a.y. 2021-2022

POLITECNICO DI TORINO

Master's Degree in Environmental and Land Engineering

Effects of climate change on snow cover in Swiss alpine terrains in the 21^{st} Century

Supervisor: Prof. Jost von Hardenberg
Co-supervisor: Dr. Adrien Michel
Co-supervisor: Prof. Michael Lehning

Candidate: Nike Chiesa Turiano
s288457

A mamma e papà
che mi hanno insegnato
che la conoscenza è un atto volontario

"Un voyage se passe de motifs.
Il ne tarde pas à prouver qu'il se suffit à lui-même.
On croit qu'on va faire un voyage mais bientôt c'est le voyage qui vous fait ou vous défait."
-Nicolas Bouvier

Acronyms

95HS 95 quantile Snow Height

DW Wind Direction

GCM Global Climate Model

GHG Green House Gas

HS Snow Height

ILWR Incoming Long-Wave Radiation

IMIS Intercantonal Measurement and Information System

ISWR Incoming Short-Wave Radiation

MCH MeteoSwiss

MDTAA0 Monthly number of Days with Air Temperature Above 0°C

MHS Mean Snow Height

MMTA Mean Monthly Air temperature

MPSUM Monthly Precipitation

MS SNOW Snow precipitation rate

NLWR Net Long-Wave Radiation

NSWR Net Short-Wave Radiation

OLWR/RLWR Outgoing/Reflected Long-Wave Radiation

OSWR/RSWR Outgoing/Reflected Song-Wave Radiation

PSUM Precipitation

QM Quantile Mapping

RCM Regional Climate Model

RCP Representative Concentration Pathway

RH Relative Humidity

SSE Snow Season Ending date

SSL Snow Season length

SSS Snow Season Starting date

SWE Snow Water Equivalent

TA Air Temperature

TSG Ground Surface Temperature

TSS Snow Surface Temperature

VW Wind Velocity

Contents

Abstract

Snow is a key element in alpine terrains as it highly affects not only the surrounding environment in terms of hydrology and ecosystems of the catchment but also for socioeconomic aspects such as electricity production and winter tourism. The future changes in air temperature and precipitation as integral part of projected climate change are expected to affect the snow cover. To analyse the magnitude of this impact, in this study Snow and Climate Metrics, evaluated in two periods of the future (2020-2050 and 2069-2099), are compared to the values of the past (1971-2001). To do so, measurement data from 18 Intercantonal Measurement and Information System (IMIS) stations situated across the Swiss Alpine arc, and 6 climate change model chains, in 2 RCP scenarios (RCP2.6 and RCP8.5), from EURO-CORDEX at 50km resolution, were used. The 18 stations are spread over the Swiss Alpine Arch above 2000 m.a.s.l. and clusteredin 4 regions, 3 on the northern side (North-West, North-Center, North-East), 1 on the southern one (South). As a complete dataset including Incoming Short-Wave Radiations and precipitation, variables not directly measure ad IMIS stations, was necessary the reconstitution of the latter was carried out thanks to the use of measurement data at MeteoSwiss stations. The climate model chains were then downscaled to IMIS stations using quantiale mapping. The downscaled datasets underwent a disaggregation process from daily to hourly resolution and were subsequently fed to the physical-based snow model SNOWPACK to obtain the evolution of the snowcover from 1971 to 2099.

All stations showed a future clear reduction in Snow Season Length (SSL), with, as main cause, an earlier ending (SSE), rather than a delayed starting (SSS). SSE is, in fact, expected to be 15-18 days in advance for RCP2.6 and 55 for RCP8.5, in contrast with a delay of 7-11 days for RCP2.6 and 13-22 days for RCP8.5 for SSS. Delays and anticipations are expected to result in a shortening of the SSL of 20-30 days for RCP2.6 and 80-92 days for RCP8.5 by 2069-2099. Furthermore, the snowcover is also awaited to be affected in its mean and maximum thickness. South and North-Center stations are the most affected ones, experiencing a reduction of 12-16% (16-20 cm) in 2020-2050, and 14-45% (20-60 cm) in 2069-2099. Even though an increase of precipitation in winter in expected on both sides, the reason of these changes is to be traced back mainly to the rise in temperatures along the whole year. For both RCPs and periods (Mid and End of Century) the Northern side is expected to experience a larger increase in air temperature and precipitation with respect to the South, however, the Monthly number of Days with Air Temperature Above 0°C (MDTAA0) is awaited to be larger in the South, resulting in a stronger reduction in MHS on this side.

The most direct impacts of the changes in the snowcover are on the hydrology of the surrounding catchments. The flux of meltwater coming from snowpacks, historically bell-shaped centered on the beginning of June with a long tail in winter, for RCP2.6 is expected to end in summer and the timing of its maximum release to be anticipated of 11-18 days, for RCP8.5 the flux becomes continuous along winter and spring and drops to 0 by the end of July, its peak is anticipated by 40 days. These impacts on the runoff behaviour can be linked to the increase in air temperature. By the end of the century, according to RCP8.5, the MDTAA0 is going to be much larger in every month causing a continuous melt of the snowpack and thus a continuous meltwater runoff from from later autumn to early summer.

1 Introduction

This thesis is a research study carried out under the supervision of Dr. Adrien Michel. It was implemented partially at the *Laboratory of Cryospheric Sciences*, CRYOS, of the Ecole Polytechnique Fédéral de Lausanne (EPFL), Lausanne and partially in the *Snow Processes* research group at the WSL Institute for Snow and Avalanche Research SFL in Davos, both coordinated by Prof. Michael Lehning. The laboratory of cryospheric sciences, as well as the Snow Processes group, investigates the processes that shape snow and ice in mountains and polar regions. In particular, snow cover processes, snow-atmosphere interactions and mountain hydrology are in the focus of current research. In addition, the work was kindly reviewed by Professor Jost von Hardenberg, lecturer and researcher at Politecnico di Torino.

Alpine snow cover has significantly decreased during the past decades [1, 2] and further reduction are expected, with clear projections for low elevations and more uncertainties for high altitudes [3, 4]. Studies by Beniston et al. (2003) [5] showed a reduction from 40 to 80% in snow volume for altitudes below 1500 m.a.s.l., and from 10 to 60% in the altitude band of 2000-2500 m.a.s.l. by mid-century and from 30 to 80% by the end of century. Snow volumes are expected to be more affected at lower elevations due to the fact that the mean air temperature, throughout all winter, is already close to the melting temperature [6, 2]. Increases at all elevations of both winter precipitation and air temperature [7] [8] are expected and Schmucki et al. (2015) [9] showed how the changes in snow cover, and specifically in snow height, are going to be mainly caused by changes in temperatures rather than changes in precipitation, which cause a shift of the precipitation phase towards liquid.

The importance of snow cover, especially at high altitudes, stands in the fact that it is a natural reservoir that can supply water throughout the year. Over a whole year, in fact, in Switzerland, over 40% of the river runoff comes from melted snow [10]. The impacts on the water system are projected to result in a smaller contribution of the snow melt to the water balance of the catchments, with an increase in the winter flows, a reduction in the summer runoff and an anticipation of the peak flow [11]. Besides the effects on the hydrology of the catchment and water supply, a change in runoff would affect the hydropower production which, in Switzerland, covers 60% of the domestically produced electricity and accounts for 12.3% of the total energy consumption [12]. Furthermore, changes in snow cover would affect the economy of mountain communities whose income can be related to up to 90% to winter tourism [13], as well as the life of plants and animals which strongly respond to changes in snow depth and snow seasons timing [14].

Several previous studies on climate change on the Alps considered different resolutions, data, methods and locations. Two main types of studies have been found: either location-specific studies such as on specific catchments (e.g. Bavay et al, 2009 [15]), or large scale ones such on the whole Alpine arc (e.g. Kotlarski et al, 2022 [8]). Furthermore, a preference for either using raw climate models or downscaling them with the Delta method was spotted. Due to the abundance of measurement stations and low elevations and scarcity at high elevations, most of the studies mainly focus on the effects on climate change up to 2000 m.a.s.l. [9] [2].

This study tries to be the conjunction link between these studies providing a broad overview on the Swiss Alpine arc above 2000 m.a.s.l. starting from station data, and downscaling climate models to the stations using the Quantile Mapping method. The research question of the present thesis is to investigate whether the future effects of climate change on the snow cover in Alpine terrains above 2000 m.a.s.l. would be different in two macro-regions of Swiss Alps, Northern and Southern sides of the ridge, considering in detail the effects on four different regions within these two macro-regions: North-West, corresponding approximately with Valais Canton; North-Center, area where the Cantons of Bern and Uri come together; North-East, part of Grison Canton; and South, belonging to Canton of Ticino. To do so, measurement data from several alpine meteorological stations, were used in couple with projections in the changes of the climate, available thanks to the EURO-CORDEX initiative which provide gridded climate change projection data from 1971 to 2099 at 50km resolution. With a set of six GCM-RCM model chains and two emission scenarios, RCP2.6 and RCP8.5, it was possible to assess the differences in snow cover projected for the stabilization scenario (RCP2.6), that supposes a 50% cut in Green House Gasses emissions by mid century, and for the non-intervention scenario (RCP8.5). The evolution of the snowcover and meteorological variable from 1971 to 2099 is obtained at the station scale thanks to the use of the physical-based snow model SNOWPACK. Thanks to a multi-step process a suitable dataset to be fed to SNOWPACK to obtain such evolution is obtained: the climate model signal was downscaled to stations and, then a disaggregation process from daily to hourly resolution, necessary to fit SNOWPACK requirements, allowed the reconstruction of daily cycles of meteorological variables. The differences in snow cover in mid century (2020-2050) and end of century (2069-2099) with respect to the Historical period of reference (1971-2001) were assessed thanks to the use of metrics which provide information on the snow season length, its starting and ending dates, as well as the mean and maximum snow height throughout the snow season. Furthermore, links between the observed changes in snow cover characteristics and changes in meteorological variables, such as precipitation and air temperature, were drawn.

1.1 Climate of the Swiss Alps

The climate of a region is defined as the average weather conditions over a period of years as exhibited by temperature, wind velocity, and precipitation. Its nature depends on the latitude, altitude, closeness to waterbodys (e.g. lake, sea, ocean), presence of mountains and prevailing wind.

In the Alps the presence of mountainous topography affects the atmospheric motion of heat and humidity by deflecting airflows both horizontally and vertically, causing more complex precipitation patters. In fact, when air encounters an obstacle, such as a mountain range, it is forced to lift. Consequently, the relative humidity increases, water vapor condensates around condensation nuclei forming clouds, forcing the precipitation to occur.

Being located in the center of Europe, in the so-called *temperate climate zone* [16], the Alps are influenced by 4 main air masses which act as drivers: westerly, mild and moist flow from the Atlantic Ocean, cold polar wind from northern Europe, air masses from the East, and warm flows from the Mediterranean sea. Both in summer and winter the main contribution comes, in order of importance, from west, north-west, south-west and north (Figure 1) [17].

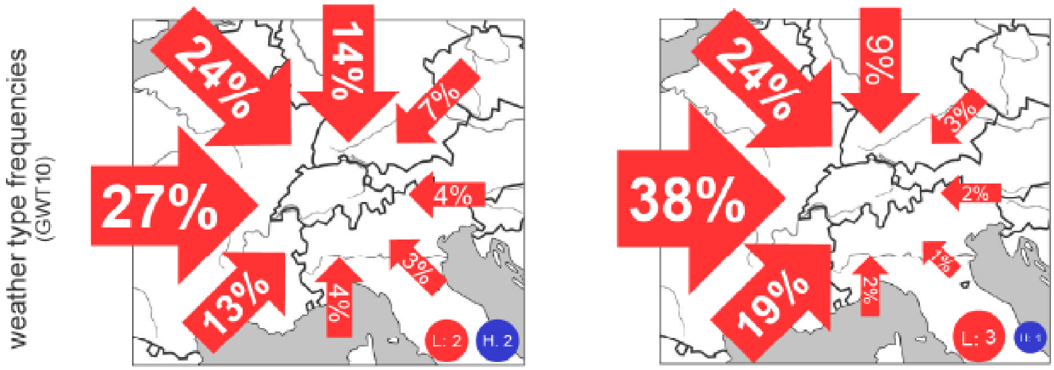

Figure 1: Figure taken from CH2018 report [17]: Illustration of air flows and their magnitude over Switzerland in Winter months (DJF), on the left, and Summer months (JJA), on the right. L: low pressure, H: high pressure. The period considered is 1981 - 2010

.

The most important local and occasional winds are Föhn, which crosses the mountain ridge, and Bise, a deflected wind. There is a northern and a southern Föhn according from where it blows from.

The climate on southern side of the Swiss Alps (dark red in Figure 2) is in fact determined both by the influence of the Mediterranean sea, mainly in summer, and by the northern Föhn, key factor in shaping the winter climate.

Figure 2: Illustration of the borders of the biogeographical major region on the south side of the Alps (in reddish brown) according to the Swiss Federal Office of the Environment (FOEN) [18]

The resulting climate in Canton Ticino, which covers most of the southern side of the Swiss Alps, is characterised, by mild and relatively dry winters, warm summer with frequent thunderstorms, heavy rains in autumn. At 2000-2500 m.a.s.l., altitude band on interest in this study, this pattern is conserved as visible in Figure 3 and Figure 4 where mean monthly air temperature and mean monthly precipitation, respectively, are show for the Southern and Northern side of the Swiss Alps. In the graph, the Northern side is subdivided in 3 regions, North-West, North-Center and North-East, according to the regions of interest of this study (Section 2.1.1).

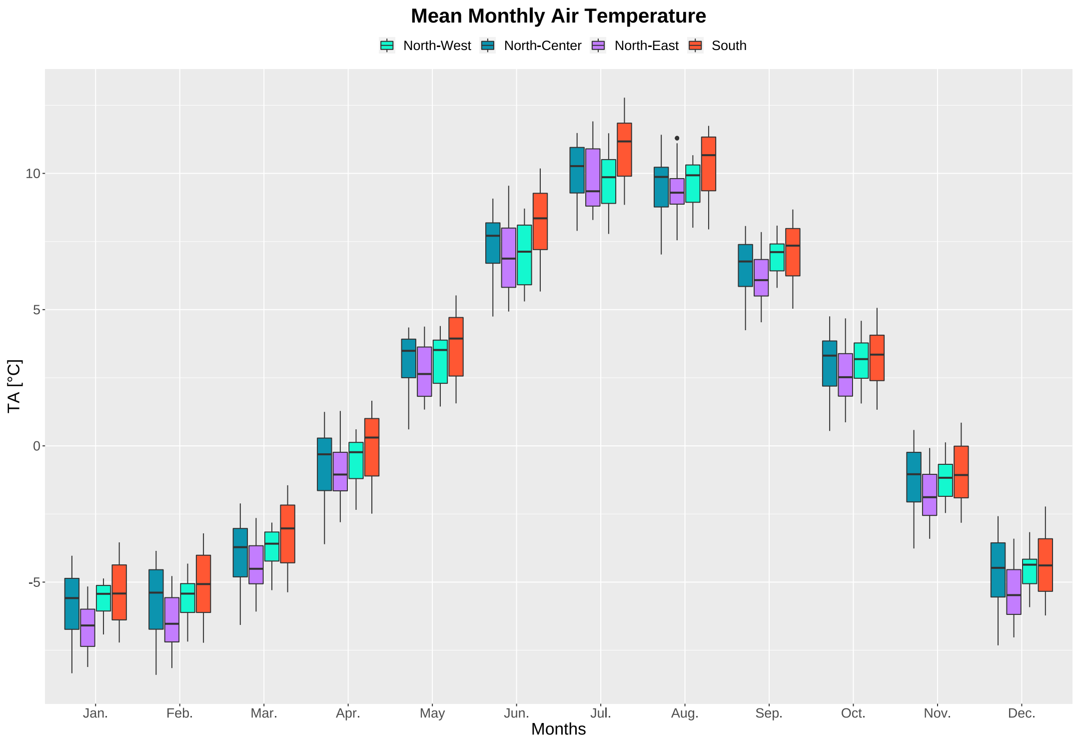

Figure 3: Mean Monthly Air Temperature on the northern (North-West, North-Center, Nort-West) and southern side of the Alps above 2000 m.a.s.l. from measurement data in the period 2005-2019

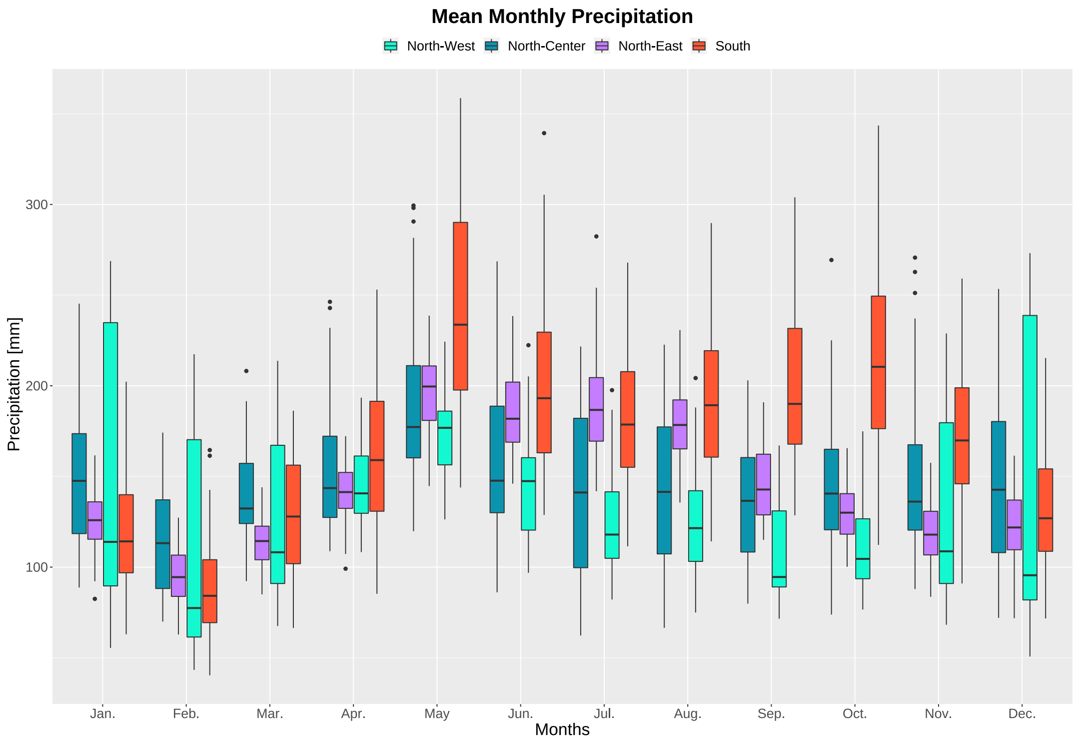

Figure 4: Mean Precipitation on the northern (North-West, North-Center, Nort-West) and southern side of the Alps above 2000 m.a.s.l. from measurement data in the period 2005-2019

The climate of the northern-side of Swiss Alps is highly determined by the influence of both the Atlantic Ocean and the Alps. The prevailing westerly and northwesterly wind currents bring humidity from the Ocean towards the inland, which is then released as precipitation due to the uplifting cause by the Alps. The Southern Föhn has a warming effect between autumn and spring, especially in valleys north-south oriented such as the western part of Valais, belonging to the North-West region (Figure 3).

The highly complex topography of the Northern Alps causes large differences in precipitation in the different regions: Valais valley shows a dry climate as it experiences $\sim$ 600 mm/year of precipitation whereas for some regions of the central Swiss Alps it goes up to $\sim$ 3000 mm/year [17]. The histograms in Figure 5 display how different precipitations can be in the different regions month by month (circled in red the regions of interest in this study). It is noteworthy how, in summer, the Nort-West (in the graph called Valais) is drier with respect to the other Regions: North-Center (in the graphs called Central Alps), South (in the graphs called Southern Alps), and North-East (in the graphs called Northern central Grisons), while, in winter (DJFM), it is characterised by more precipitation (together with Bern+Uri).

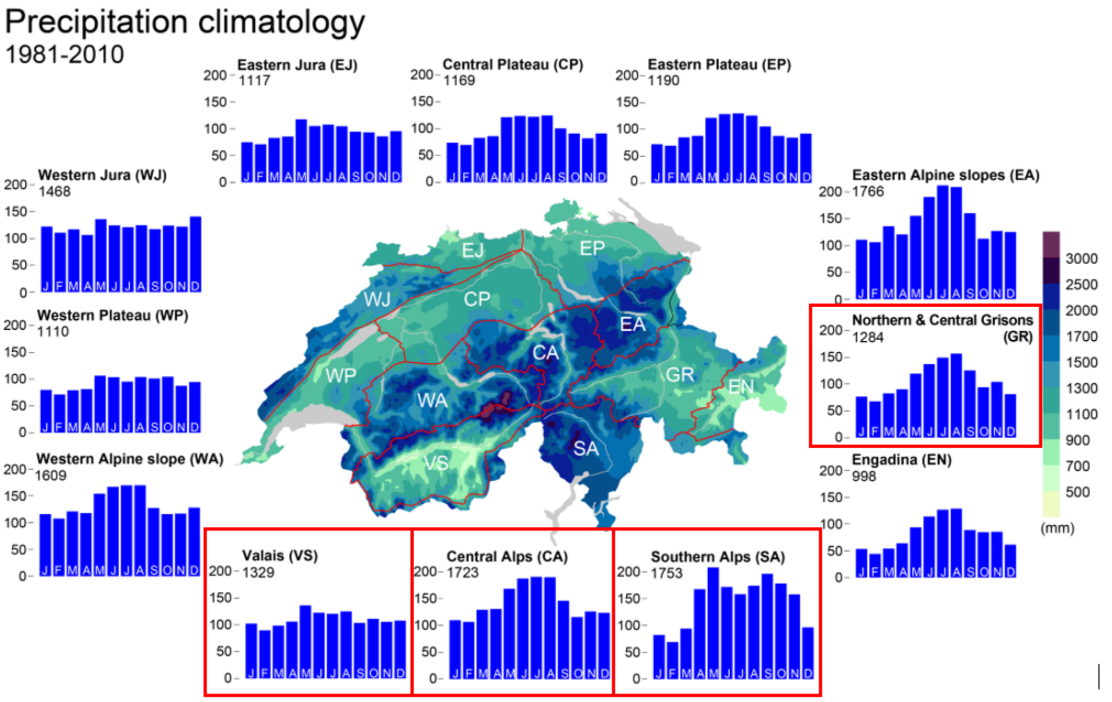

Figure 5: Gridded annual mean precipitation and monthly sums for the twelve Swiss climate regions [19]

It is noteworthy to note how the differences in precipitation patterns among the different regions do not persists at 2000-2500 m.a.s.l. altitude band as visible in Figure 4: while on average the North-West keeps being the driest region, the North-East becomes more rainy in the summer months with respect to the North-Center. In autumn and winter the North-Center is the region experiencing the largest mean precipitation. The long boxplots characterising the North-West have to be attributed a larger variability of the local precipitation phenomena across the region, which is not traceable back to the variability in air temperature which is quite little (Figure 3).

Due to low temperature, most of the precipitation, above 1200-1500 m.a.s.l. falls mainly as snow [20], but the measurable number of days with snowfall still strongly depends on altitude. In the alpine region, in fact, generally, snow days can range from 30 to 120: the North-Center shows a mean of roughly 90-100 days, while Valais, Ticino and Grison drop to 60-70 (Figure 6). Snow Water Equivalents (SWE) values do not draw a different picture with respect to snow days, but the difference between Valais and Grison is noteworthy: 400 mm in the former and only 150 mm in the latter.

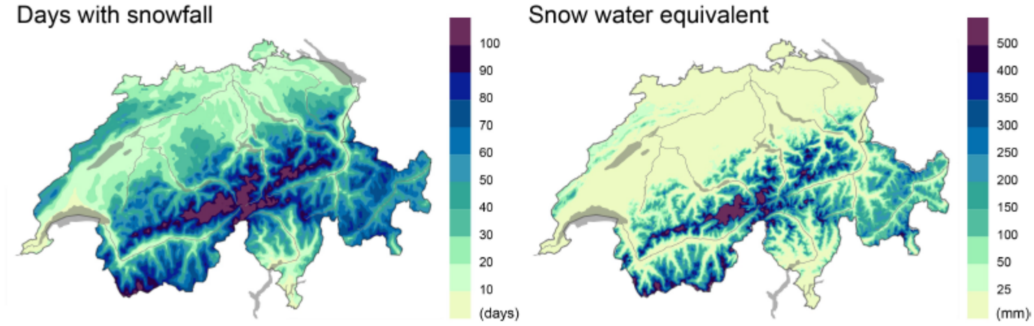

Figure 6: 1981 - 2010 snow climatology for the extended winter season (September - May). Left: Mean number of days with measurable snowfall based on (days with new snow sum 1 cm). Right: Mean snow water equivalent [21].

For measurement site in the 2000-2500 m.a.s.l. altitude band (Figure 7) North-Center and North-East, the snowiest regions, are rather homogeneous in terms of mean values but the former show a larger variability. North-West is the least snowy in terms of mean but, once again, shows a high inner variability. The South stands in between.

Figure 7: Mean Solid Precipitation on the northern (North-West, North-Center, Nort-West) and southern side of the Alps above 2000 m.a.s.l. from measurement data in the period 2005-2019

1.2 Introduction on Climate change

Climate Change can have natural cause, as well as athropogenic ones. Geologic records indicate how dramatic changes occurred in the past during which the Earth went through cooling and warming phases in absence of humans [22]. Natural drivers for these changes include Sun's intensity, orbital forcing, volcanic eruptions, aerosol emissions and changes in natural Green House Gases (GHG) emissions. Since the 19^{th} Century human activities have been the main drivers of changes in global and regional climate: the records show that a much faster warming, that can not be explained by natural causes, is occurring [22]. In fact, the greenhouse effect, that naturally keeps the Earth warm thanks to the absorption of thermal radiation, significantly increased due to the rise in athropogenic emission of GHG [22].

As a result of the higher GHG concentrations in the atmosphere the mean air temperature of the Earth is now $\sim 1.1°C$ warmer than at the end of the 19^{th} Century. It is a great challenge to predict the evolution of the climate system in relation to the human activities, especially if the predictions have to be adequate enough for countries to adjust their behaviour and plan policies to limit the impacts. The most complex task is to foresee the evolution of human activities, which are related to social, economical and political aspects, and their repercussions on the climate system. This is where the concepts of climate scenarios and climate models nest.

1.2.1 Climate Change models

"Climate models are computer programs that simulate weather patterns over time" [23]. They can be visualised as layers of 3D cells surrounding the Earth (Figure 8) where each cell contains the mathematical equations that govern the exchanges and motion of mass and energy.

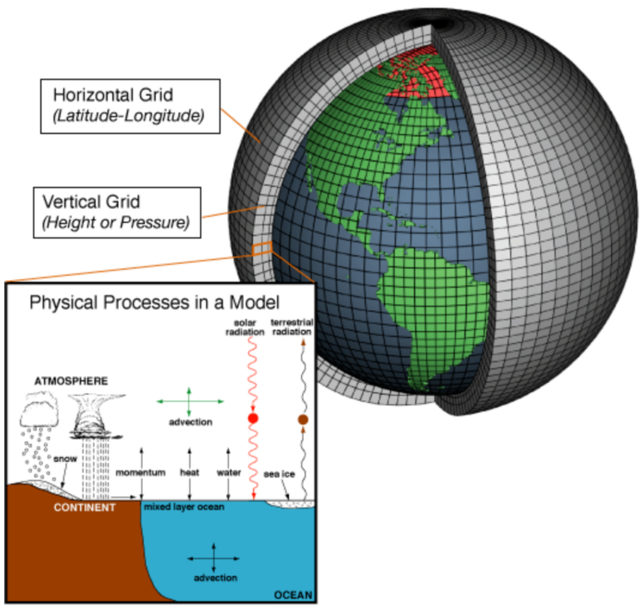

Figure 8: Visualisation of climate models grids and the inner interaction of physical processes [24]

As climate models simulate Earth's weather, they are governed by physical principles. The atmospheric component of climate models is defined by the following seven principles:

- Conservation of air mass
- Conservation of water mass
- Conservation of energy
- Conservation of momentum of air in the three directions
- Ideal Gas Law

The results of the equations describing these seven physical principles for each grid cell is communicated to the neighbouring cells to model the exchange of mass and energy. The complexity of climate models is related to the number of processes and correlations among the climate drivers that are included. The detail with which each process is described depends to the importance of it in the climate system. The cells' size determines the resolution of the model, smaller cells imply higher resolution on the processes. For what concerns phenomena (e.g. convection, clouds, sea-land breeze, snow) which are smaller than the size of a cell, parameterizations are applied.

Resolution, usually, goes hand in hand with the type of climate model and its extension:

- Global Climate Models (GCMs): they cover the whole Earth with cells of hundreds of kilometers-long sides.

- Regional Climate Models (RCMs): they cover specific areas (e.g. Europe) with a finer resolution of tens of kilometers-long sides.

While GCMs are used to grasp the evolution of the climate system, especially in response to human actions, RCMs, being more locally accurate, help understanding the climate change effects on specific areas. The existence of both types of climate models allows to predict the effects of global changes simulated by the GCMs, at the regional scale. It would be, in fact, very time-expensive to run a model with the resolution of RCMs on a global scaled for time sake. The transfer of information from a GCM to a RCM occurs thanks to *Dynamical Downscaling*. The dynamical downscaling involves nesting the RCM into the GCM, a technique thanks to which lateral boundaries of the RCM are provided by the GCM. Usually, the provided information are atmospheric fields (e.g. wind, pressure, temperature and humidity) and sea surface temperature [25]. The validation of climate models, called *Hind-Casting*, consists in running the models from past to present and comparing the results with observed measurements. Once validated, a climate model can be run to the future. Runs in the future strictly require the forcing to be set to change according to a scenario. The term *Scenario* includes the evolution of any type of forcing, such as population growth, land use, climate forcing [24]. Scenarios are used as boundary conditions of climate models, in fact, the first definition of scenarios, responded to the need of making different and independent models comparable. Indeed, if models were run using different assumptions and starting points, then, it would be hard to compare the outputs.

1.2.2 Climate Change scenarios

The *Intergovernmental Panel on Climate Change*, also known as IPCC, is an organisation that publishes reports to share the current knowledge on the drivers of climate change, their future impacts, their potential risks, and how adaptation and mitigation can help in reducing those risks [26]. In 2014, IPCC described a new set of possible future scenarios called *Representative Concentration Pathways* or RCPs in the fifth Assessment Report (AR5). Each RCP consists of a set of starting values and evolution of emissions up to 2100 based on the projection of several factors such as economic activity trends, energy sources and population growth. They are specifically focused on the concentration of GHGs in the atmosphere in 2100, expressing their effects on the radiative forcing in terms of $[Wm^{-2}]$ [24]. A *radiative forcing* is the magnitude of influence that a factor has on altering the balance of incoming and outgoing energy in the atmosphere [27]. It is important to know that, as the name itself suggests, they are not a simple specific long-term concentration prediction but rather the trajectory, or pathway, over time to reach such concentration.

There are 4 main RCPs pathways:

- RCP2.6: radiative forcing peaks at 3 $\mathrm{W\,m^{-2}}$ within the 21^{st} century and declines afterward, stabilizing the increase of global mean temperature at <$2°C$. It is also known as *2°C-compliant mitigation*.
- RCP4.5: radiative forcing stabilises at 4.5 $\mathrm{W\,m^{-2}}$ with an average increase of global mean temperatures predicted by models of $\sim 2.5°C$. It is also known as *2°C-non compliant mitigation*
- RCP6: radiative foring peak of 6 $\mathrm{W\,m^{-2}}$ around 2080, then decline. Temperature rises of 3-4$°C$ by the end of the 21^{st} century.
- RCP8.5: raditive forcing crosses 8.5 $\mathrm{W\,m^{-2}}$ and the global mean temperature rises of 4-5$°C$ by the end of the 21^{st} century. It is also known as *Unabated emissions*

In Figure 9 and Figure 10 a visualisation of the evolution of the GHGs concentration for each RCP and the relative radiative forcing trends are shown. For what concerns CO_2 emissions (Figure 9, left graph), while RCP8.5 is characterised by a rapid concentration increase, RCP6 and RCP4.5 stabilise in the second part of the century, and RCP2.6 exhibit a peak around 2050 to then have a decline. As a result of the relatively short lifetime of CH_4 emission reductions, as in the RCP2.6 and RCP4.5 lead to an emission peak much earlier in the century (Figure 9, central graph). For N_2O (Figure 9, right graph), in contrast, a relatively long lifetime imply an increase in concentrations, in all RCPs [28].

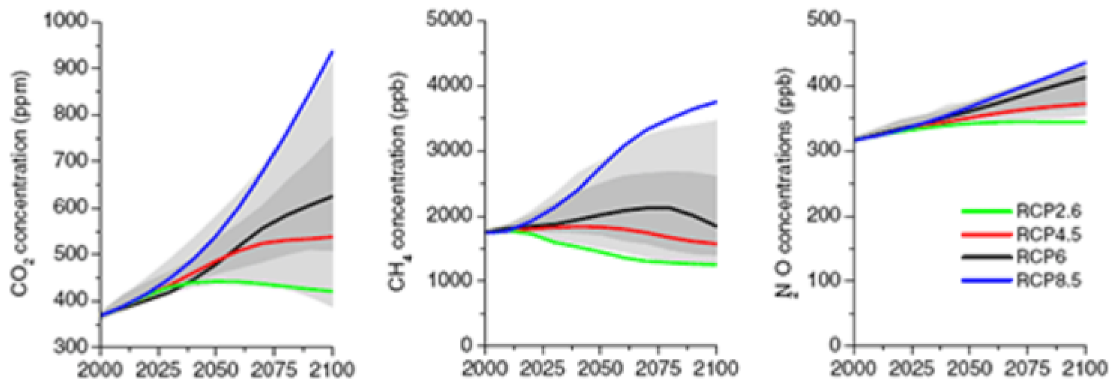

Figure 9: Trends in concentrations of GHG. Grey areas indicates the 98th and 90th percentiles (light/dark grey) [29].

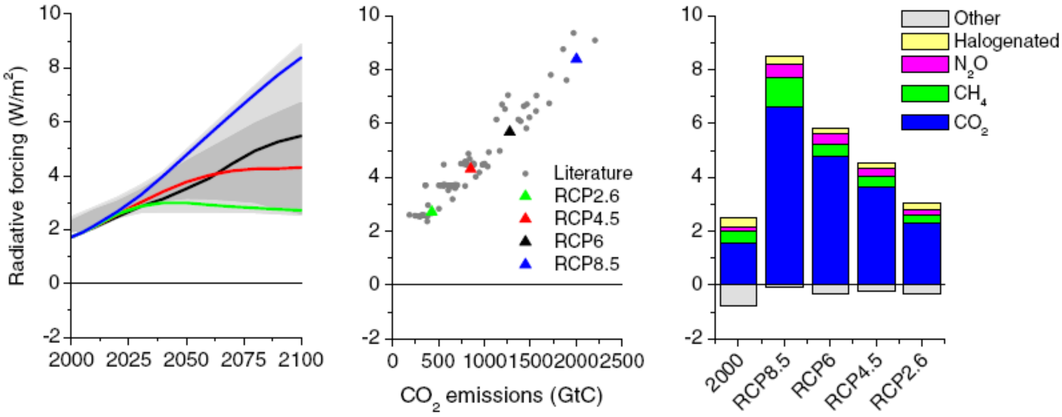

Figure 10: Trends in radiative forcing (left), cumulative 21st century CO_2 emissions vs 2100 radiative forcing (middle) and 2100 forcing level per category (right). Grey area indicates the 98th and 90th percentiles (light/dark grey) of the literature. The dots in the middle graph also represent a large number of studies. Forcing is relative to pre-industrial values and does not include land use (albedo), dust, or nitrate aerosol forcing [29].

It is important to note that in 2021 IPCC released a new set of scenarios in the sixth Assessment Report (AR6) [30]. These Shared Socioeconomic Pathways (SSP) scenarios describe possible different developments of socioeconomic factors such as population growth, economic growth, urbanisation and technological development. RCPs and SSPs are meant to be combined as the analysis of the evolution of emissions and different socioeconomic pathways highlights which climate policy can achieve the forcing levels set by each RCP. These scenarios are going to be used in the next generation of climate models.

1.2.3 Climate Change uncertainty

Climate Change projections are affected by uncertainty due to their nature. There are three types of uncertainty [31]:

- Natural variability: It is the variation of the atmospheric system around a mean state due to natural processes.
- Scenarios uncertainty: scenarios are based on hypothesis of socio-economic trends, population growth and resources consumption which are associated with unforeseeable developments. The made assumptions span possible futures but can not be predicted with certainty.
- Model uncertainty: It is due to the incomplete knowledge of the relationships between physical, chemical and biological processes occuring in the atmosphere, as well as the impossibility to mathematically precisely describe each one of them. Furthermore, parameterisations may differ from model to model.

Figure 11 shows how the importance of each uncertainty varies with time. Internal variability and model uncertainty are the main sources of uncertainty in the short-term, but at the end of the century such role is taken over by the the scenario uncertainty.

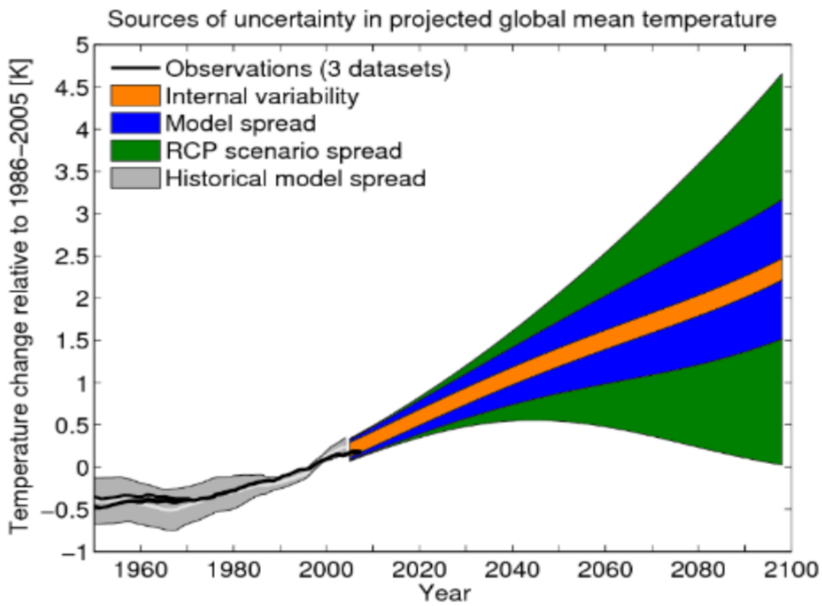

Figure 11: Sources of uncertainty and their contibution to the total uncertainty over time [32].

To deal with these uncertainties, it is important to take into account several climate models rather an a single one to be aware of how wide the range of possibilities is [33].

1.2.4 Bias Correction Methods

RCMs are characterised by fine resolutions which, however, can be too coarse for subsequent applications such as the assessment of climate change effects at local scales, especially, in regions with highly complex terrains, like the alpine region, which show a strong variability in the space of a few kilometers. To face the problem of coarsely resolved and potentially biased climate model outputs, several statistical downscaling (SD) and bias correction (BC) methods have been developed in time.

Two of the most commonly used methods to post-process and bias-correct the climate models output are the *Delta change* method and the *Quantile Mapping* (QM) method.

The Delta method implies two steps (Figure 12) [17]:

1. Extraction of Delta change: the raw climate model considered for an historical reference period, is compared with the raw climate model itself but for a future period. Their difference is defined as the Delta change.

2. Production of downscaled future signal: the Delta change is applied to the observations in order to obtain the signal in the future for the same future period considered in the Delta change computation.

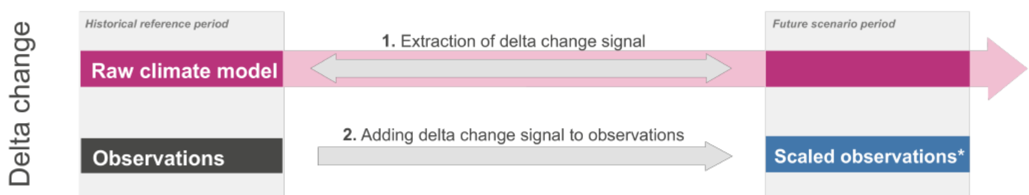

Figure 12: Methodological overview of the delta-change [17]

Beside the easy implementation and robustness of this method, it presents two main downsides: that future scenarios show the same temporal evolution of the observations, and it does not provide information between the observation period and the chosen future period (Figure 13).

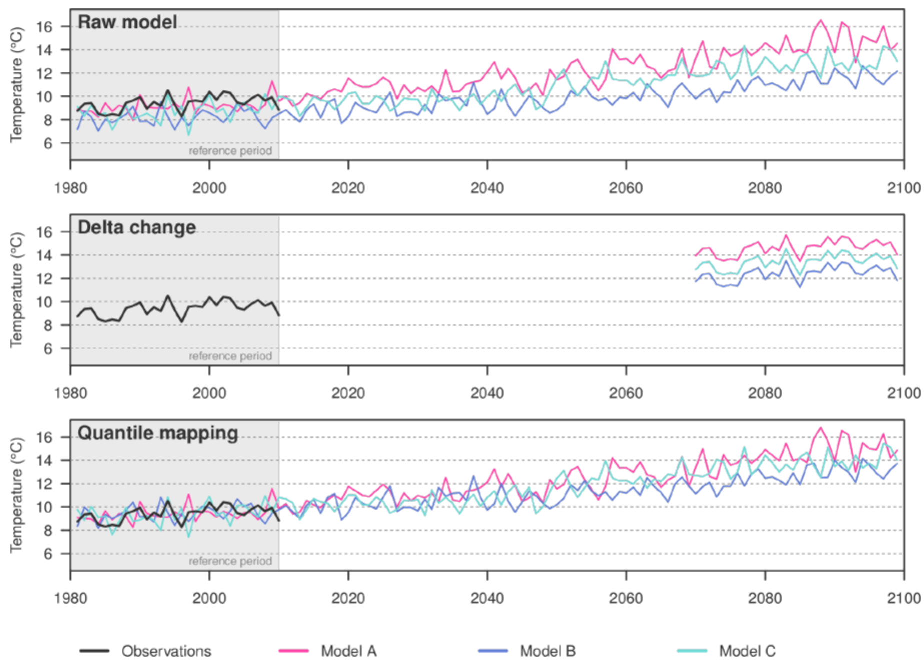

Figure 13: Comparison of Delta change and Quantile Mapping for the case of annual mean temperature at the Zurich/Fluntern (SMA) station and for three EURO-CORDEX model chains (referred to as A, B, and C). Top: Observations and raw model output. Middle: Delta-change method, consisting of a simple scaling of the observed time series with the annual mean temperature-change signal between the reference and the scenario period. Bottom: Quantile mapping. [17]

QM, on the other hand, is a bias-correction technique which removes only certain biases (e.g. biases in the mean), as it is unable to correct biases in temporal sequences. QM is designed such that it corrects the distribution of raw modeled climate data so that simulated quantiles match the counterpart on observational data and, subsequently, applies the correction, *correction function*, to future climate model outputs data (Figure 14). Thus, corrected Climate models reproduce accurately the quantiles of the variables but not their values one by one. The adjustment on the distribution of the data results in the correction of both the errors related to the different scales of climate models and observational data, and possible systematic model biases [34]: as visible in Figure 13, the row climate models are corrected in order to share the same mean with observations

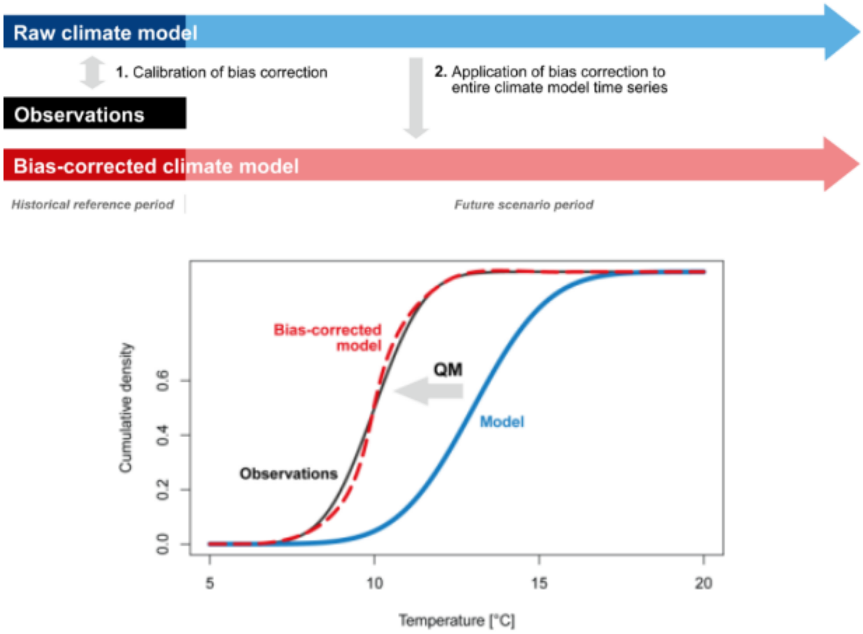

Figure 14: Top: Overview on the bias correction approach: a bias correction function is calibrated by comparing raw climate model output to observations in a common historical reference period. The calibrated correction function is then applied to the entire raw model output in order to produce a bias-corrected time series out into the future scenario period. Bottom: A biased simulated distribution (blue) is corrected towards an observed distribution (black). In the example shown the raw simulated distribution is subject to both a bias of the mean and a bias in variance. The resulting bias-corrected distribution (dashed red) approximates the observed one but is typically not identical to it (e.g. due to the sampling uncertainty during the calibration of the correction function or details of the specific QM implementation) [35]

Since thanks to QM climate models are corrected to match observational data, the procedure implicitly results in a downscaling process from grid data to the local scale of the meteo station (Figure 15) [17].

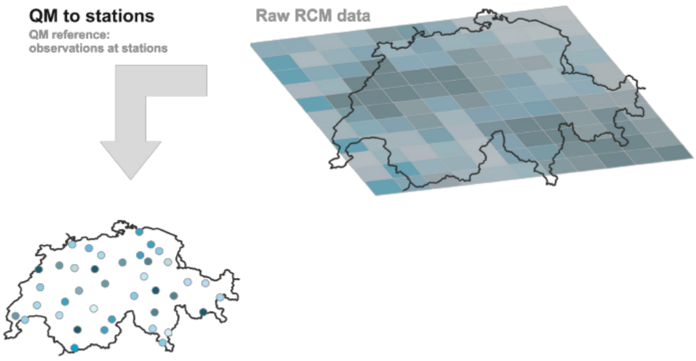

Figure 15: Application of QM from grid data to station [17]

In this study, as bias correction method, the choice fell on QM as the author wanted to obtain, for the present work and possible future ones, a continuous dataset of meteorological variable carrying the climate change signal from 1971 to 2099. The application of QM is further reported in Section 3.6

1.2.5 Snow Modelling

Snow is a complex material which constantly changes as result of heat and mass exchanges occurring between snowpack, atmosphere, underlying ground and, if present, the surrounding canopy. Studies on the processes that shape a snowpack require modelled descriptions of the physical properties of snow. Hydrological studies [11], avalanche forecasting [36] and climate modeling [37] are some of the reasons for which snow models are nowadays widely used and continuously improved in the accuracy with which the physical processes are described. In Figure 16 the main players in the mass and energy balance on a snowpack are reported together with the main processes: Incoming Short radiation from the sun are partially reflected (Outgoing Short Wave radiations) and partially absorbed in the snowpack according to the albedo of the snow surface, which depends on the aging of the snow grains; a different amount due to cloudiness of Incoming Long Wave radiations are absorbed and emitted according to the temperature and emissivity of the snow; rain and meltwater can refreeze inside the snowpack releasing laten heat or percolate till the soil creating an outgoing runoff; moisture gradients between atmosphere and snowpack drive latent heat fluxes while temperature differences cause sensible heat fluxes; snow can be moved, deposited or eroded by the action of the wind. Mass and energy balances are necessary to express all these parallelly on-going processes.

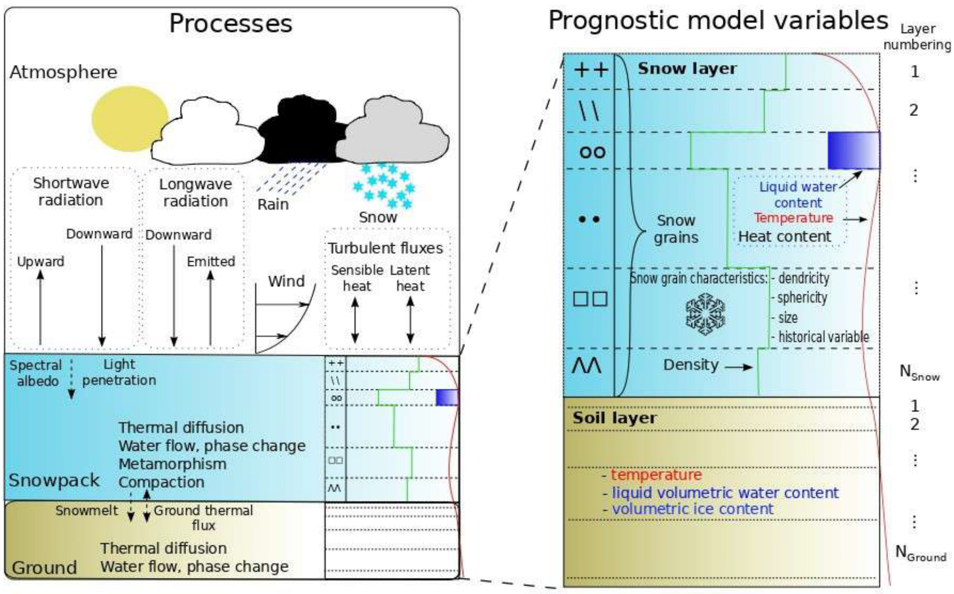

Figure 16: Scheme of the main physical processes and occurring in a snowpack [38]

The accuracy of a snow model depends on its use and computationally expense that can be supported [39]. They can be grouped in three levels of accuracy: low accuracy, intermediate accuracy and high accuracy [40]. In the first group fall the snow models included in global climate models as, generally, the snowpack is represented as a single layer with fixed density and specific characteristics such as low thermal conductiviy and high albedo. Intermediate-accuracy snowpacks are, instead, described by to 2 to 5 layers in order to account for processes like settling and percolation [40] and their properties are parameterized as function of of snow density. An example is the ISBA-Explicit Snow model [41] which is used in couple with hydrological and atmosphere models for local scale hydrological simulations. High accuracy snow models such as SNOWPACK [36] (Section 2.2), Crocus [38] and SNTHERM [42] go down to the description of the evolution of the miscrostructure of snow. They provide a wide knowledge on the vertical layering of snowpack but they can not be directly implemented in RCM or GCM As they are highly computationally demanding. However, several studies (e.g. Schmucki et al., 2014 [43], Marty et al, 2017 [44]), this one included, have been conducted on the effects on climate change with the help of these models. They can be, in fact, used to locally reconstruct the evolution of snowpack with high accuracy using as climate variables the ones coming from climate models.

2 Data and Software

In the present study two type of data were used: measured and modelled data. Measurements, also called observational data, are required as reference for validations (section 3.4) as well as for bias-correction processes (section 3.6). They come from both IMIS meteorological stations [45] and MeteoSwiss meteorological stations [20]. Modelled data, on the other hand, are necessary to obtain the change in signal of climate variables at the sites of interest and come from EURO-CORDEX data. Measured data span from 2006 to 2019, period that is going to be called *Calibration period*; climate model data go from 1971 to 2099.

The use of SNOWPACK software [36], allows to obtain the evolution of the snowpack providing meteorological variables.

2.1 Data

2.1.1 Measurement data: IMIS and MeteoSwiss stations

The sources of measurement data are as follow:

- IMIS stations [45]: these stations, operated by the WSL *Institute for snow and avalanches research* (SLF), are high-alpine stations located outside the electricity grid, above the tree line, between 2000 and 3000 m.a.s.l. As electricity supply is necessary to heat up snow gauges, its absence results in the inability to assess snow precipitation rate (PSUM).

  Furthermore, the risk of snow covering the instruments, jeopardising the continuity of measurements, is very high and results in the limitation of measured radiative fluxes. Only Reflected Short-Wave Radiation (RSWR) is measured, neglecting the Incoming Short-Wave Radiation (ISWR).

  As PSUM and ISWR are quantities modelled in climate models, their magnitude at the sites of interest, can not be discarded and must be reconstructed (Section 3.2.2 and Section 3.2.3). In Table 1 the variables measured at IMIS stations are shown.

Variables measured at IMIS stations		
Variable Name	**Standard Name**	**Units**
TA	Air Temperature	K
TSS	Snow Surface Temperature	K
HS	Snow Height	m
RH	Relative Humidity	-
VW	Wind Velocity	m s^{-1}
DW	Wind Direction	°
RSWR	Reflected Short-Wave Radiation	W m^{-2}
TSG	Temperature Surface Ground	K

Table 1: Variables measured at IMIS stations.

In the Northern macro-region of the Swiss Alps 11 IMIS stations were selected; in the Southern macro-region 7 (Table 2). The choice fell on these 18 stations as they are compliant with the necessity of having the longest time series possible, with no large data gaps, and the high alpine location. The northern stations are distributed along the whole Swiss Alpine arc, belonging, from west to east, to the Cantons of Valais, Bern, Uri and Grison. The southern stations are entirely located in the Canton of Ticino (Figure 17). In the following study the clusters of stations will be addressed with their geographical position (North-West, North-Center, North-East, and South) according to the Canton(s) they belong to (Valais, Bern+Uri, Grison).

IMIS				
SOUTH - TICINO				
ID	**Name**	**Altitude [m.a.s.l.]**	**Latitude [°]**	**Longitude [°]**
BED3	Cassinello	2101	46.491153	8.521914
CAM2	Fontane	2216	46.465719	8.717473
DTR2	Preda	2057	46.542860	8.869060
FRA2	Efra	2100	46.338232	8.853177
MES2	Pian Grand	2384	46.414007	9.160296
NAR2	Bassa di Nara	2077	46.472985	8.868635
SIM2	Piano del Simano	2450	46.467451	8.980823
NORTH WEST - VALAIS				
ID	**Name**	**Altitude [m.a.s.l.]**	**Latitude [°]**	**Longitude [°]**
ARO3	Arolla:Breona	2602	46.087417	7.562051
CON2	Conthey:Etang_de_Trente_Pas	2229	46.289738	7.274200
ZER4	Zermatt:Alp_Hermetje	2408	45.997986	7.702383
NORTH CENTER - URI+BERN				
ID	**Name**	**Altitude [m.a.s.l.]**	**Latitude [°]**	**Longitude [°]**
GUT2	Guttannen:Homad	2115	46.679304	8.289692
LUK2	Lukmanier:Lai_Verd	2555	46.604147	8.783521
MEI2	Meiental:Laucheren	2220	46.743762	8.551015
TUJ3	Tujetsch:Nual	2211	46.647026	8.740223
NORTH EAST - GRISON				
ID	**Name**	**Altitude [m.a.s.l.]**	**Latitude [°]**	**Longitude [°]**
DAV2	Davos:Baerentaelli	2558	46.698887	9.819410
DAV3	Davos:Hanengretji	2455	46.788831	9.773990
KLO2	Klosters:Madrisa	2147	46.909113	9.873862
PAR2	Parsenn:Kreuzweg	2290	46.851723	9.804846

Table 2: IMIS stations used in the study with the relative information of altitude, latitude and longitude

- MeteoSwiss stations (MCH): these stations belong to the Swiss Federal Office of Meterology and Climatology. They are supplied by the electric grid and equipped with several measurement instruments, among which automatic gauges for the measurement of the precipitation (PSUM) as well as instruments to measure the solar radiation (Table 3). Since neither PSUM nor ISWR are available at IMIS stations, MeteoSwiss measurements have to be taken into account. However, these stations are located at lower altitudes and need corrections to assess snow precipitation and solar radiation occurring higher in the mountains (Section 3.2.2 and Section 3.2.3).

Variables used among the ones measured at MeteoSwiss stations		
Variable Name	**Standard Name**	**Units**
ISWR	Incoming Short-Wave Radiation	$W m^{-2}$
PSUM	Snow Precipitation Rate	$Kg\, m^{-2} h^{-1}$

Table 3: Variables used among the ones measured at MeteoSwiss stations.

6 and 4 MCH stations were selected on the northern and southern side of the Alps, respectively (Table 4). The process through which MCH stations were selected, further explained in Section 3.2, implies a spatial distribution of the stations analogous to the IMIS stations one, spread across the whole northern arc, and grouped in Ticino for the south (Figure 17).

MCH				
SOUTH				
	Name	**Altitude [m.a.s.l.]**	**Latitude [°]**	**Longitude [°]**
PIO	Piotta	990	46.514809	8.688032
CIM	Cimetta	1661	46.200466	8.791643
SBE	S. Bernardino	1638	46.463545	9.184682
COM	Acquarossa/Comprovasco	575	46.459518	8.935472
NORTH				
ID	**Name**	**Altitude [m.a.s.l.]**	**Latitude [°]**	**Longitude [°]**
EVO	Evolène	1825	46.112209	7.508637
MVE	Montana	1422	46.298796	7.460817
WFJ	Weissflujoch	2691	46.833323	9.806370
GRH	Grimel Hospiz	1980	46.571691	8.333251
GUE	Gütsch, Andermatt	2286	46.652435	8.615046
GRH	Grimel Hospiz	1980	46.571691	8.333251
ZER	Zermatt	1638	46.029269	7.752436

Table 4: MeteoSwiss (MCH) stations used in this study with the respective altitude, latitude and longitude.

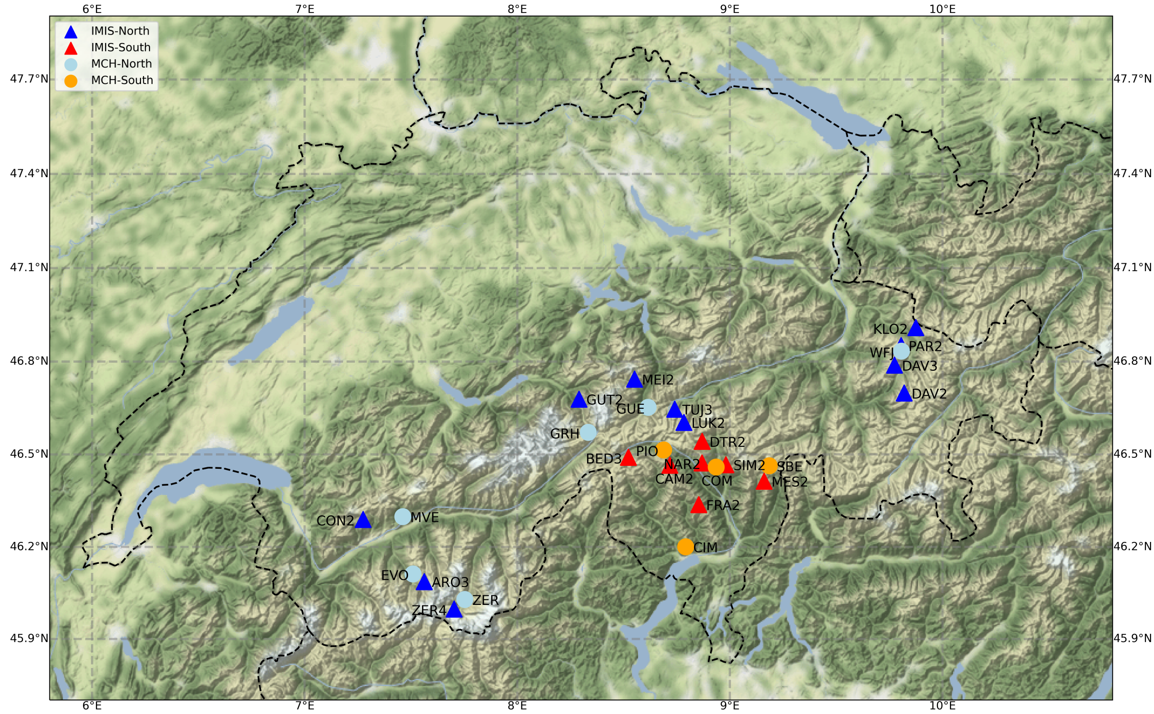

Figure 17: Localisation of IMIS (triangles, blue for the norther side, red for southern side) and MeteoSwiss (circles, light-blue for the northern side, red for the southern side) stations on the Swiss territory

2.1.2 Climate models data: EURO-CORDEX data

EURO-CORDEX is the European branch of the International Coordinated Regional Climate Downscaling Experiment (CORDEX), which is a program sponsored by the World Climate Research Program (WRCP) to organize an internationally coordinated framework to produce improved regional climate change projections for all land regions world-wide. The EUR-44 realisation, used in this study, provides gridded data with a resolution of $\sim 49km \times 49km$ ($0.44° \times 0.44°$) which represents the Alpine orography only in a coarse level.

Climate model data are available for three future greenhouse gas emissions scenarios, RCPs: RCP2.6, RCP4.5 and RCP8.5. However, in this study, only RCP2.6 and RCP8.5 are taken into account as RCP4.5 falls in between the other two. For each RCP scenario, a varying number of transient regional climate scenarios models are available for the set of variables visible in Table 5.

EURO-44 VARIABLES		
Variable Name	**Standard Name**	**Units**
evspsbl	water evaporation flux	kg m-2 s-1
hurs	Relative humidity	%
huss	Specific humidity	1
mrro	Surface runoff flux	kg m-2 s-1
mrso	Soil moisture content	kg m-2
orog	surface altitude	m
pr	Precipitation	kg m-2 s-1
rsds	Surface Downwelling Shortwave Radiation	W m-2
sfcWind	Near-Surface Wind Speed	m s-1
sfcWindmax	Daily Maximum Near-Surface Wind Speed	m s-1
sftlf	Land Area Fraction	%
snw	Surface Snow Amount	kg m-2
tas	Air Temperature near surface, at 2 m	K
tasmax	Daily Maximum Air Temperature	K
tasmin	Daily Maximum Air Temperature	K
uas	Eastward Wind at 10 m	m s-1
vas	Northward Wind at 10 m	m s-1

Table 5: Variables available in EUR-44

The transiet regional climate scenarios are the combination of Global and Regional Climate Models (GCMs, RCMs): GCMs provide boundary conditions data to RCMs. The ones considered in the present study are the following (RCM+GCM):

- KNMI-RACMO22E + MOHC-HadGEM2-ES
- SMHI-RCA4 + ICHEC-EC-EARTH
- SMHI-RCA4 + MIROC-MIROC5
- SMHI-RCA4 + MOHC-HadGEM2-ES
- SMHI-RCA4 + MPI-M-MPI-ESM-LR
- SMHI-RCA4 + NCC-NorESM1-M

The choice fell on these six models as they were the ones providing all the needed variables to then run SNOWPACK simulations, as explained in Section 2.2. It is important to note that the RCM is the same for 5 of the 6 transient regional models, while the GCM varies.

As EURO-CORDEX data comes in the form of *NetCDF* files covering the whole European territory, a grid point extraction had to be run to obtain the values at the IMIS stations locations. The procedure is further explained in Section 3.5.

EURO-CORDEX data is publicly available via the nodes of the Earth System Grid Federation[46] and the Copernicus Climate Data Store [47], however, for this study the elaboration used by MeteoSwiss in the recent CH2018 report was used [17].

2.2 SNOWPACK software

SNOWPACK is a one dimensional, physically-based, numerical model that uses the finite-element method to solve the partial differential equations related to the mass and energy conservation within snowpacks [36]. Snow is modelled as a three-component (air, water, ice) porous material whose behaviour is governed by temperature equations (energy conservation), vapour diffusion equations (mass conservation of air phase), water transport equations (mass conservation of water phase), and settlement equations (momentum conservation) [36]. Phase changes between the components are simulated assuming that each layer is described by the sum of the volumetric fraction of each component, and the mechanical and thermodynamical properties depend on the snow microstructure [36].

To run a simulation on SNOWPACK, several informations are required and, according to their nature, they are contained within different input files (Figure 18) [48]:

- .smet file (Meteo input)
- .ini file (INI input)
- .sno file (SNO input)

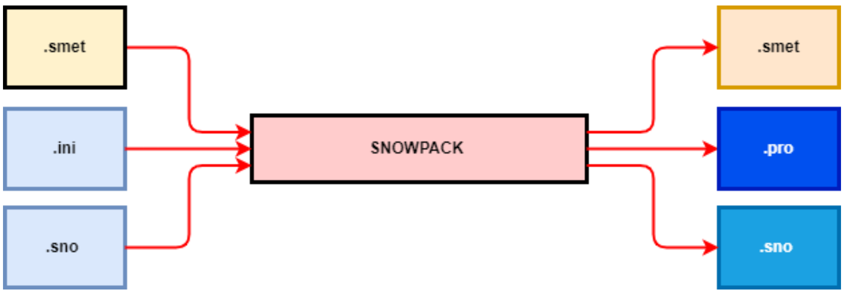

Figure 18: input and output files in a SNOWPACK simulation

The .smet file contains the input data:

- the description of the place where the snowpack has to be simulated: latitude, longitude, elevation, slope
- the time series of the various meteorological parameters. At least:
  - Air Temperature (TA)
  - Relative Humidity (RH)
  - Wind speed (VW)
  - Incoming Short-Wave Radiation (ISWR) and/or Reflected Short-Wave Radiation (RSWR) or net short wave radiation
  - Incoming Long-Wave Radiation (ILWR) and/or Snow Surface Temperature (TSS)
  - Precipitation (PSUM) and/or Snow Height (HS)

In case ILWR or ISWR are not provided, as in the first simulation run in this study (see Section 3.2.2), SNOWPACK has to rely on alternative pathways to reconstruct the missing variable. If ISWR is not provided, SNOWPACK parameterises the albedo of the snowpack and back calculates the ISWR from the RSWR. The albedo parameterisation, based on the data from an albedo research-campaign carried out in Weissfluhjoch by SLF, follows the changes in reflectivity by varying its value according to the aging of the snow and to the presence of soil once there is no longer snow on the ground.

The .ini file contains the setting for the simulation and the model parameters: filters, interpolations and advanced parameters. Two important settings for a simulations, which highly affect the output, are:

- ENFORCED MEASURED SNOW HEIGHT
- CHANGE BC

Both settings can be either set to TRUE or FALSE.

ENFORCED MEASURED SNOW HEIGHT, if set to TRUE, forces the simulation to run on the input values of snow height, if set to FALSE, forces the simulation to run with the precipitation data. In the former case, the computation of snow precipitation rate in SNOWPACK is based on the determination of the amount of new snow that falls during every snowfall event. Such value is defined as the difference between the measured snow height and the snow height modelled in case of no snowfall event. To avoid biases, this process is allowed only if both Relative Humidity (RH) shows values larger than 50%, the difference in Air and Snow Surface temperature (TA,TSS) is lower than 3°C [49]. The fact that the modelled snow precipitation rate is linked with the snowpack height explains the existing relation in SNOWPACK between radiative fluxes and the newly snow precipitation evaluation: as radiative fluxes influence the energy balance of the snowpack, they also influence the melting rate and consequently the height. In the second case, instead,from the precipitation rate [$\mathrm{mm\,h^{-1}}$] the snowpack height [m] is back calculated on an hourly resolution taking into account density parameterisations and compaction processes.

To solve the energy balance and settlement equations, SNOWPACK model requires either the temperature measured at the snowpack surface, called Dirichlet boundary conditions, or the radiative components to establish the energy fluxes, Von Neumann boundary condition. The setting CHANGE BC defines which of the conditions have to be applied in the simulation. In case it is set to TRUE, if $T <$ -1 °C, the snow-cover surface temperature equals the measured temperature, otherwise it is estimated computing energy fluxes which require the use of ILWR and ISWR. If set to FALSE, only energy fluxes are taken into account.

The .sno file specifies the initial state of the various soil and snow layers.

As output SNOWPACK provides three main files (Figure 18):

- .smet file: contains the data of the simulations in terms of 1D variables and fluxes such as measured snow height, modelled snow height, air temperature, relative humidity, latent heat, sensible heat, etc.
- .pro file: it contains the evolution of the state of the snowpack in time in terms of inner variables providing information also on the micro-structure
- .sno file: it is a copy of the input .ini file

Some default parameterisation may change from version to version of SNOWPACK, in this study September 2020 version was applied.

3 Data Preparation

In this section, the steps necessary to obtain a suitable input dataset for a SNOWPACK run that would produce the evolution of the snowpack from 1971 to 2099 at each station are described. Every station must have its own dataset with 3 characteristics:

1. it has to contain the meteorological variables of TA, RH, VW, ISWR, PSUM at the station (Section 3.2).

2. it has to to include the climate change signal from 1971 to 2099 at the stationc(Section 3.6)

3. it has to have hourly resolution (Section 3.7)

Figure 19 shows the steps, or processes, (green boxes) necessary to achieve the above mentioned requirements and the relative inputs and outputs (yellow boxes). Each process is further explained in the following subsection of this chapter. For clarity sake, the author decided to describe methods and results of the steps in consecutive sections, as the output of one step and the relative considerations were often necessary for subsequent task.

The Data Preparation (current Section) and the Data Analysis (Section 4) were mostly conducted thanks to the use of the language for statistical computing and graphics, R [50].

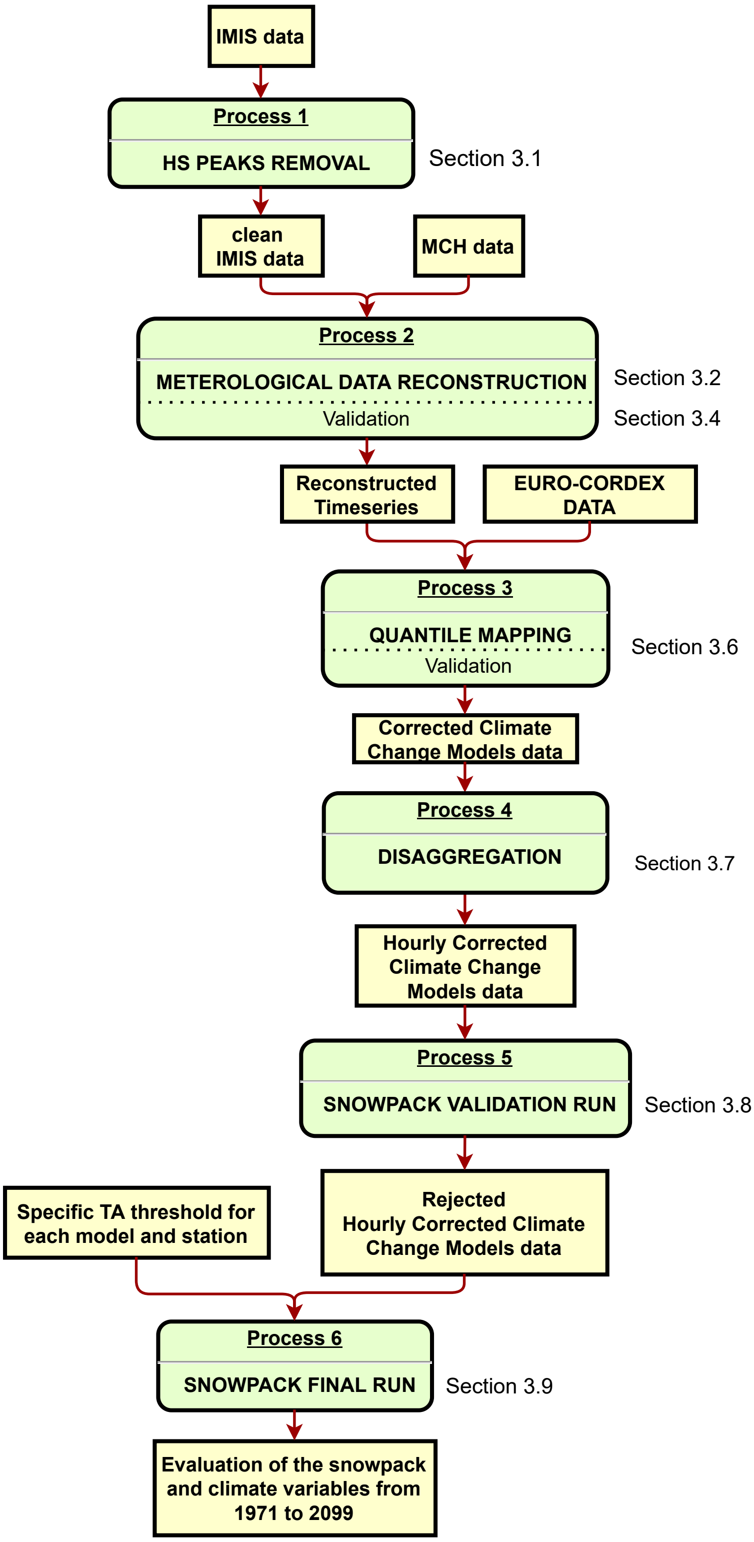

Figure 19: work flow of the data preparation

3.1 Data Cleaning: peaks and gaps removal

It is not unusual to find outliers, inexplicable fluctuations, or missing values within measurement data. IMIS datasets were not an exception. Cleaning the values was necessary because outliers and gaps strongly affect the snowpack modelling, resulting in unreliable outcomes or in the inability of SNOWPACK to proceed in the modelling. SNOWPACK, to avoid such interference, relays on filtering processes to remove outliers and generator processes to compute reliable values in case of missing values. For what concerns gaps, SNOWPACK is able to fill gaps if they are smaller than a set number of seconds, in this case, it was set to 12 hours (43200 seconds). To do so interpolations techniques are applied to all the points falling within the gap.

For what concerns peaks a clean input dataset was wanted and thus an *a priori* cleaning and detection was carried out.

The detection of peaks was carried out only on the HS variable by setting a maximum variation threshold of $\Delta = 50\,\text{cm}$ between two consecutive values of the HS timeseries. "NaN" values (Not a Number values) were turned into peaks and treated analogously. The cleaning was carried out by substituting each unwanted value with the mean between the previous HS value and the first subsequent meaningful HS value. In case of multiple consequent unwanted values, the same mean value was assigned to each of them.

3.2 Meteorological data reconstruction

This first step consists in reconstructing a meteorological dataset at every IMIS station so that, beside the meteorological variables directly measured in such locations (Table 1), this dataset could also include Precipitation (PSUM) and Incoming Short-Wave Radiation (ISWR). The need of reconstructing a meteorological dataset for each IMIS station roots in two facts:

- IMIS stations measure Snow Height (HS) and Outgoing Short-Wave Radiation (OSWR) which are scarcely reliable in climate models data as they computed thanks to parametrisation at large scale while at small scale they are the result of multiple processes (e.g. compaction) and feedbacks (e.g. albedo) which are hard to predict and control. Climate models include PSUM and ISWR.
- SNOWPACK requires a meteorological input dataset including either ISWR or RSWR, and either PSUM or HS.

In Figure 20 the work flow to reconstruct and validate a new, but reliable, meteorological dataset is reported. The flow is subdivided into two steps: step 1 is the work necessary to reconstruct the meteorological dataset, step 2 is the work necessary to validate the dataset and ensure its applicability. Processes are represented as green boxes, outputs and inputs of the processes are shown in orange and yellow respectively. If an output is used as it is as input, the box stays orange. SNOWPACK simulations are visualised as red boxes, and the .ini file they required in blue. The latter report the applied settings for energy fluxes (MEAS TSS and CHANGE BC), short wave radiation (SW MODE), and forcing variable (ENFORCE MEASURED SNOW HEIGHT). Within each step several processes are reported: Process 1 is the peak removal on HS (Section 3.1), Process 2, subdivided in a (Section 3.2.3), b (Section 3.2.2), c(Section 3.2.2), d, are the processes to reconstruct ISWR and PSUM, Process 3 (Section 3.4) is the validation, Process 4 is the check on the boundary conditions set on SNOWPACK (Section 3.4.

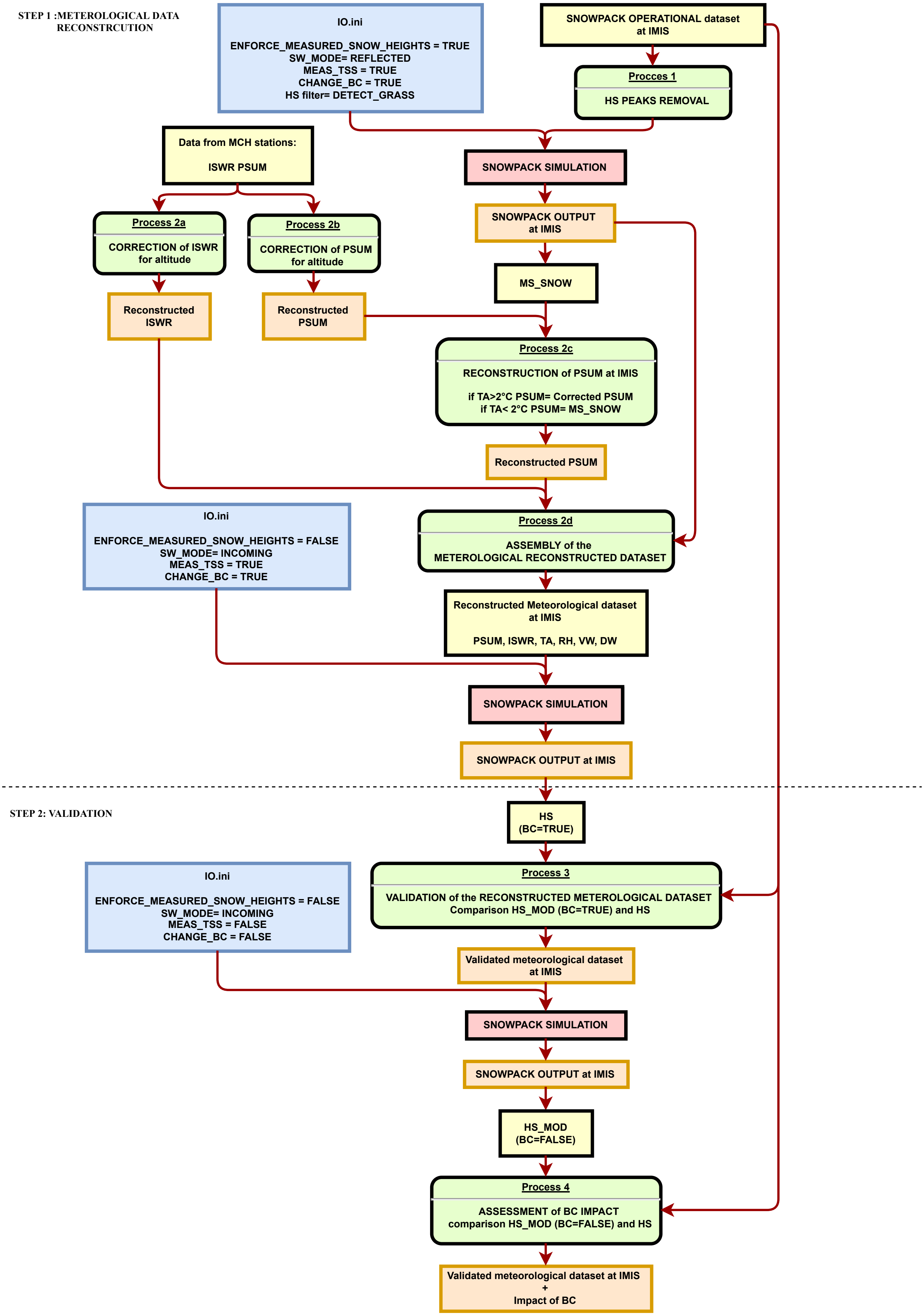

Figure 20: work flow for meteorological data reconstruction

3.2.1 Matching of MeteoSwiss and IMIS stations

As further explained in Section 3.2.2 and Section 3.2.3, in order to reconstruct precipitation and radiations at IMIS stations, a coupling between the latter and MCH stations was required. MCH data was, indeed, used as starting point for the data reconstruction at IMIS stations.

The coupling of the stations required a few steps: MCH stations which are known to be frequently hit by avalanches, were a priori discarded, as well as those which have timeseries shorter than 15 years. The final coupling process was driven by selecting the closest MCH station in crow-fly distance to the relative IMIS station. In Table 6 the definitive couples of IMIS and MCH stations are reported.

SOUTHERN ALPS					
IMIS			**MCH**		
ID	**Name**	**Altitude [m.a.s.l.]**	**ID**	**Name**	**Altitude [m.a.s.l.]**
BED3	Cassinello	2101	PIO	Piotta	990
CAM2	Fontane	2216	PIO	Piotta	990
DTR2	Preda	2057	PIO	Piotta	990
FRA2	Efra	2100	CIM	Cimetta	1661
MES2	Pian Grand	2384	SBE	S. Bernardino	1638
NAR2	Bassa di Nara	2077	COM	Acquarossa/Comprovasco	575
SIM2	Piano del Simano	2450	COM	Acquarossa/Comprovasco	575
NORTHERN ALPS					
IMIS			**MCH**		
ID	**Name**	**Altitude [m.a.s.l.]**	**ID**	**Name**	**Altitude [m.a.s.l.]**
ARO3	Arolla:Breona	2602	EVO	Evolène	1825
CON2	Conthey:Etang de Trente Pas	2229	MVE	Montana	1422
DAV2	Davos:Baerentaelli	2558	WFJ	Weissflujoch	2691
DAV3	Davos:Hanengretji	2455	WFJ	Weissflujoch	2691
GUT2	Guttannen:Homad	2115	GRH	Grimel Hospiz	1980
KLO2	Klosters:Madrisa	2147	WFJ	Weissflujoch	2691
LUK2	Lukmanier:Lai_Verd	2555	GUE	Gütsch, Andermatt	2286
MEI2	Meiental:Laucheren	2220	GUE	Gütsch, Andermatt	2286
PAR2	Parsenn:Kreuzweg	2290	WFJ	Weissflujoch	2691
TUJ3	Tujetsch:Nual	2211	GUE	Gütsch, Andermatt	2286
ZER4	Zermatt:Alp_Hermetje	2408	ZER	Zermatt	1638

Table 6: Matched IMIS and MeteoSwiss(MCH) statios

3.2.2 Precipitation reconstruction

The aim of the precipitation reconstruction process was to obtain a reliable timeseries of precipitation data for the whole calibration period (2006-2019) at every IMIS station. SNOWPACK software can be used to back compute, from the evolution of the measured HS, the snow precipitation (*MS*

SNOW) that, in time, generates such snowpack (step 1 in Figure 20). This process is reliable during the accumulation period, period during which the snowpack builds up, but not as much during the melting period in which rain precipitation play an important role. This is due to the fact that, not providing measured ILWR, SNOWPACK reconstructs it thanks to parameterisations that use RH, TA, ISWR in the process [51]. Generally, the Net Short-Wave Radiation (NSWR) is the dominant flux of the energy balance of a snowpack, however, Net Long-Wave Radiation (NLWR) is often the kickstarter of early spring melting and is highly relevant in alpine terrains as the surrounding topography can be an additional source [52]. Studies on SNOWPACK sensitivity to missing radiative forcings show how the reconstruction of ILWR results in an overestimation during melting period and thus in a faster melt [43]. In cascade, this results in a larger amount of modelled precipitation as more snow precipitation is required to match the measured snow height. In fact, the computation of snow precipitation rate in SNOWPACK is based on the determination of the amount of new snow that falls during every snowfall event. Such value is defined as the difference between the measured snow height and the snow height modelled in case of no snowfall event. The fact that the modelled snow precipitation rate is linked with the snowpack height explains the existing relation in SNOWPACK between radiative fluxes and the newly snow precipitation evaluation: as radiative fluxes influence the energy balance of the snowpack, they also influence the melting rate and consequently the height.

Thus, for the melting and summer periods, alternative ways to reconstruct the precipitation had to be considered. To do so, this study considered the precipitation recorded at the MCH stations. Since precipitation are highly location-dependent, a correction had to be applied so that the precipitation at MCH stations could be transported at IMIS stations locations (Step 1, Process 2b in Figure 20). A previous study of Bender et al [53] used a combination of back calculated solid precipitation from SNOWPACK and multiple linear regression values calculated from the 2 best near-by MCH stations. The decision tree to select the value from one or the other data source for each timestep was based on HS and TA thresholds. In this study an analogous but simpler approach was used: back calculated solid precipitation from SNOWPACK and corrected MCH precipitation were used. The correction of MCH values in order to transport the precipitation values to IMIS shapes in a multiplicative factor called $Ratio\ factor$ (Eq. 1), that has to be applied to the MCH PSUM (Eq.2). It is defined as follows:

$$Ratio factor = \frac{\sum_{t=Start\ acc}^{End\ acc} MS\ SNOW_{IMIS_t}}{\sum_{t=Start\ acc}^{End\ acc} PSUM_{MCH_t}} \tag{1}$$

$$PSUM_{MCH->IMIS} = Ratio\ factor \cdot PSUM_{MCH} \tag{2}$$

where $Start\ acc$ and $End\ acc$ are the starting date and ending date of the accumulation periods, $MS\ SNOW_{IMIS}$ is the solid precipitation computed by SNOWPACK from the evolution of the measured HS in time at IMIS stations, $PSUM_{MCH}$ is the precipitation occurring at MCH stations, cleaned of possible rain events (i.e. $TA_{IMIS} > 1.5°$). The starting and ending dates of the accumulation periods were defined as the day for which the snowpack is going to be stably over 5 *cm* for at least the following 100 days, and the day with the highest HS in a window of 5 days characterised

by the highest sum of HS, respectively.
The correction (Eq.2) assumes that the ratio between the precipitation that falls at IMIS and at MCH stations is constant along the whole year. Such strong assumption is considered not to strongly affect the results of the study as it affects melting and summer periods, which are not the target-periods of this study.

For sake of higher precision, the distinction between MS SNOW data from SNOWPACK and corrected PSUM from MCH stations to build up the new precipitation dataset $PSUM_{IMIS}$, was not based solely on the starting and ending dates of accumulation or melting/summer periods, but rather on the physical conditions required to have snow precipitations (Step 2, Process 4 in Figure 20):

$$PSUM_{IMIS} = \begin{cases} PSUM_{MCH->IMIS} & \text{if } TA_{IMIS} > 2^\circ \\ MS\ SNOW_{IMIS} & \text{if } TA_{IMIS} < 2^\circ \end{cases} \tag{3}$$

3.2.3 Radiation reconstruction

As radiation is attenuated the further it travels in the atmosphere, its magnitude at specific locations depends on the altitude. The study carried out by Marty C. et al. in 2002 [54] on the dependence to altitude of surface radiation fluxes in the Swiss Alps states that annual mean values of global radiation shows an altitude gradient of $\pm 1.3[\mathrm{W\,m^{-2}}]/100[\mathrm{m}]$. Thus, to transport ISWR values from MCH to IMIS stations the following correction was applied (Step 1, Process 2a in Figure 20):

$$ISWR\ Correction = \frac{1.3\ [\mathrm{W\,m^{-2}}] \cdot \Delta Altitude\ [\mathrm{m}]}{100\ [\mathrm{m}]} \tag{4}$$

$$ISWR_{IMIS} = ISWR\ Correction\ +\ ISWR_{MCH} \tag{5}$$

where $\Delta Altitude$ is the difference, with sign, in altitude between an IMIS station and its relative MCH station.

It is important to note that possible differences in exposition and shading between coupled MCH and IMIS stations are not taken into account. This is due to the fact that inhomogeneity in insolation between stations was not faced in reference studies, such as CH2018 [17], either.

3.3 Climate and snow metrics

Climate change effects are traditionally assessed thanks to average values of selected parameters among samples of 30 years, as the natural variability and uncertainties do not allow reliable results for shorter timespans. Thus, a set of parameters, that will be addressed as *Metrics*, had to be defined in order to study and compare the climate change effects in time on the snowpacks and on meteorological variables such as PSUM and TA. Specifically, the snowpack is studied thanks to the Metrics called *Snow Metrics*, the meteorological variables through the *Climate Metrics*. The metrics are used both to study the results (Section 4) and to validate specific steps during the work flow (Section 3.4).

Snow Metrics include: Snow Season Length (SSL), Snow Season Starting date (SSS), Snow Season Ending date (SSE), Mean Snow Height (MHS), 95^{th} quantile of Snow Height (95HS).

SSL is defined as the number of days (at least 100 consecutive days) with at least 5 cm on the ground. The threshold of 100 days allows to avoid taking into account the first snow days in autumn which do not contribute to the building up of the major and continuous snowpack of the season. The threshold on the HS of 5 cm allows to avoid alteration due to possible wrong measurements due to the presence of grass on the ground. SSS and SSE are the first and last days for which the snowpack is continuously above 5 cm, they allow to study whether there will be delays or anticipation in the snow seasons. MHS in case of study of climate effect is defined as the mean snow height along the snow season, thus every year it is evaluated on the extent of the SSL of that year, in case of validation, instead, is evaluated on a fixed snow season length of the reference data. 95HS is used in place of the maximum snow height as it is more representative than detecting a peak in HS which might be an anomaly.

Climate metrics include: Mean Monthly Air Temperature (MMTA), Monthly number of Days with Air Temperature Above 0°C (MDTAA0), and Monthly Precipitation (MPSUM).

MMTA allows to understand whether there will be changes in TA and if there will be, which months are going to be the most affected ones. MDTAA0 lets understand how many days the snowpack might melt for for each month. MPSUM is the amount of cumulative precipitation fallen each month, taking into account both liquid and solid precipitation. It is used to study the possible changes in precipitation distribution along the whole year.

A sum up of the used Climate and Snow Metrics is shown in Table 7.

Snow Metrics	
SSL	Snow Season Length: number of consecutive days for which snowpack height>5cm
SSS	Snow Season Starting date: first day of the snow season
SSE	Snow Season Ending date: last day of the snow season
MHS	Mean Snow Height: mean snow height throughout SSL
95HS	95 quantile of Snow Height: value of Snow Height that computed as the 95^{th} quantile of the Snow Height throughout the SSL
Climate Metrics	
MMTA	Mean Monthly Air Temperature
MDTAA0	Monthly number of Days with Air Temperature Above 0: number of days per month that show a mean air temperature above 0°C
MPSUM	Monthly Precipitation

Table 7: Climate and Snow Metrics

3.4 Validation of Meteorological data and assessment of SNOWPACK boundary conditions effects

Once having built up a complete dataset of meterological variables two checks had to be run: check the reliability of the dataset itself, thus the reliability of the reconstructed PSUM and ISWR, and check the effects of the boundary conditions that will have to be imposed in SNOWPACK runs forced with Climate Change models data.

3.4.1 Method

In order to assess the reliability of the processes of Precipitation and Radiation reconstruction illustrated in Section 3.2.2 and Section 3.2.3, a validation had to be carried out. To do so, a SNOWPACK simulation was launched imposing:

- Forcing meteorological variables = PSUM (ENFORCED MEASURED SNOW HEIGHT = FALSE) and ISWR (SW MODE = INCOMING),
- Energy balance boundary conditions = using measured snow surface temperature if T < -1°C and computed energy fluxes otherwise (CHANGE BC = TRUE)

The HS computed as output of such SNOWPACK simulation had to be compared with the measured HS at the IMIS stations (Step 3, Process 6 in Figure 20). As Snow Metrics (Section 3.3) play the major role in this study, to better assess the reliability of the reconstruction process, they were applied to both the HS datasets. The results are visible in the following Section 3.4.2.

Since climate change models do not provide Snow Surface Temperature and Ground Heat Fluxes as they are too complex to be modelled, SNOWPACK, for Climate Change scenarios, can not be run with CHANGE BC=TRUE. This implies that a CHANGE BC=FALSE setting has to be applied, varying the energy balance of the snowpack and thus, the melting and compaction processes. The difference in output due to the change in boundary conditions have to assessed to be aware of its extent and was carried out thanks to the application of the Metrices to HS modelled forcing with PSUM, ISWR and imposing CHANGE BC=FALSE. The results are visible in the following Section 3.4.2.

3.4.2 Results

In Figure 21 the monthly mean HS for three datasets is shown: Measured HS in orange, HS obtained by forcing SNOWPACK simulation with PSUM and ISWR, and allowing or not the change in boundary conditions in red and blue, respectively. It is visible how using the reconstructed PSUM and SNOWPACK introduces a bias in the evolution of the height of the snowpack with respect to the observations. This bias is larger if the change in energy boundary conditions is not enabled. A quantitative evaluation of mean difference in mean HS and in mean 95HS is reported in Table 8. The use of reconstructed PSUM as input for SNOWPACK results, on average, in an increase of 8 cm in the mean HS and of 5 cm in the 95HS. Disabling the energy fluxes and the change in boundary conditions, instead, causes the mean difference to rise to 24 cm and 37 cm respectively.

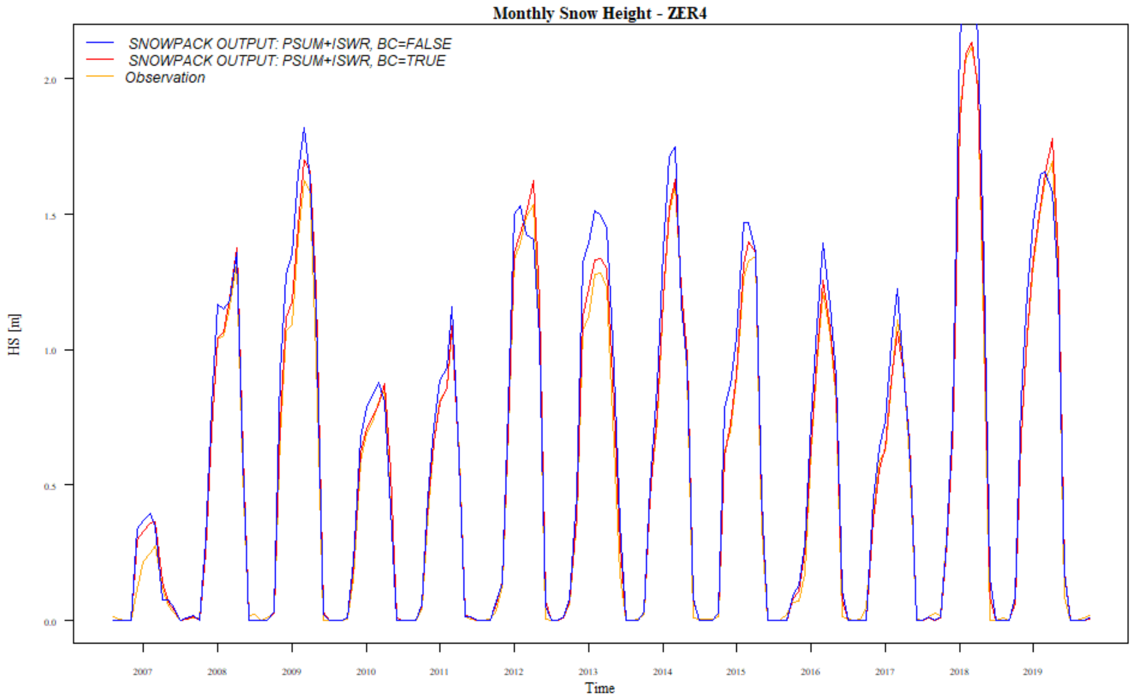

Figure 21: Example of monthly Snow Heights (HS) at the IMIS station ZER4 for different datasets: Measured HS (Orange), reconstructed HS with a SNOWPACK simulation forced with reconstructed PSUM, reconstructed ISWR and CHANGE BC=FALSE (Blue), and reconstructed HS with a SNOWPACK simulation forced with reconstructed PSUM, reconstructed ISWR and CHANGE BC=TRUE (Red)

Mean Metrics Statistics		
Metrics	**BC=TRUE**	**BC=FALSE**
SSL [days]	23	27
SSS [days]	-12	-12
SSE [days]	9	10
MHS [cm]	8	24
95HS [cm]	5	37

Table 8: Mean of differences in Metrics values of SNOWPACK forced with CHANGE BC=TRUE and CHANGE BC=FALSE with respect to the Metrics on the Observations

In Figure 21, due to the monthly average applied for visual clarity, the difference at the beginning and ending of the snow season which affect the values of Metrics SSL, SSS, and SSE is not visible. To better visualise the difference, violin plots were considered: Figure 23 reports an example for the IMIS Station ZER4. A mean evaluation of the difference in the mentioned Metrics showed how enabling or not the change in boundary conditions does not highly affect the effect that using PSUM as forcing meteorological variable already has. The mean difference in SSL is, in fact, +23 and +27 days respectively. This increase is both due to an earlier beginning of the season (-12 days in both cases) as well as a later ending (+9 and +10 days).

Thus, the reconstruction of PUSM and ISWR can be considered reliable as the evolution of the snowpack in terms of HS varies of $\sim 3\%$.

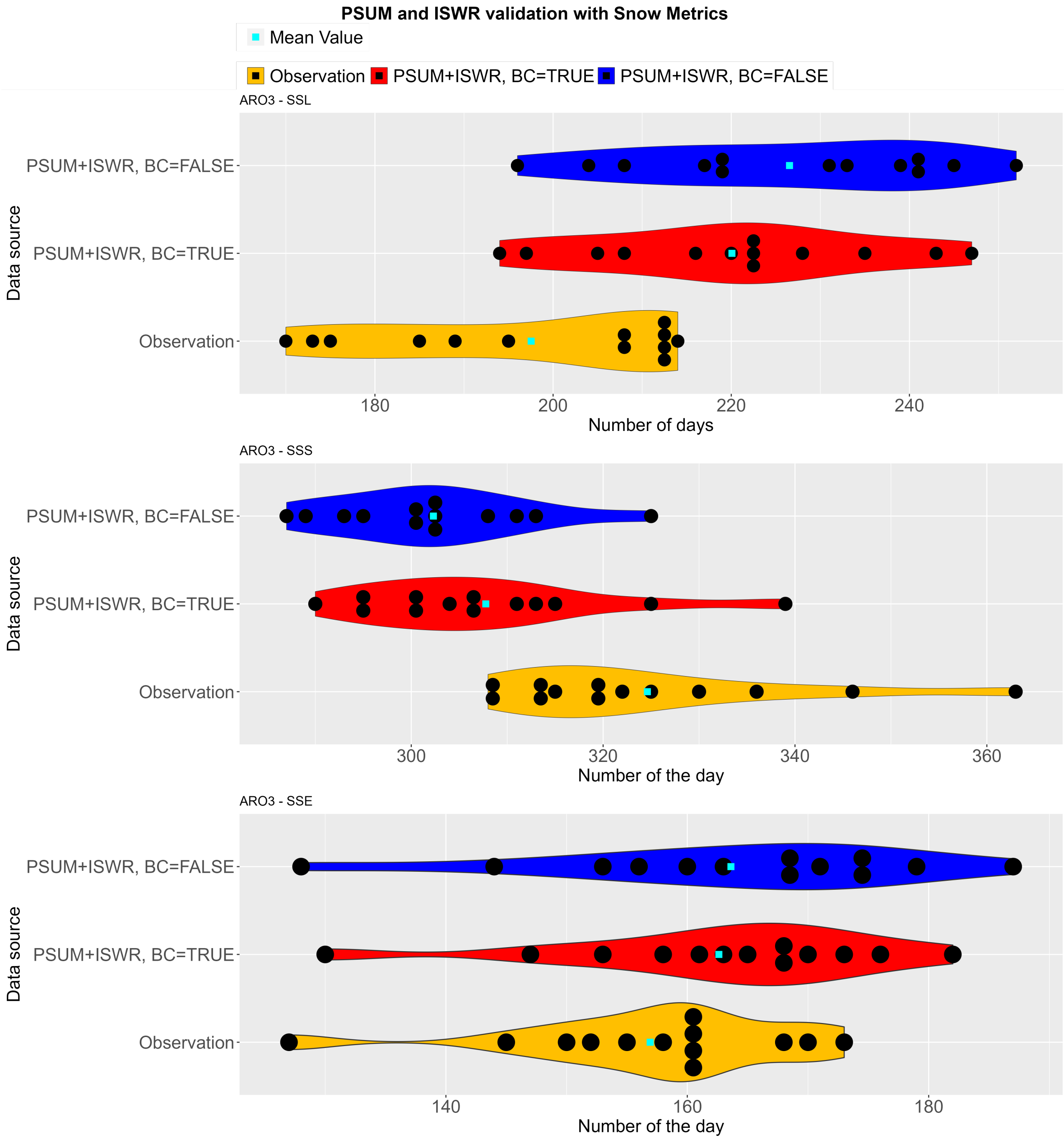

Figure 22: Comparison in Snow Metrics SSL,SSS and SSE between Measured HS (Orange), reconstructed HS with a SNOWPACK simulation forced with reconstructed PSUM, reconstructed ISWR and CHANGE BC=FALSE (Blue), and reconstructed HS with a SNOWPACK simulation forced with reconstructed PSUM, reconstructed ISWR and CHANGE BC=TRUE (Red).

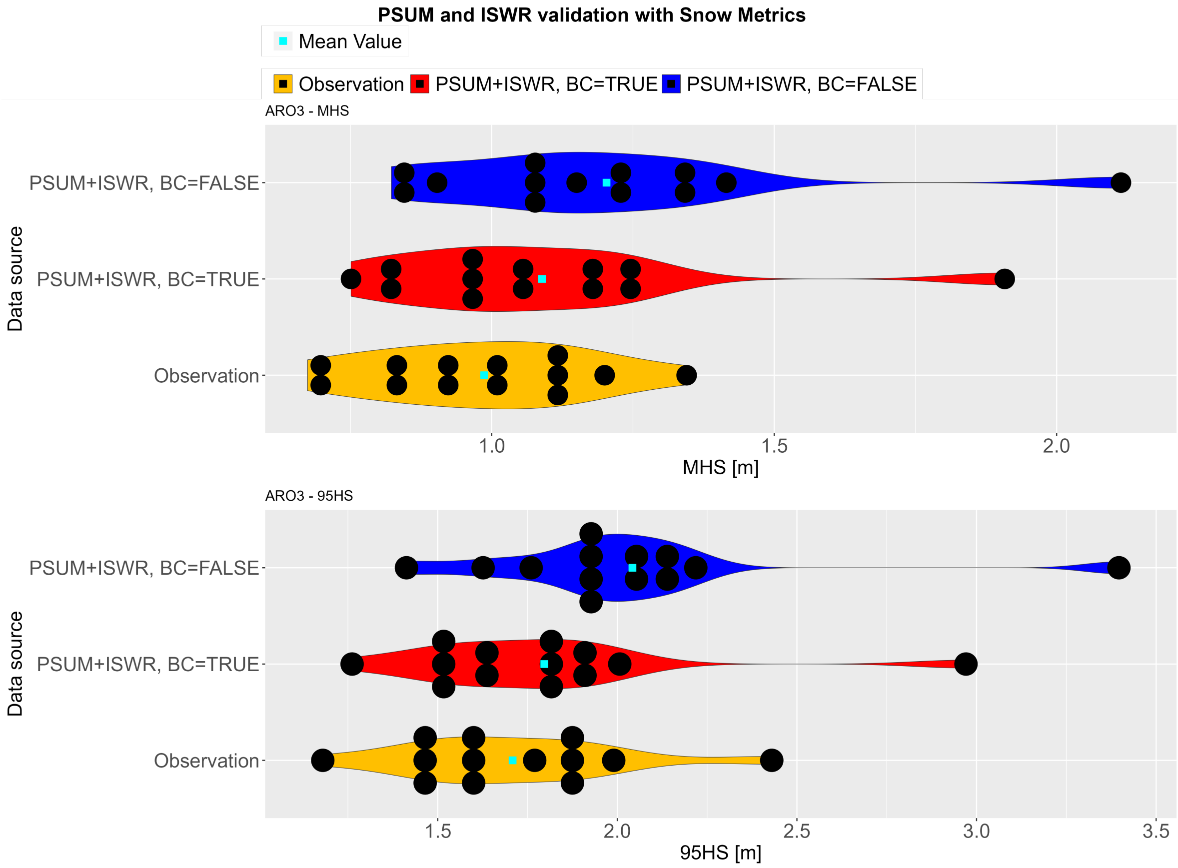

Figure 23: Comparison in Snow Metrics MHS, 95HS between Measured HS (Orange), reconstructed HS with a SNOWPACK simulation forced with reconstructed PSUM, reconstructed ISWR and CHANGE BC=FALSE (Blue), and reconstructed HS with a SNOWPACK simulation forced with reconstructed PSUM, reconstructed ISWR and CHANGE BC=TRUE (Red).

3.5 EURO-CORDEX data extraction and homogenisation

In this section it is explained how the Climate Change data were obtained and the preliminary manipulation to homogenised them is described.

3.5.1 Method

EURO-CORDEX data come in the form of *NetCDF* files: gridded data covering the whole European territory extension. Variables values are stored as function of their localisation (latitude and longitude) and time. To gather the whole set of needed variables (TA, TA_{max}, TA_{min}, PSUM, VW, ISWR, RH) at the wanted location and time-span, it was necessary to pick out the necessary grid points. Such points, or, as will be here called, *pixels*, are defined as the closest grid points to the considered IMIS stations in terms of latitude and longitude, taking into account the center of the pixel and the geolocalisation of the stations. Thanks to the use of Swiss National Supercomputing Centre (CSCS), operating in *Linux* [55], the manipulation of such a large amount of data was possible on *Piz Daint* node.

Regional climate models can be based on several different calendars: 360-days, 365-days, Gregorian, Proleptic-Gregorian. 360-days datasets are characterized by 12 equally long months (30 days). Thus, the homogenization to a Gregorian calendar required both the artificial insertion of missing days and the removal of excessive ones. For 365-days datasets, days were added in order to take into account leap years. The variable values for the artificially-made days were defined, in both cases, as the mean of the previous and following day.

3.5.2 Results

Figure 24 shows the localisation of the IMIS stations (blue triangles for IMIS station on the northern side, red triangles for IMIS station on the southern side) and and the respective, extracted EURO-CORDEX pixels. As climate models have a coarse resolution of ∼49 km ×49*km*, several stations are associated to the same pixel.

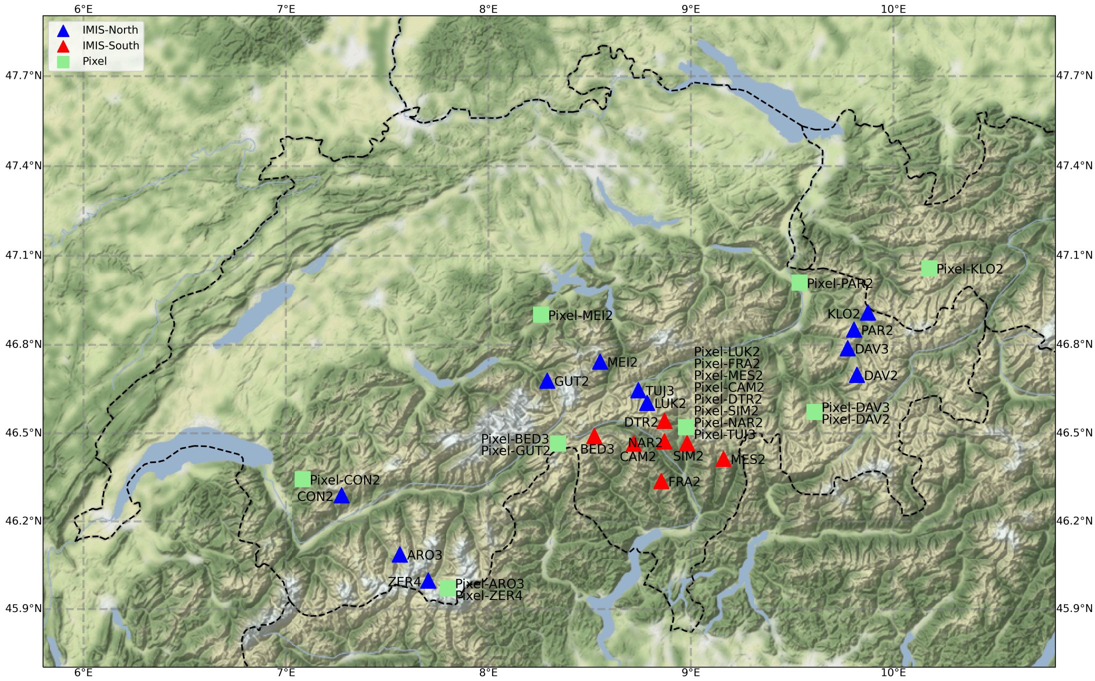

Figure 24: Map of IMIS stations (triangles: northern side in blu, southern side in red) with the respective EURO-CORDEX pixel (square)

3.6 Quantile Mapping

Once the Reconstructed Timeseries is available at each station and climate change models data is extracted for every necessary pixel, a downscaling of the climate change signal from the pixel scale down to the station scale has to be run. This allows to obtain a dataset of meteorological data from 1971-2099 carrying the Climate Change signal at the station.

To do so, in this study, the process of uni-variate Quantile Mapping is used. As mentioned in Section 1.2.4, QM is bias-correction method which corrects statistical biases in the data, but, since it is corrected to match the statistics of Reconstructed Timeseries, it implicitly results in a downscaling to the station. It is important to note that, being an uni-variate method, each meteorological variable is separately treated.

3.6.1 Method

The QM applied on EURO-CORDEX data was run thanks to the implementation of QM method, *qmCH2018*, available in *R - Software Environment for Statistical Computing and Graphics*. This R package was developed at ETH Zurich and MeteoSwiss and was used within the framework of the CH2018 Swiss Climate Change Scenarios project [34].

The implementation is based on the *Empirical Quantile Mapping* approach as previous works by Themeßl at al. showed how using constructed empirical cumulative distribution functions (*ecdf*) [56] is generally applicable to all possible meteorological parameters. Every raw climate model timeseries X of a meterological parameter at the day of the year (DOY), at time *t* and location *s* is corrected to a timeseries Y according to the *ecdf* of the observations (*obs*) and climate model timseries (*mod*) during the calibration period (*cal*) taking into account the following equation:

$$Y_{t,s} = ecdf_{DOY,s}^{obs,cal^{-1}}[ecdf_{DOY,s}^{mod,cal}X_{t,s}] \tag{6}$$

Thus, the corrected value $Y_{t,s}$ corresponds to the observed value with the same quantile in the observed distribution. The transformation is achieved by applying a *correction function g* to the modelled value $X_{t,s}$ [17]:

$$Y_{t,s} = X_{t,s} + g(X_{t,s}) \tag{7}$$

where g, for a quantile p_i, is defined as:

$$g(p_i) = ecdf_{DOY,s}^{obs,cal^{-1}}[ecdf_{DOY,s}^{mod,cal}(p_i)] - p_i \; with \; i \in [1,99] \tag{8}$$

Values of $X_{t,s} > p_{99}$ or $X_{t,s} < p_1$ are corrected as if thery were $X_{t,s} = p_{99}$ or $X_{t,s} = p_1$, respectively.

g is defined for each day of the year using a 91-day moving window centered on the day of interest in order to have more available values to define the *ecdf*.

To be used, the *qmCH2018* toolbox requires:

- Daily climate model data: in this case the EURO-CORDEX data extracted at the station locations
- Daily observational data: dataset obtained from the hourly Reconstructed Timeseries. According to the variable the daily observational data were computed differently: daily mean value for temperature, solar radiations, relative humidity and wind speed, sum along the whole day for precipitations.
- Definition of *calibration period*: it is subjected to the necessity of complete calendar-years, thus, it was defined as the time span from 2006-01-01 to 2019-12-31.

3.6.2 Results

The process of QM, as seen in Section 3.6, results in a bias-correction of the mean of the values to the observational one. Thus, the validation of the QM process consists in verifying whether this happened. As the study is focused on snow precipitation, it is also important to investigate whether the precipitation of the *Corrected Climate Change Models data* and Reconstructed Timeseries cumulate analogously. It is, however, important to remember that QM is not able to transform raw climate models data so that their values correspond one to one to the observations (Section 3.6), thus, a perfect match between the variables will not be found, but rather a close trend. In Figure 25 an example of QM efficiency for one model chain for ARO3 station is reported. It is qualitatively visible how QM process brought the raw Climate Change Models data (Before QM, in black) closer to the Reconstructed Timeseries values (in blue) : Climate Change Models after QM (in orange) share the same trend and range of variability with the Reconstructed Timeseries. Furthermore, the lines showing the cumulative precipitation over the whole calibration period (bottom-right graph), are very close.

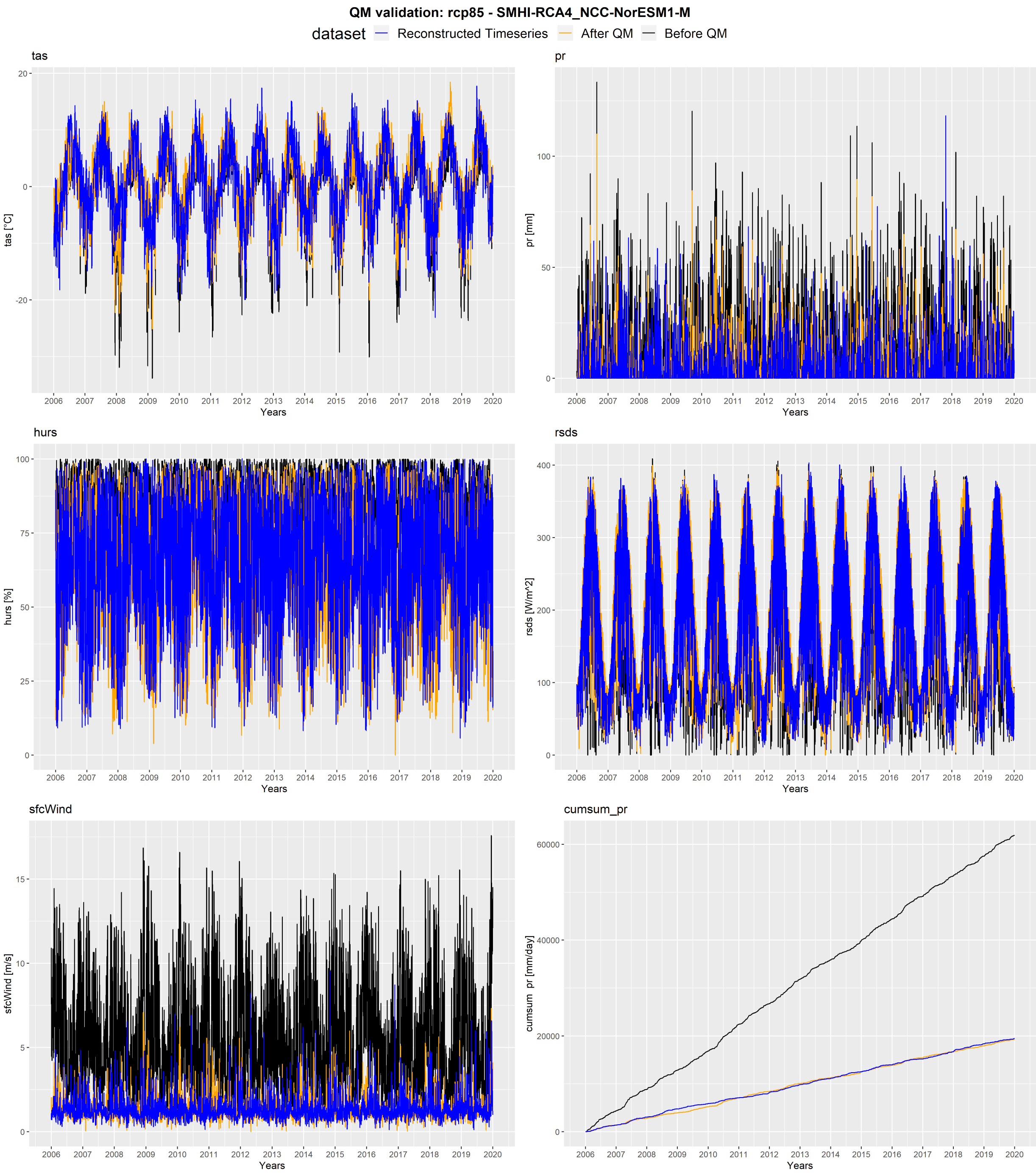

Figure 25: Comparison of Reconstructed Timeseries data (blue), Climate Models data before and after undergoing Quantile Mapping (black and orange respectively). In reading order: air temperature (tas), precipitation (pr), relative himidity (hurs), solar radiation (rsds), wind speed (sfcWind), cumulative precipitation over the whole calibration period (cumsum$_p$r.

3.7 Disaggregation: Temporal downscaling from daily to hourly time-steps

The disaggregation of Corrected Climate Model data from daily to hourly is necessary to meet SNOWPACK requirements on the input data format (Section 2.2). To do so, a toolbox written in *Python* scripting language [57] was used. The applied MEteoroLOgical observation time series DISaggregation Tool, MELODIST [58], is a open-source toolbox that consists of several disaggregation functions for each meteorological variable. Every disaggregation functions provides the possibility to specify the method to use, among a pool of available methods.

To choose the best disaggregation function setting for each variable, every method was tested on Reconstructed Timeseries data: firstly hourly data from Reconstructed Timeseries were merged into daily ones (mean value for TA, RH, VW, ISWR, sum for PSUM), secondly all the disaggregation functions were applied to these daily values, thirdly disaggregated hourly values were compared with the hourly Reconstructed Timeseries values. Thanks to statistical metrics (mean, R^2, root mean square error (RMSE)) the goodness of each disaggregation function could be evaluated and, thanks to a decision tree, the best disaggregation function could be selected for each meteorological variable. The decision tree followed the following steps:

1. As mean values, for future data analysis, play an important role, the first skimming step was to select the functions which would not alter it.

2. Since R^2 shows how well the Reconstructed Timseries are replicated by the disaggregated values, the functions with higher R^2 were selected among the remaining.

3. As RMSE gives how much the obtained values (disaggregated value) vary around the predictions (Reconstructed Timeseries), the function with minor RMSE was selected among the functions remaining from step (2)

The adopted methods are:

- Temperature: Mean course mean
- Relative Humidity: Equal
- Incoming Shortwave radiations: Pot. rad
- Wind Speed: Cosine
- Precipitation: Cascade

3.8 SNOWPACK Validation run

At this stage, the Climate Change Models data that underwent Quantile Mapping (Section 3.6.1) and, subsequently, disaggregation (Section 3.7) had to be validated. This dataset is going to be addressed as *Hourly Corrected Climate Change Models data*

3.8.1 Method

To validate the Hourly Corrected Climate Change Models dataset, the HS outputs of a SNOWPACK run forced with Reconstructed Timseries data and one with the Hourly Corrected Climate Change Models data were compared. Specifically, the mean-year HS were compared.

The Mean-year of a variable is defined as the artificial year for which its value, for each day, is computed as the mean value of the values assumed by the variable on that same day but in different years (e.g. the value assumed on the 1^{st} of January for the mean year is the mean of the value assumed in all the $1^{st}s$ of January of the years from 2006 to 2019) (Figure 26).

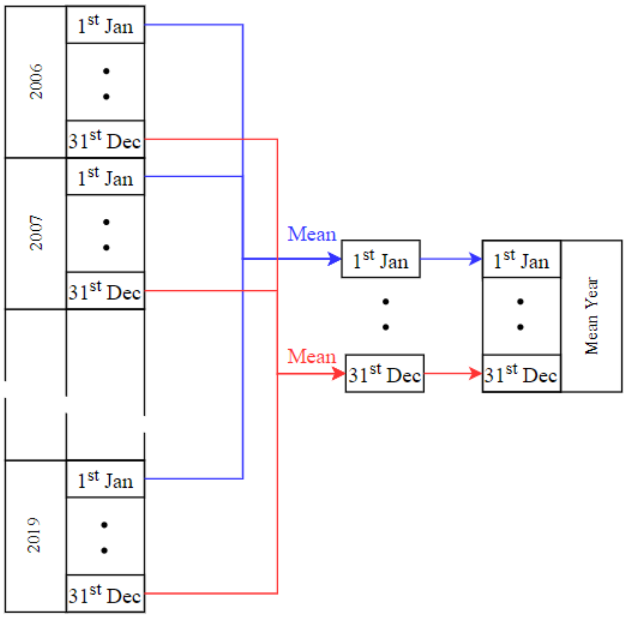

Figure 26: Scheme on how mean-years are constructed from a dataset spanning several years

3.8.2 Results

In order for the Hourly Corrected Climate Change models data to be accepted, the mean-year HS of each model has to be contained within the upper and lower standard deviation of the mean-year HS of the Reconstructed Timeseries. The fulfilment of this conditions ensures both that the Hourly Corrected Climate Change model values are close to the Reconstructed Timeseries one. In Figure 27 an example of the HS comparison is shown for the station BED3, model chain SMHI-RCA4+MIROC-MIROC5. As visible, the mean-year HS of the Hourly Corrected Climate Change model was not compliant with the requirement of the Validation.

The discrepancy shown in HS between the two datasets could both lie in a discrepancy in precipitation as well as wrong air temperatures. A focused investigation highlighted how both temperature and precipitation of Hourly Corrected Climate Change model were consistent with the Reconstructed Timeseries, but the SNOWPACK output of Snow Water Equivalent (SWE) would not build up analogously over any of the snow seasons. Being SWE a parameter that measures the mass of snow (converted in water), it revealed how a much smaller amount of snow would fall in the SNOWPACK output of the Hourly Corrected Climate Change models data with respect to the Reconstructed Timeseries one. SNOWPACK runs the partition of the precipitation in solid and liquid phase thanks to a threshold on TA: for TA>1.2°C precipitation is seen as rain. With a co-analysis of temperature and precipitation a repetitive phenomenon could be spotted: precipitation would occur mainly on warm days and warm hours. This bias is present in the climate models. The process of uni-variate QM applied to Climate Change Models data (Section 3.6.1) allows a bias-correction on the statistics of the data, however, it presents several limitations which might undermine the reliability of the data. One of these limitations lies in the fact that uni-variate QM treats independently each meteorological variable resulting in a possible inconsistency in the inter-variable behaviour [17] that are present in the reality of climate system. In this study, this flaw resulted in the inability of QM to correct the bias present in the models of the occurrence of precipitation on warm days. Since SNOWPACK runs the precipitation partition based on temperature, the occurrence of precipitation on warm days, would result in an incorrect partition of the solid and liquid precipitation in favour of the latter. Section 3.9 illustrates how this issue was solved.

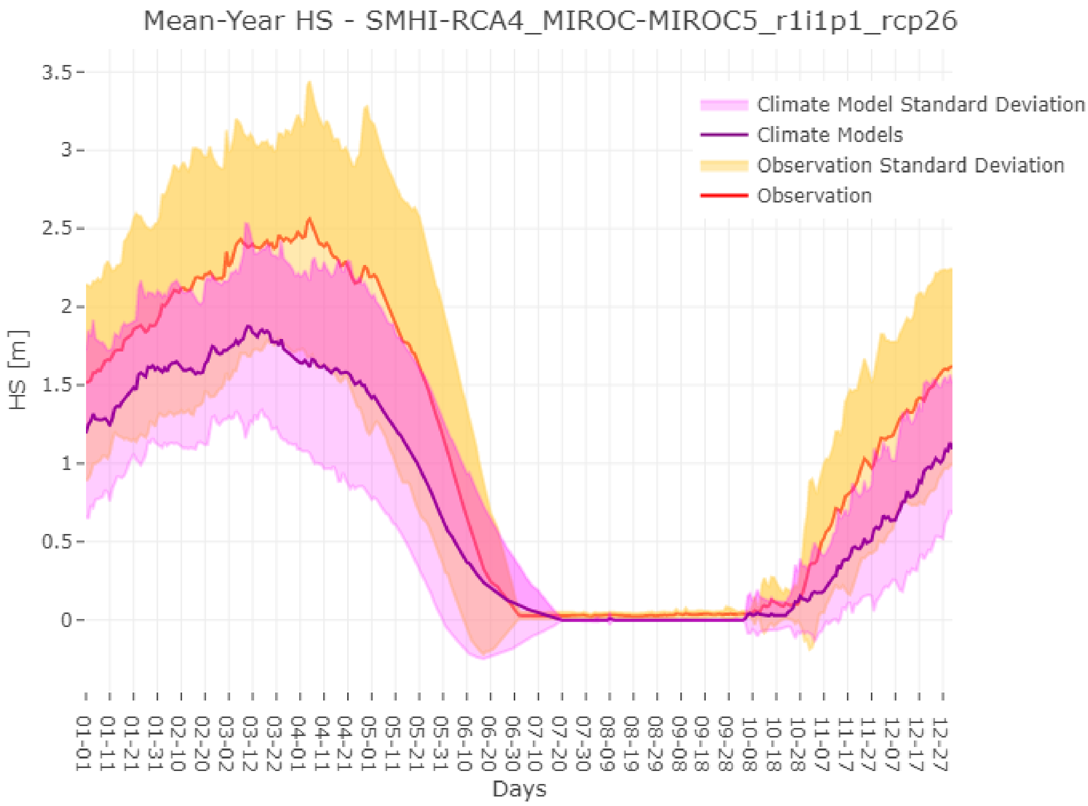

Figure 27: Example of comparison between mean-year HS: Reconstructed Timeseries in red, Hourly Corrected Climate Change model. Standard deviation in yellow and pink for Reconstructed Timeseries and Hourly Corrected Climate Change model respectively.

3.9 SNOWPACK final run

Before running the final SNOWPACK run, the issue raised by the failed validation of the Hourly Corrected Climate Change models data (Section 3.8.2) had to be fixed. In agreement with Kotlarski S., Head of Climate Evolution at MeteoSwiss, the solution applied, in order to obtain a proper partition of precipitation phase in SNOWPACK, was to set different TA thresholds above which precipitation is labeled as rain.

3.9.1 Method

A new TA threshold was determined for each station and model by comparing, during the calibration period (2006-2019), the *ecdf* of Snow precipitation for the mean-year of the Reconstructed Timeseries and the one of Hourly Corrected Climate Change models data. In a range spanning from 1.2°C to 4°C, the TA threshold that allowed the *ecdf* of Snow Precipitation of the Hourly Corrected Climate Change models data to be the most similar to the Reconstructed Timeseries one, was used. The TA thresholds used for each model and station are reported in Appendix A.

3.9.2 Results

As visible in Figure 28, 29 and 30 the setting of specific TA thresholds allowed the Hourly Corrected Climate Change models data to pass the validation as its mean-year HS (coloured curves) is always contained within the standard deviation bands (yellow areas) of the Reconstructed Timeseries one. However, differences between models and Reconstructed Timeseries (black-solid) are still visible and are station dependent. Figure 28 shows the case of Station FRA2, while Figure 29 the one of Station PAR2. In the former the models tend to underestimate the mean-year HS, in the latter, on the contrary, to overestimate it. 7 stations (ARO3, CAM2,DAV2, LUK2, NAR2, PAR2, SIM2) exhibit an overestimation, 6 (DAV3, DTR2, FRA2, GUT2, MEI2, ZER4) an underestimation, and 5 (BED3, CON2, KLO2, MES2, TUJ3) both behaviours according to the model and month.

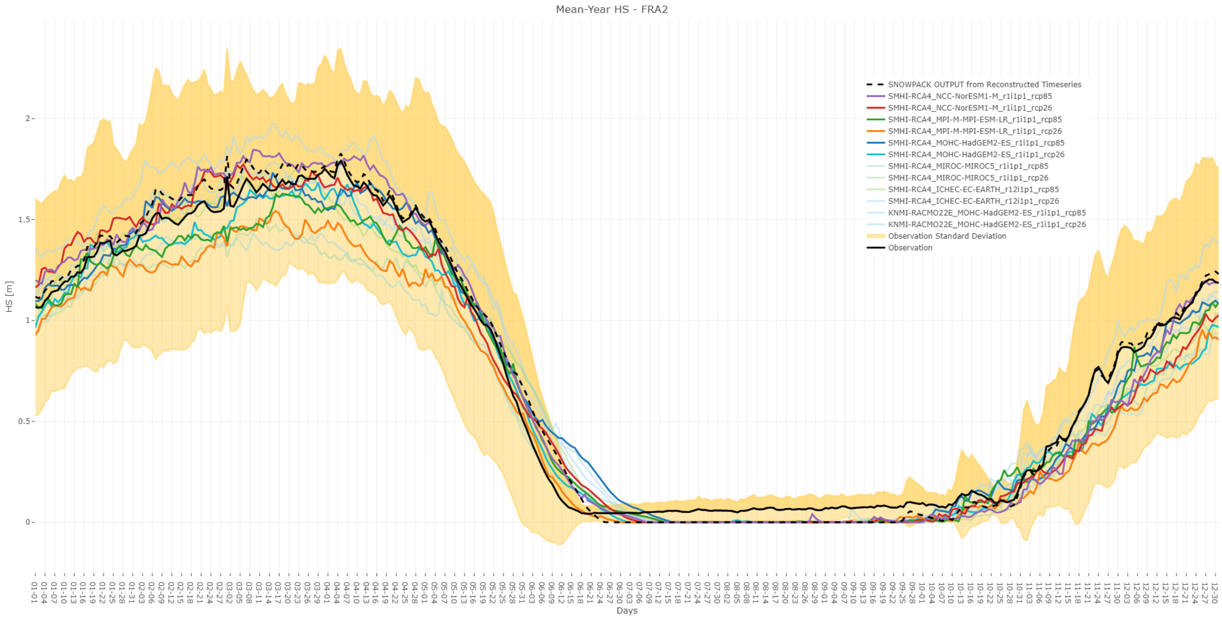

Figure 28: Comparison of mean-year HS data of Reconstructed Timeseries (black-solid), SNOWPACK output (black-dashed), Climate Change Models (several colors). In yellow the daily standard deviation of the Reconstructed Timeseries values.

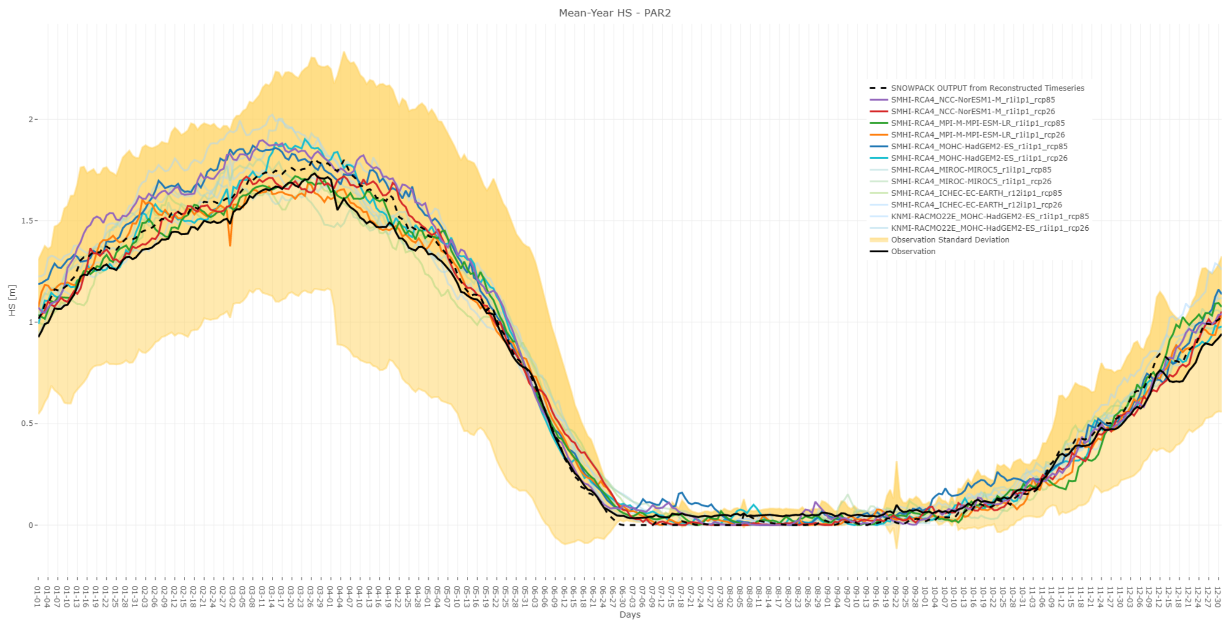

Figure 29: Comparison of mean-year HS data of Reconstructed Timeseries (black-solid), SNOWPACK output (black-dashed), Climate Change Models (several colors). In yellow the daily standard deviation of the Reconstructed Timeseries values.

Figure 30 shows how, in contrast with Figure 28 and 29, the melting period of the models is strongly delayed. Half of the stations show a delay, the other half well fit the Reconstructed Timseries mean-year HS during the melting period. It is important to note how this behaviour is not induced by the use of SNOWPACK: in Section 3.8.2 it has been highlighted how forcing SNOWPACK with PSUM can create a bias in the output-HS with respect to the measured one. In this case, however, the models curves diverge from the SNOWPACK output-HS (black, dashed). This can create some biases in the application of the Snow Metrics for the single station, however, since means among stations are run, it is believed that this biased-influence is mitigated.

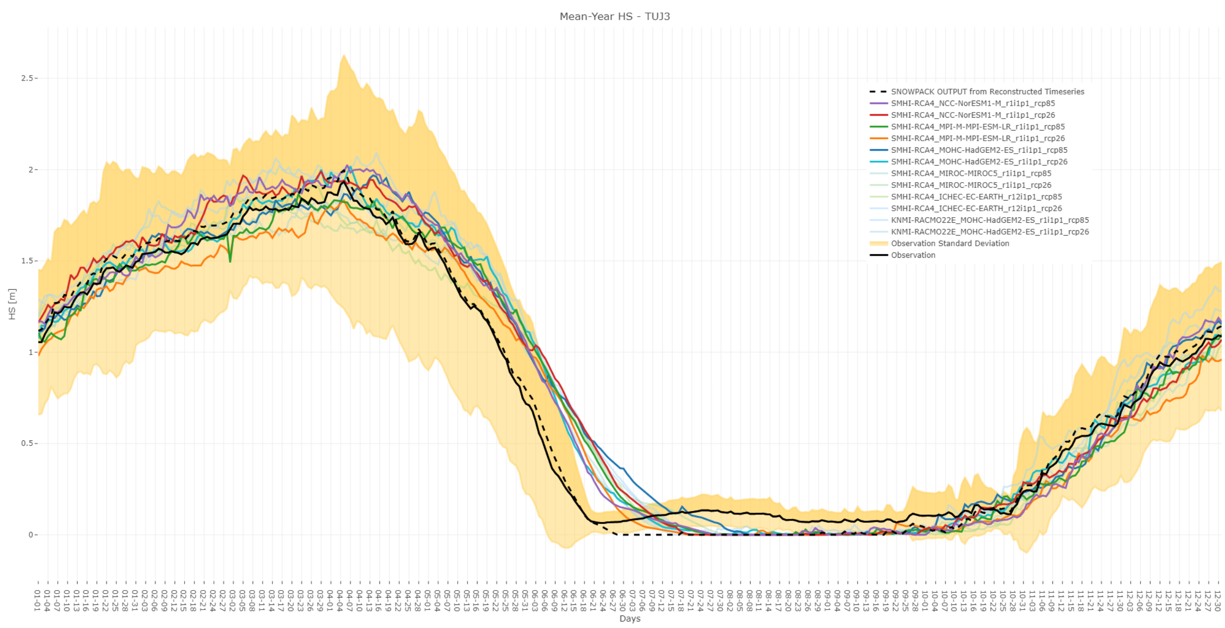

Figure 30: Comparison of mean-year HS data of Reconstructed Timeseries (black-solid), SNOWPACK output (black-dashed), Climate Change Models (several colors). In yellow the daily standard deviation of the Reconstructed Timeseries values.

Since the validation was passed, the final SNOWPACK run from 1971 to 2099 could be run with, as meteorological variables, the Hourly Corrected Climate Change data (ENFORCED SNOW HEIGHT = FALSE), boundary conditions set to false (CHANGE BC = FALSE). An example of a used .ini file is reported in Appendix B.

3.10 Validation of Climate Metrics on Reconstructed Timeseries and Joined Climate Change models

The previously defined Climate and Snow Metrics (Section 3.3) required, at this point, a validation as they could result unreliable once applied, further in the analysis, to the output of the SNOWPACK final run, which is going to be addressed from now on as *Climate Change Models data*

3.10.1 Method

To validate their applicability, a check on the values obtained if applied, for the calibration period (2006-2019), on the SNOWPACK output from Reconstructed Timeseries with respect to Climate Change Models data was run. To be able to run such comparison a Joined CC Models dataset was created as the union of the single Climate Change Models data. No partition in RCP2.6 and RCP8.5 is necessary for the calibration period as the values do not differ much for the same model chain.

3.10.2 Results

In Figure 31 the boxplots of the mean differences, between the values of the metrics applied to the Joined CC Models dataset and the ones of the Reconstructed Timeseries are shown. The single values of mean, median, 95 and 25 quantiles are available at Appendix C. SSL is represented in coral-red, SSS in green-lime, SSE in green, MHS in blue, 95HS in purple. In Table 9, the mean values of Absolute and Relative difference for each Snow Metric are reported. The relative difference of a Metric M is defined as follows:

$$M_{Relative\ difference} = \frac{M_{Future\ period} - M_{Historical\ period}}{M_{Historical\ period}} \cdot 100 \tag{9}$$

Running a comparison between the values of Table 8, where the Absolute differences in Snow Metrics between measured and SNOWPACK outputs are shown, it is visible how the values are comparable. These values of absolute differences correspond to the mean error of the analysis that will be run in the future Section *Data Analysis: Statistical analysis of Metrics at different scales* (Sections 4). However, it is important to remember that, since differences will be run between different periods of the same dataset, these errors will cancel out.

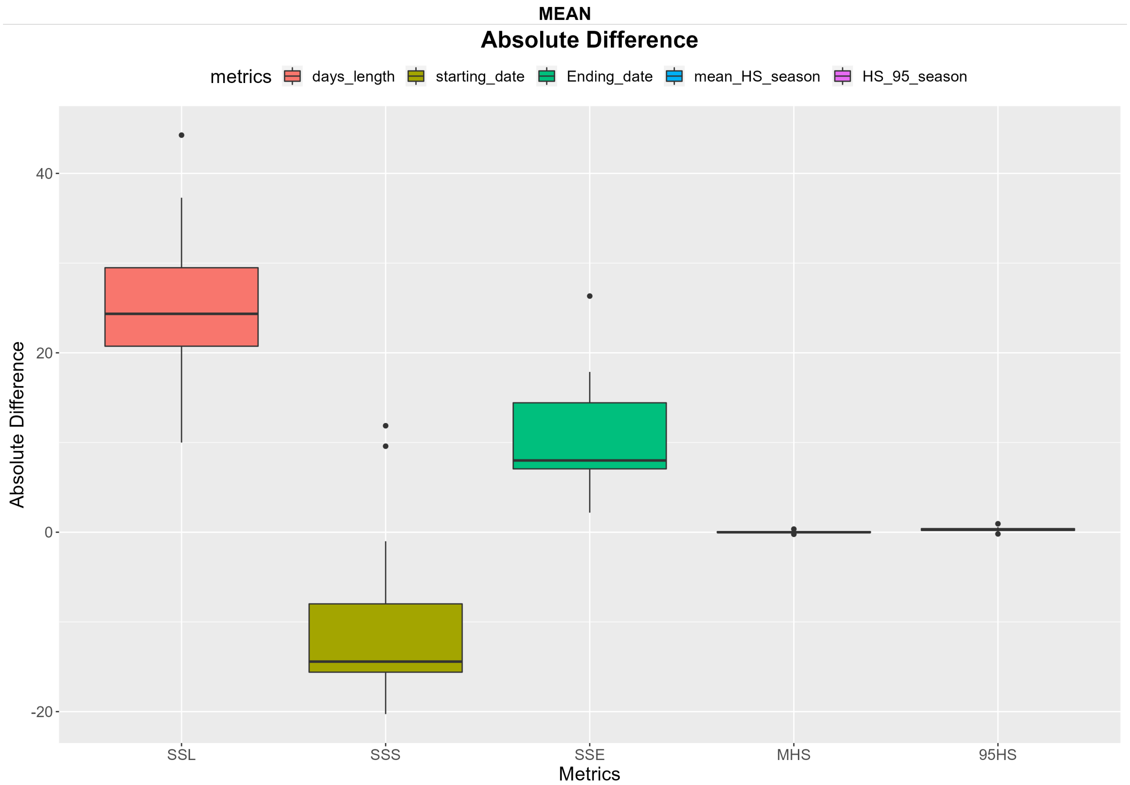

Figure 31: Boxplots of the Absolute differences in mean between the Snow Metrics applied to the Joined CC data and to the Reconstructed Timeseries. SSL in coral-red, SSS in green-lime, SSE in green, MHS in blue, 95HS in purple

Mean		
Metrics	**Absolute Difference**	**Relative Difference [%]**
SSL [days]	25	12
SSS [days]	-11	-
SSE [days]	11	-
MHS [cm]	2	1.5
95HS [cm]	30	13.95

Table 9: Absolute and Relative differences of in Snow Metrics values between Joined CC data and Reconstructed Time-series data.

4 Data analysis: Statistical analysis of Metrics at different scales

This section consists on the analysis of the application of Metrics to historical and future Climate Change model data at different geographical scales, from the smallest to the largest: station scale, regional scale, and macro-region scale. The station scale analysis (Section 4.1) points out common behaviour detected among the 18 studied stations, the regional scale(Section 4.2)focuses on comparing trends and altitude-related effects among the 4 geographical regions (North-West, North-Center, North-East, South), the macro-region scale (Section 4.3) explores the nature of climate change signals on the norther and southern sides of the Alps ridge drawing links with changes in precipitation and air temperature.

Climate Changes is, usually, studied in periods of 30 years to avoid the influence of natural variability, thus, 3 periods of 30 years each were defined throughout the available period spanning from 1971 to 2099:

- *Historical*: from 1971 to 2001
- *Mid Century*: from 2020 to 2050
- *End of Century*: from 2069 to 2099

The *Historical* period is taken as reference period to which future changes in climate (*Mid Century* and *End of Century*) are related to. The nature of the evolution of both Historical and future snowpacks was observed to differ, for some models and years, from the pattern visible in the Calibration period 2006-2019 (Section 3.8.2). In fact, during the Calibration period, the snowpack was characterized by an annual cycle as it would build up and completely melt within the same hydrological year, unlike the Historical snowpack that was found, at times, to last multiple years (Figure 32), and the future snowpack that is sporadically absent (Figure 33) and often ephemeral (Figure 34). These different features required some adjustments on the definition of the Snow Metrics (Section 3.3) as they would not, otherwise, correctly capture the nature of the evolution of the snowpacks.

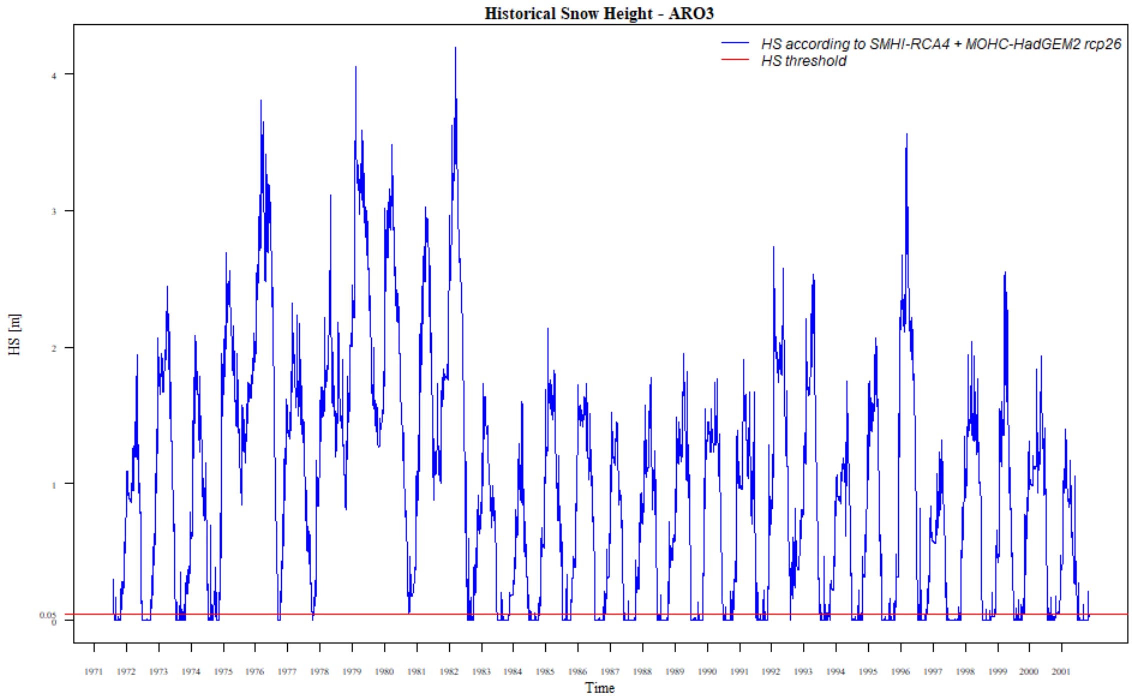

Figure 32: Example of Snow Seasons spanning more than one hydrological year into Snow seasons with yearly cycle

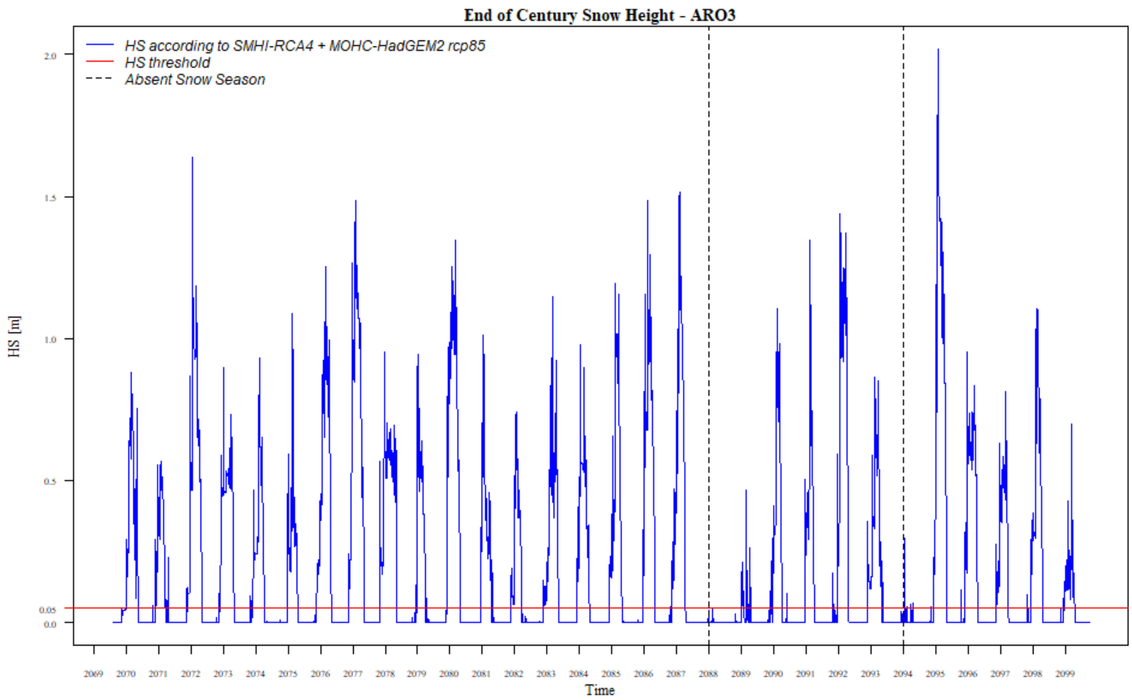

Figure 33: Example of absent Snow Season

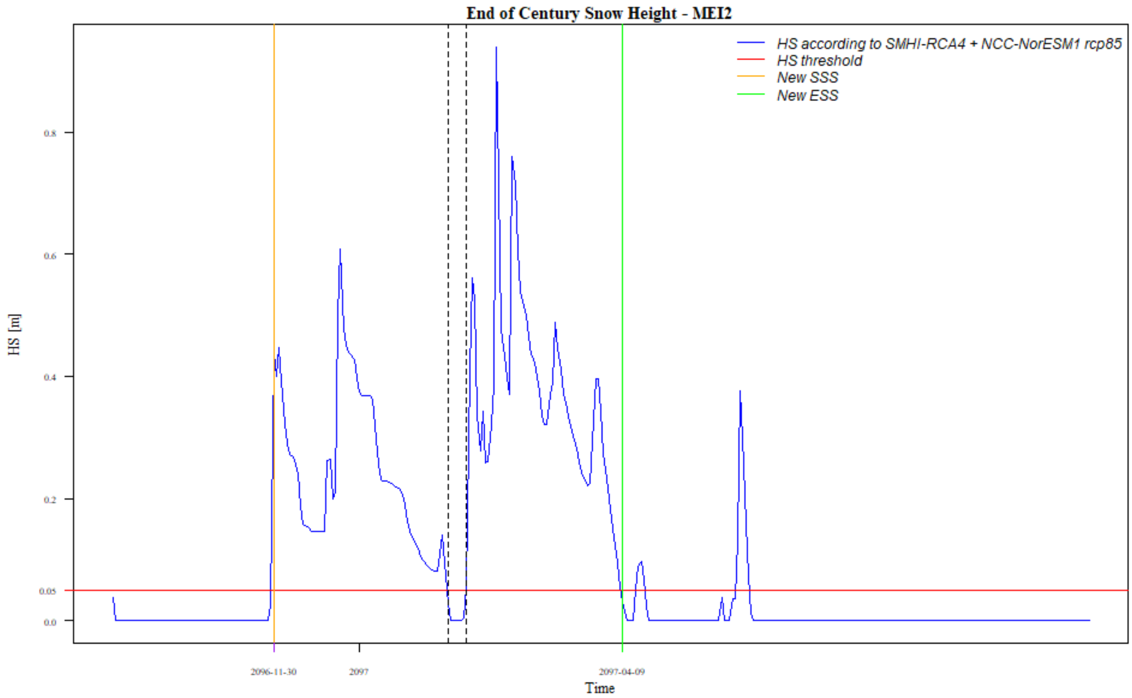

Figure 34: Example of ephemeral behaviour: multiple Snow Seasons within the same hydrological year

3 cases were detected:

- Multi-year snowpack: snowpacks last longer than 1 hydrological year (Figure 32). This feature was only found throughout the Historical period and was faced by cutting the SSL into multiple SSLs according to the hydrological years that they would span. Thus, SSS and ESS would correspond to the beginning and end of the hydrological years of interest (Figure 35).

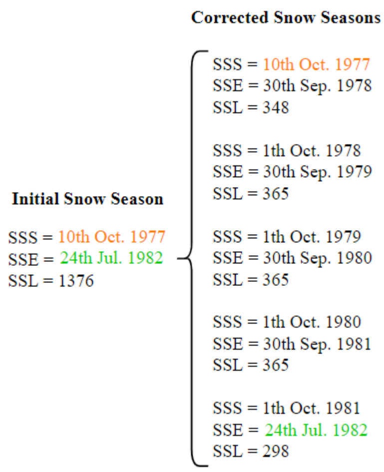

Figure 35: Example of subdivision of a Snow Season spanning more than one hydrological year into Snow seasons with yearly cycle

- Absent snowpack (Figure 33): The absence of snowpack was seldomly detected in the Mid and End of Century periods. It is important to note that the lack of snowpack detection implies that no snow (thicker than 5cm) was found on the ground for more than 20 days in a row, but does not imply that no snow fell or that no < 5cm-thick snowpack built up. In this case no SSS and SSE were defined as SSL was set to 0.

- Ephemeral snowpack (Figure 34): This case was only found throughout Mid and End of Century periods. Firstly, the days-threshold, set to define the minimum time that the snow has to be on the ground to start considering the snow season began (Section 3.3), was lowered from 100 to 50 and 20 for the periods Mid Century and End of Century respectively. Due to this lowering, two possible cases raised:

  1. Several Snow Seasons of comparable length: If several snow seasons with comparable length (length difference smaller than 80 days) were detected within the same hydrological year, the new SSL became the sum of each short season length. The new SSS became the SSS of the first short season while the ESS would be set at the date of the SSE of the last short snow season

     (Figure 36).

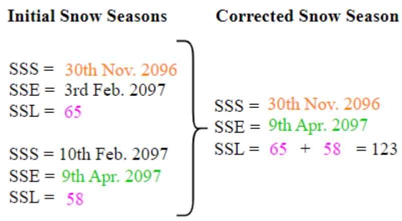

Figure 36: Example of joining short Snow Season under a single, artificial snow season

2. One short and one long Snow Season: In such a case, two seasons are respectively defined short and long if their difference in SSL is larger than 80 days. Given that this phenomenon was observed in case of long seasons of 100 days in winter and short seasons of $\sim 20 daysinautumn, theshortseasonwasdiscardedinfavourofthelongone.$

In case the snowpack was both ephemeral and absent in different years of the same period, both corrections were applied.

4.1 Station Scale Analysis

This sections aims at analysing the effects of Climate Change at the local scale in order to be able to understand whether different stations react in different ways or rather share a common behaviour.

4.1.1 Method

Once the Metrics datasets for each model, scenario, period and station (Figure 37) on yearly (Snow and Climate Metrics) or monthly resolution (Climate Metrics) were obtained, a statistical analysis had to be run as single values are not representative. The Statistical analysis was run for each station separately (Figure 38).

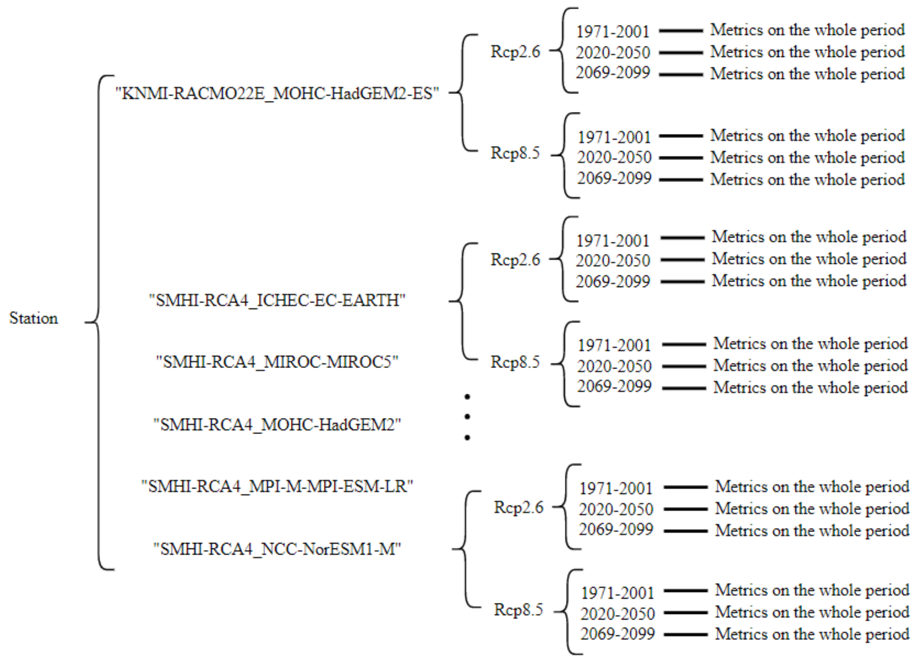

Figure 37: Example for one station of the metrics structure

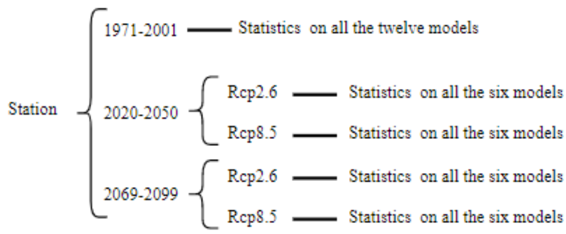

Figure 38: Example for one station of the statistic structure

The statistical analysis implied the computation of:

- mean
- median
- quantile 75
- quantile 25

for each of the metrics. Each statistical parameter was computer on both the available scenarios RCPs for the Hisotrical period, and separately for Mid and End of Century periods. To be noted that the statistics were applied separately to each model first (Figure 38).

4.1.2 Results

In Figure 39 the Metrics values for station ARO3 are displayed. Since the statistical distributions of all stations were found to have the same behaviour, Station ARO3 statistics was brought as an example. It is important to note how both SSS and SSE are not expressed in terms of date, but rather as number of the day within the year (e.g. 1^{st} of February = 32^{nd} day of the year). Boxplots show, in the box, 3 quartiles: Q1 and Q3, which are the edges of the box, correspond to the 25th and 75th percentile, while the line inside the box is the second quartile Q2 which correspond to the median. The whiskers represent the extreme of the data, while the dots the outliers.

In Figure 39 data are represented for the three periods separately: Historical, Mid Century and End of Century. Additionally, the Future periods (2020-2050 and 2069-2099) are subdivided in the two considered emission scenarios RCP2.6 (in light-blue for 2020-2050 and in blue for 2069-2099) and RCP8.5 (in orange for 2020-2050 and in red for 2069-2099). The Historical period (in purple) is not broken-down into the scenarios as it is included in the calibration period of Climate Change Models run by EURO-CORDEX itself before the release, thus, the scenarios, even though available, do not differ with each other.

The comparison of the boxplots of the Climate Metrics in the different periods show, as expected, that for each Snow Metric, the Mid Century period (for both RCPs) and the End of Century-RCP2.6 are similar, while End of Century-RCP8.5 deviates. This result is not surprising as it is related to the nature of the RCP scenarios: RCP2.6, being the best case scenario, foresees an equal change at Mid Century and End of Century as result of past emissions, rather than future ones; RCP8.5, on the other hand, being the worst case scenario, foresees an increasing difference the further the study looks in the future (Figure 9).

With different extents for the different stations, the predictions for the Snow Metrics are: reduction of SSL, delay of SSS, anticipation of SSE, and, according to the scenario, reduction of both MHS and 95HS.

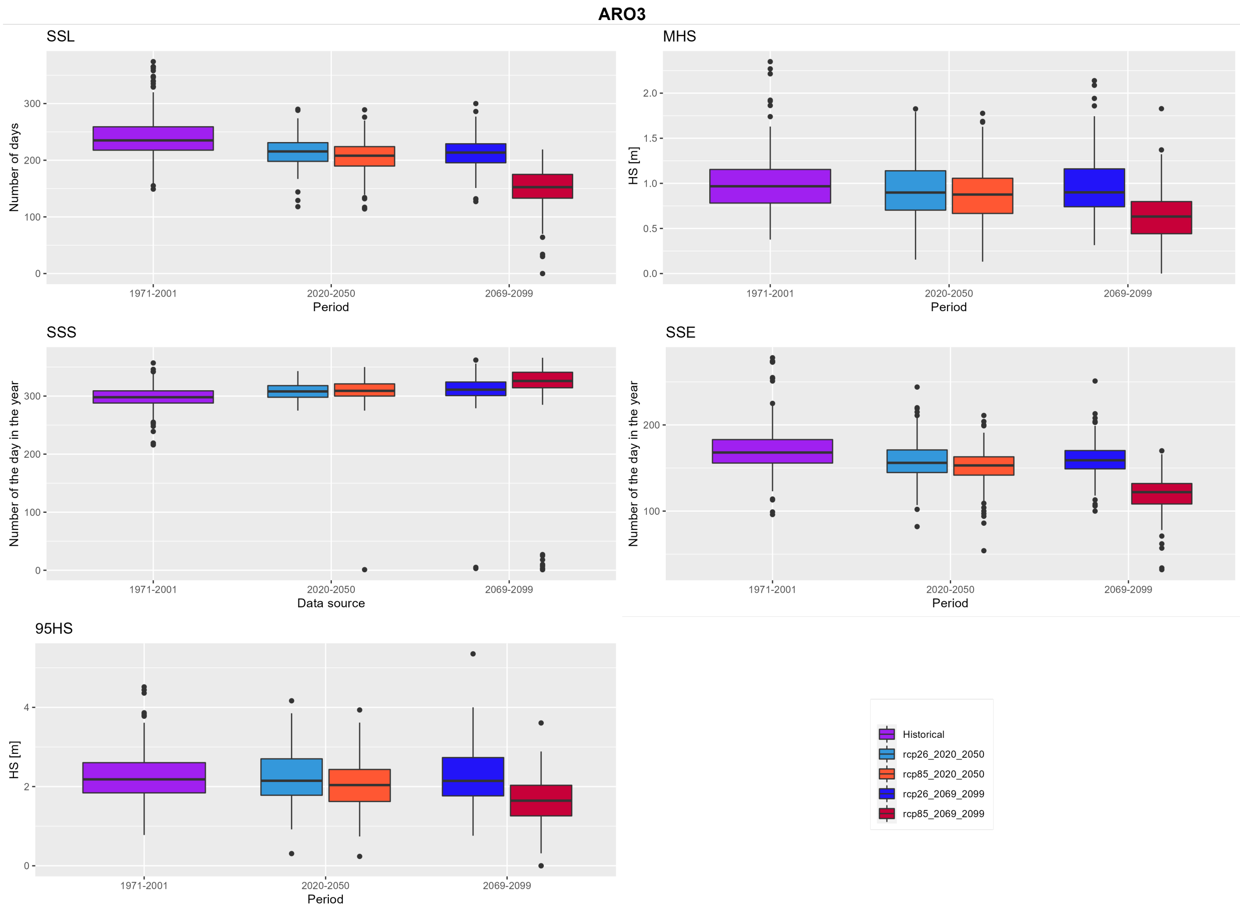

Figure 39: Example, for the station ARO3, of the boxplots as result of the application of Snow Metrics. In reading order, boxplots are shown for: Snow Season length (SSL), Mean Snow Height (MHS), Snow Season Starting date (SSS), Snow Season Ending date (SSE), 95 percentile of Snow Height (95HS). Historical values are shown in purple, Future periods (2020-2050 and 2069-2099) are subdivided in the two possible scenarios RCP2.6 (light-blue and blue respectively) and RCP8.5 (orange and red respectively).

For more than the 2/3 of the stations the reduction of SSL is mainly due to the earlier disappearance of snow on the ground, resulting in an anticipation of SSE (Figure 39); for the remaining stations, the reduction is co-caused by a later building-up of the snowpack and an earlier melting, as visible for station LUK2 (Figure 40).

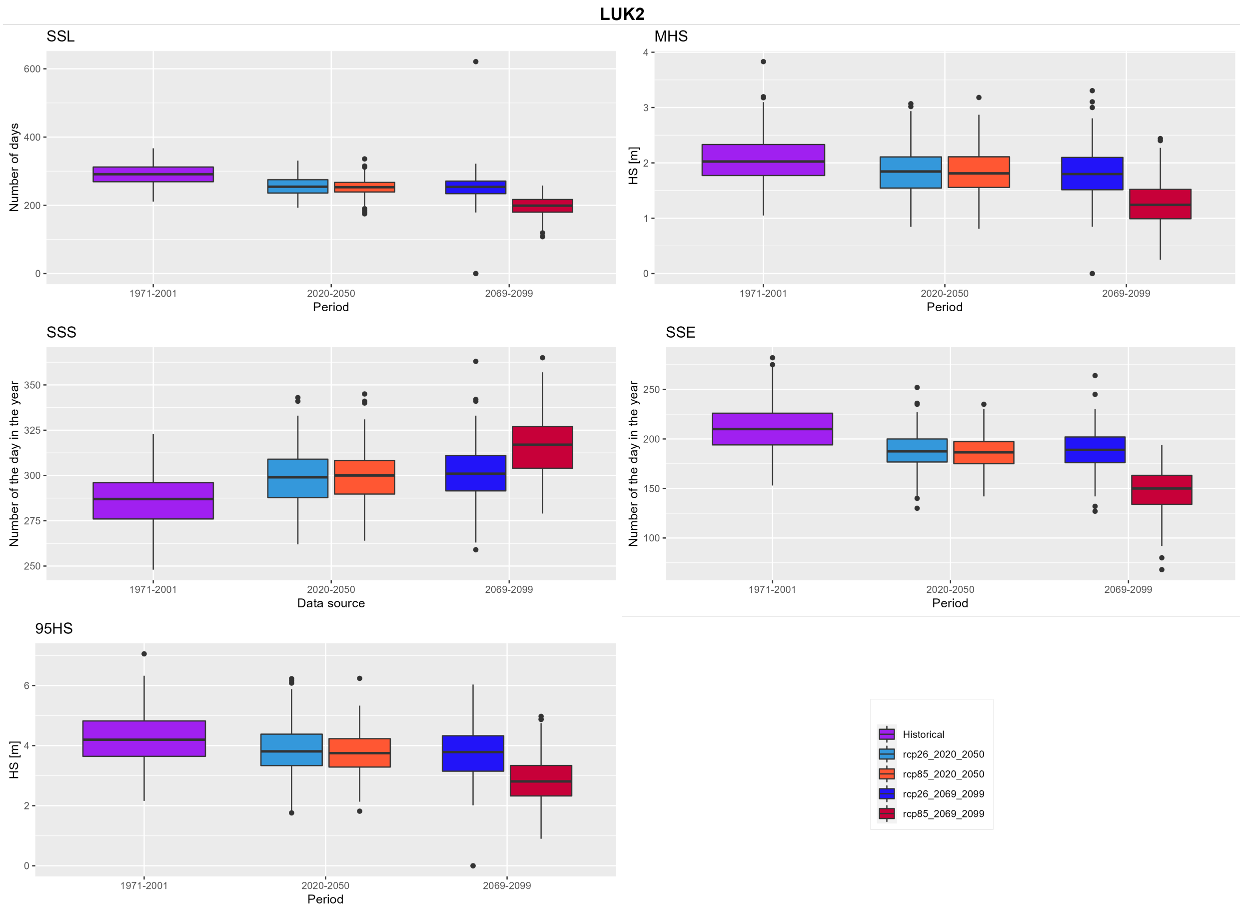

Figure 40: Example, for the station LUK2, of the boxplots as result of the application of Climate and Snow Metrics. In reading order, boxplots are shown for: Snow Season lengt (SSL), Mean Snow Height (MHS), Snow Season Starting date (SSS), Snow Season Ending date (SSE), 95 percentile of Snow Height (95HS). Historical values are shown in purple, Future periods (2020-2050 and 2069-2099) are subdivided in the two possible scenarios RCP2.6 (light-blue and blue respectively) and RCP8.5 (orange and red respectively).

As visible in third plot from the top of Figure 41, the changes in Snow Metrics values can not be directly associated to changes in precipitations as, in none of the scenarios and periods, striking changes are visible at monthly level for mean years.

On the other hand, Air Temperatures change significantly with an increase in both MDTAA0 and MMTA (first and second plot from the top of Figure 41). Regarding the changes in MDTAA0, all the stations show a more significant increase at the End of Century for RCP8.5 with respect to RCP2.6 which vary less and analogously. The larger increase in MMTA in the summer months is in accordance with several previous studies [8].

Furthermore, half of the stations is affected by an anticipation of one month (from May to April) of MMTA above 0°C for all scenarios and period, while the other half show such anticipation only at the End of Century in case of RCP8.5. Earlier Mean temperatures above 0°C cause earlier melting of the snowpack, resulting in an earlier SSE.

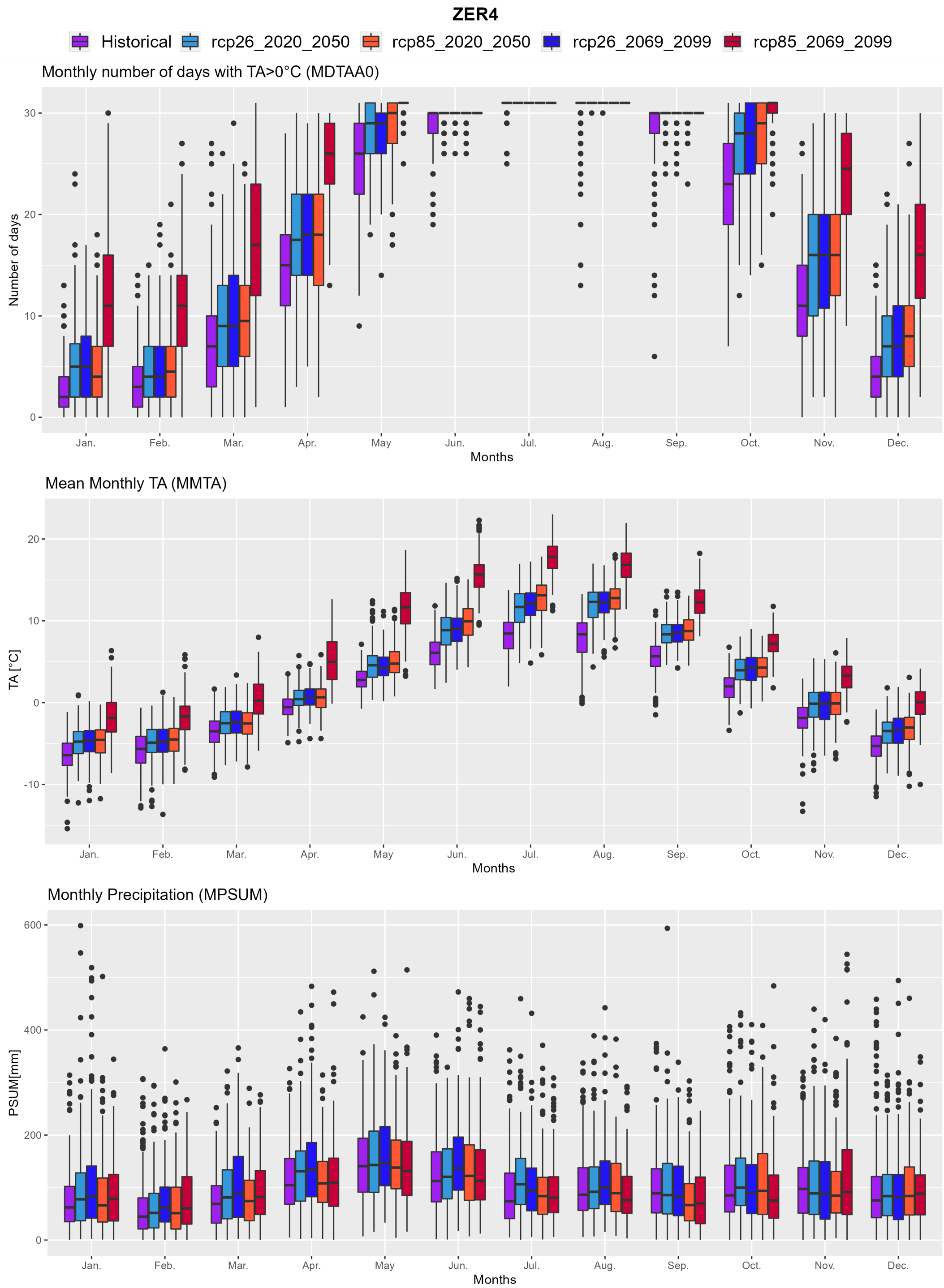

Figure 41: Climate Metrics at ZER4 station. From the bottom to the top: MDTAA0, MMTA, MPSUM. Historical values are shown in purple, RCP2.6 is shown in light-blue for 2020-2050, in blue for 2069-2099, RCP8.5 is shown in orange for 2020-2050, red for 2069-2099.

In Figure 42 the mean-year HS for BED3 is shown and it is visible how the SSE is more affected by the climate changes with respect to the SSE as in spring future HS reaches values below 0.05 m (dashed red line) way before the historical one

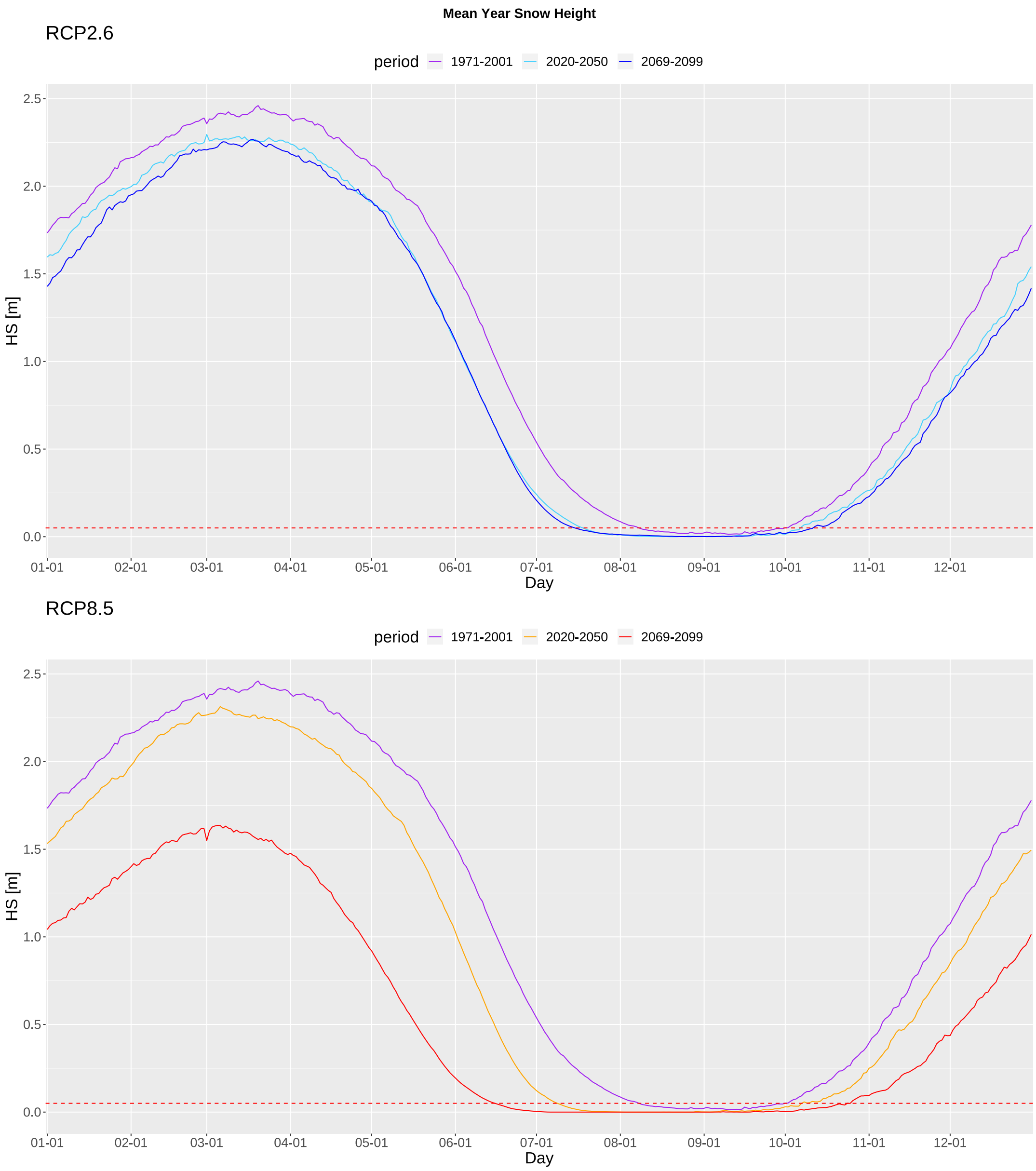

Figure 42: Mean-year HS at Station BED3. Top: RCP2.6, Historical in purple, Mid Century in light-blue, End of Century in blue. Bottom: RCP8.5, Historical in purple, Mid Century in orange, End of Century in red. In dashed red the 0.05m HS threshold.

The current study hypotheses the unsettling fact that SSS is not affected as much as SSE even thought TA is going rise in autumn as much as in spring (Figure 41) to be explainable by the radiative fluxes (Figure 43). In fact, during spring months (March, April) the mean incoming radiative flux rises from 150 Wm^{-2} to almost 225 Wm^{-2}, while in autumn (October, November) it decreases from 150 Wm^{-2} to 100 Wm^{-2}. The higher incoming radiative flux in spring fosters the melting process in spring.

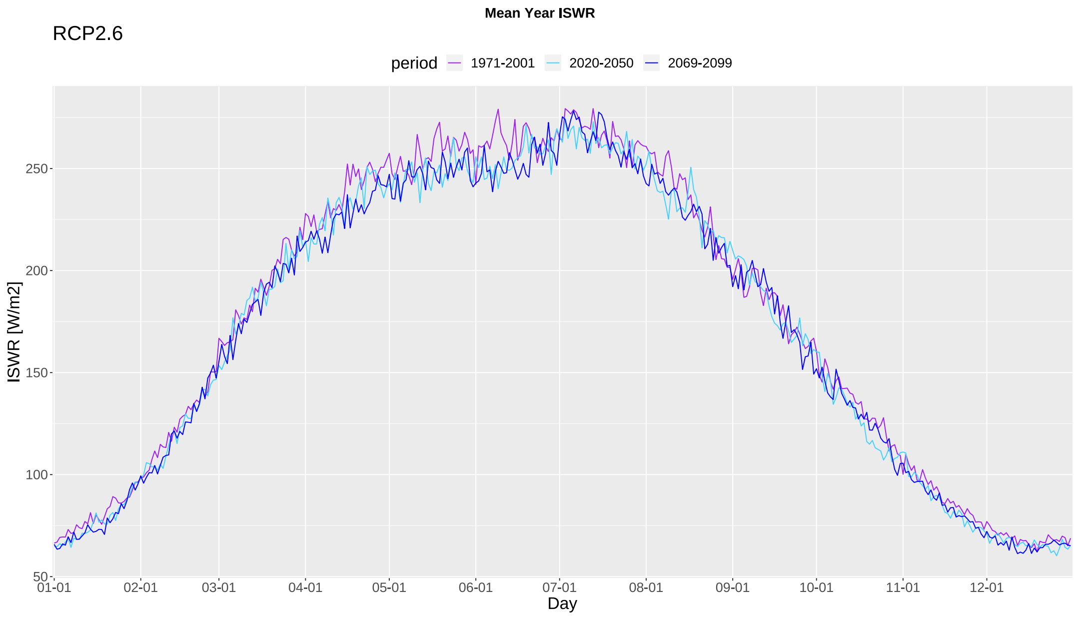

Figure 43: Mean-year ISWR. Top: RCP2.6, Historical in purple, Mid Century in light-blue, End of Century in blue. Bottom: RCP8.5, Historical in purple, Mid Century in orange, End of Century in red.

4.2 Regional Analysis

This investigation roots in the fact that, according to the First Law of geography by Waldo Tobler, *"everything is related to everything else, but near things are more related than distant things."*, and in the evidence that the four regions (Valais, Uri+Bern, Grison) are known too have, at present, on average, different climates (Section 1.1).

4.2.1 Method

The regional analysis to explore possible patterns of the Snow Metrics within changing climate was performed thanks to the statistical tool of Boxplots. Specifically, station by station, for each model (6), the mean value of the considered Snow Metric was computed over the 3 periods and for both RCPs, in order not only to obtain an average difference but its spread as well. Furthermore, the absolute and relative difference of future values with respect to the historical ones were computed model by model, scenario by scenario resulting in 4 values for each model: 2020-2050 in RCP2.6, 2069-2099 in RCP2.6, 2020-2050 in RCP8.5, 2069-2099 in RCP8.5 (Figure 44).

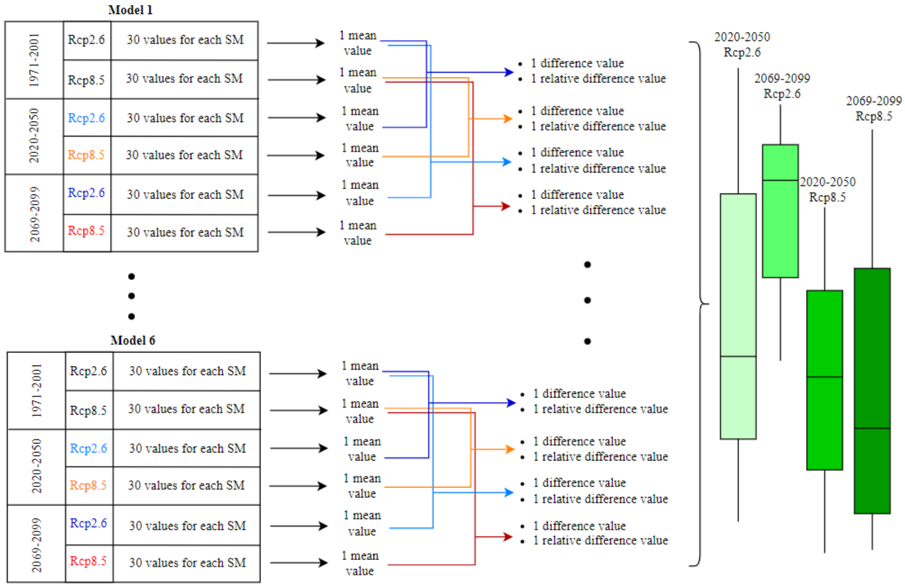

Figure 44: Workflow on how to get a boxplot for one station

4.2.2 Results

In the following figures, boxplots for each station show the absolute (MHS: Figure 45, SSL: Figure 48, SSS: Figure 50, SSE: Figure 49) and relative difference (MHS: Figure 46, SSL: Figure 48) of the Snow Metrics of the Future Periods (2020-2050, 2069-2099) with respect to the Historical period (1971-2001). No relative difference is computed for SSS and SSE as it would lose meaning. MHS and 95HS showed the same behaviour, thus, only MHS is here reported. The colors of the boxplots are related to the region the stations belong to: green for North-West, purple for North-center, blue for North-East, orange/red for South. Stations are ordered from the lowest to the highest in altitude within each region.

For what concerns the absolute difference in MHS, it is noteworthy the fact that different regions show different links to altitude, even though remaining consistent in the different periods and scenarios:

- North-West: the absolute reduction decreases with the increase of altitude.
- North-Center: the higher the altitude, the larger the reduction in MHS.
- North-East: the dependency to altitude is smoothed and stations tend to experience a more homogeneous reduction
- South: the tendency is a reduction in MHS with the increase of altitude but with a flattening at higher elevations.

As already grasped in the qualitative analysis of the Snow Metrics at the station level (Section 4.1.2), in the two future periods the difference of MHS widely differ in RCP8.5, while they are more similar for RCP2.6. In fact, in 2069-2099 for RCP8.5, the difference is averagely +30% larger than the one in 2020-2050, in comparison with the +3% for RCP2.6 (Figure 46). Furthermore, the stronger effect on the Southern side in terms of Relative reduction (Figure 46, bottom graph) is remarkable in both scenarios and periods, especially with respect to the Northern-East side.

To have a less scattered outlook on the regions, stations values were merged, model by model, into regional ones. In Figure 47 it is visible how the Southern and the Northern-center sides are the ones more largely effected in both scenarios RCPs, with a reduction of 12-16% (16-20 cm) in 2020-2050, and 14-45% (20-60 cm) in 2069-2099. The least affected stations, in the North-West, showed how no less than a reduction of 8% can be expected. (Table 10 and Table 11).

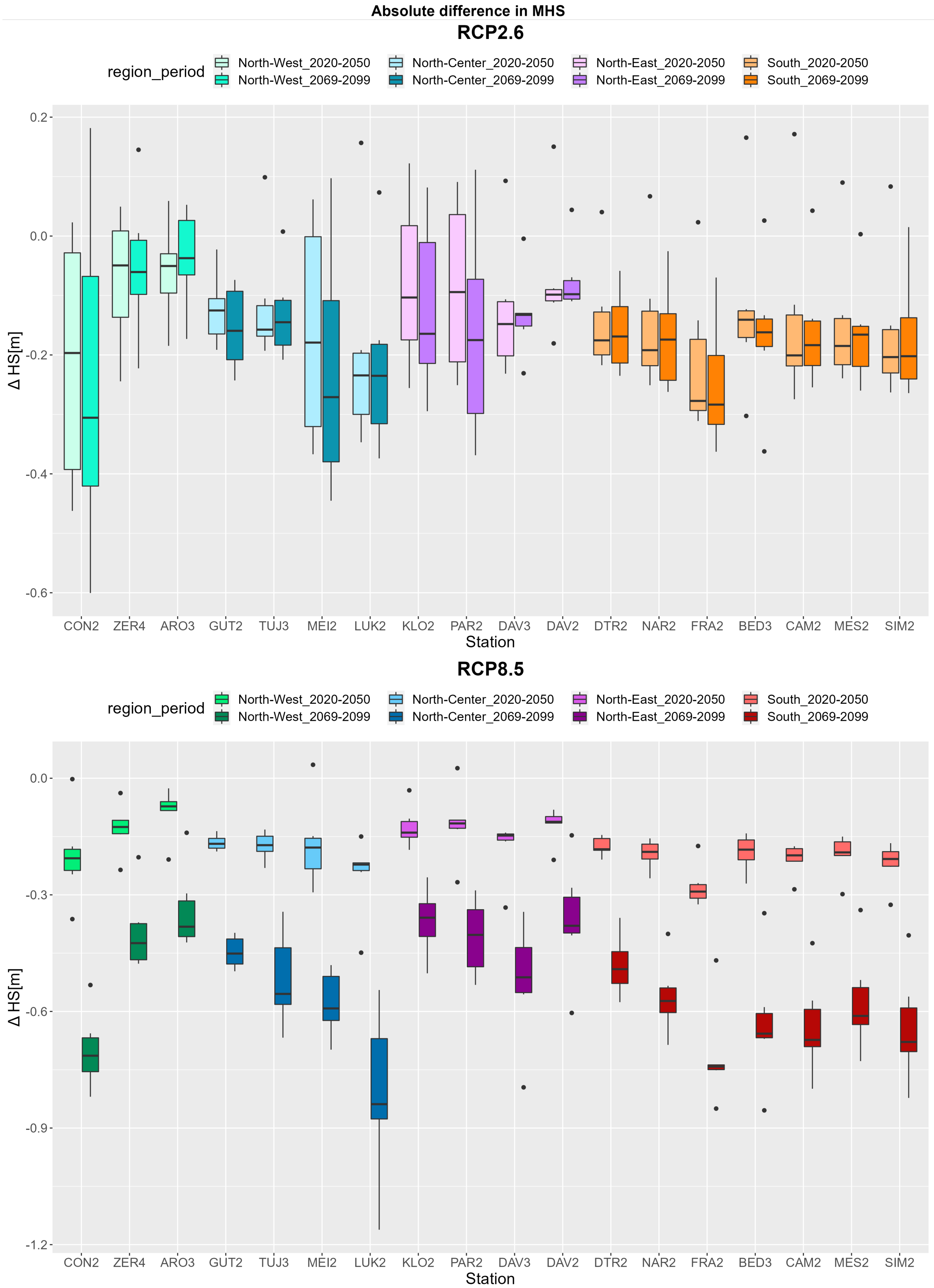

Figure 45: Absolute difference in MHS between the Future periods (2020-2050, 2069-2099) and the Historical one. Top: RCP2.6. Bottom: RCP8.5. Regions are subdivided by color: green for North-West, purple for North-center, blue for North-East, orange/red for South

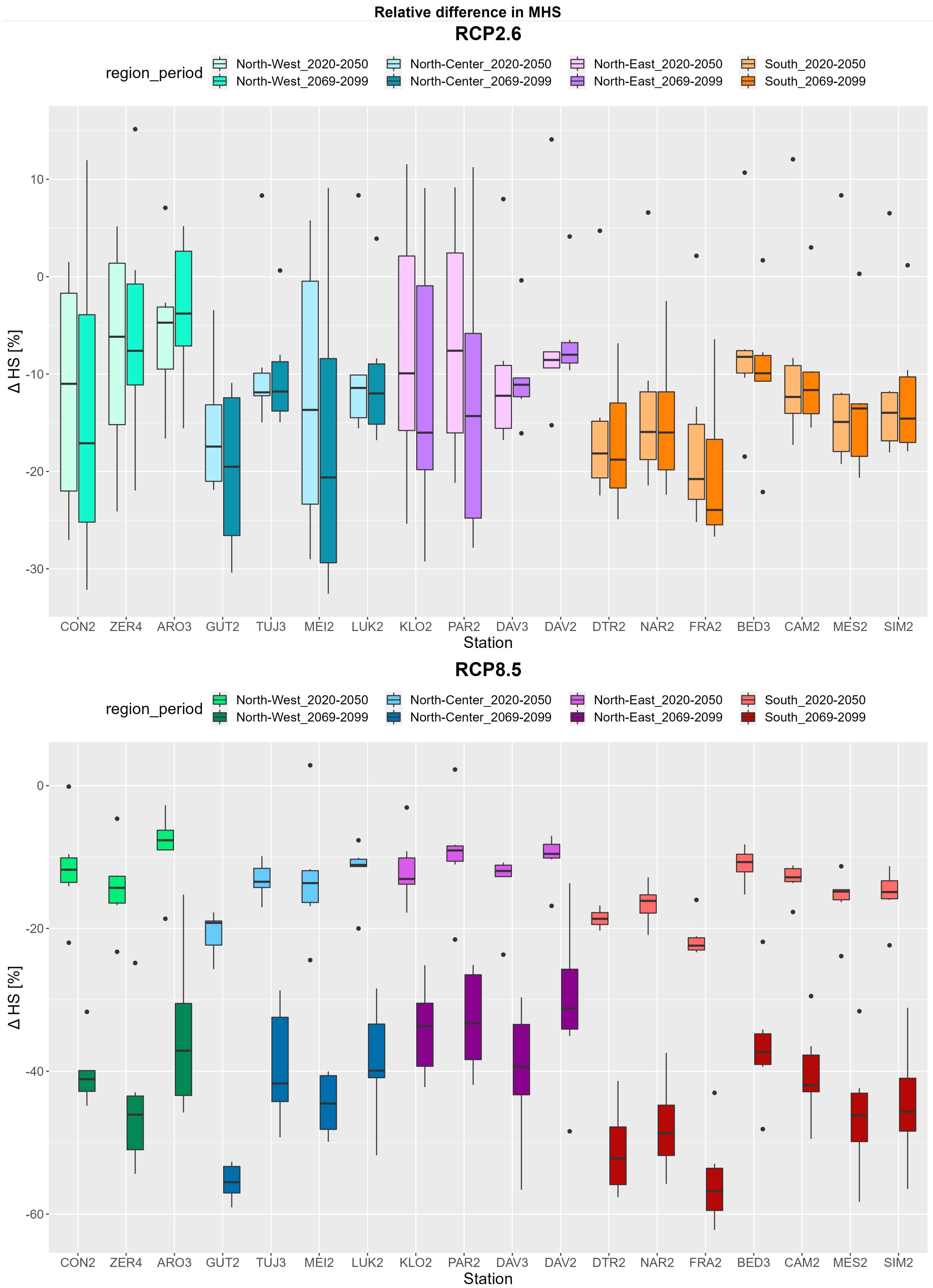

Figure 46: Relative difference in MHS between the Future periods (2020-2050, 2069-2099) and the Historical one. Top: RCP2.6. Bottom: RCP8.5. Regions are subdivided by color: green for North-West, purple for North-center, blue for North-East, orange/red for South

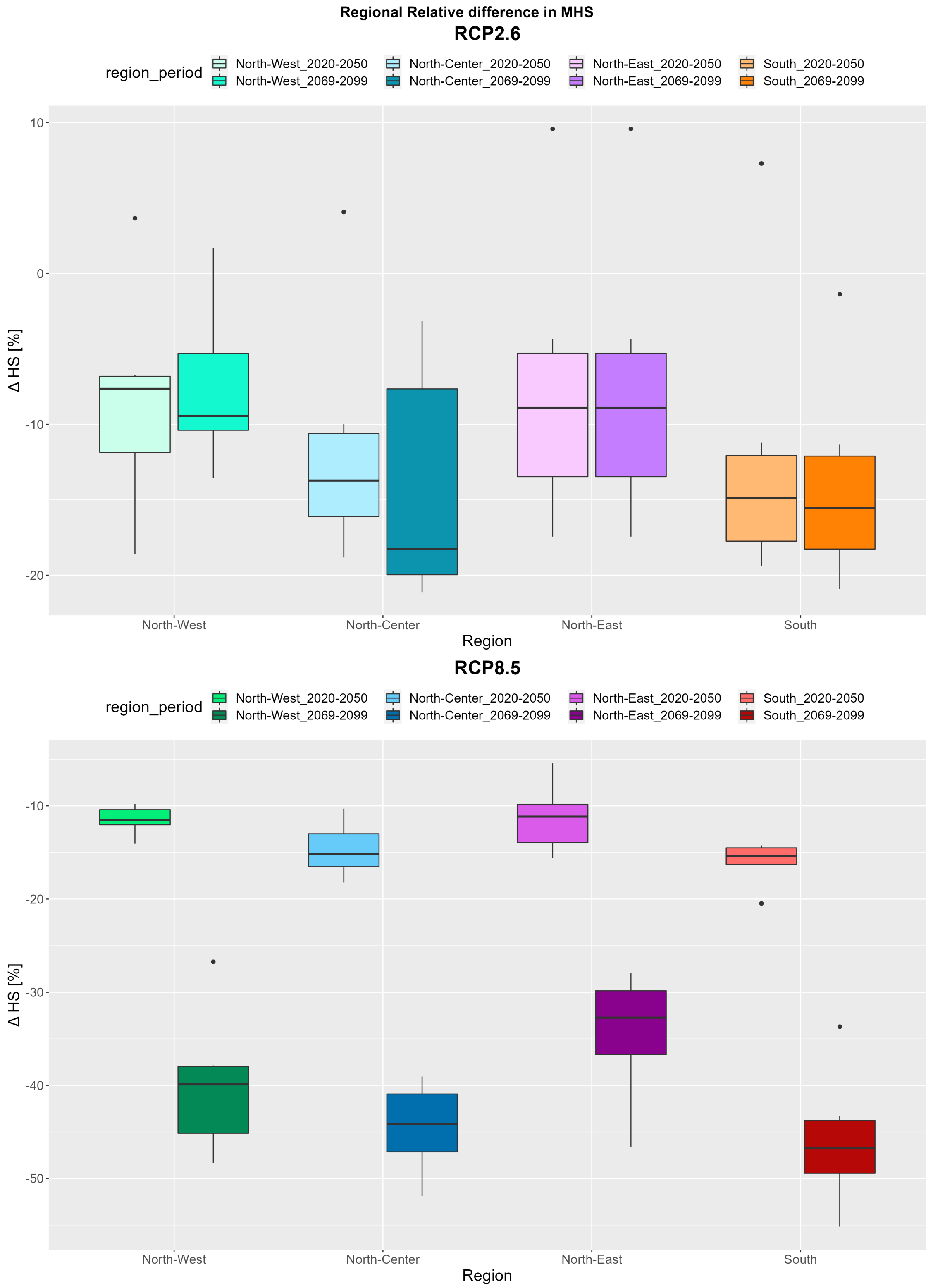

Figure 47: Relative difference in MHS between the Future periods (2020-2050, 2069-2099) and the Historical one, shown region by region. Top: RCP2.6. Bottom: RCP8.5. Regions are subdivided by color: green for North-West, purple for North-center, blue for North-East, orange/red for South

A clear link among the Snow Metrics is the one that can be drawn between SSL and SSE. Comparing Figure 48 and Figure 49 it is noticeable how SSL trend mirrors SSE one. This is due to the fact that while a strong anticipation of the SSE is foreseen, a less intense deviation is noted on the SSS (Figure 50): for the latter, a maximum mean-delay of +11 and +20 was computed in the South for RCP2.6 and RCP8.5, respectively, in contrast with the minimum mean-anticipation of -13

Table 10: Mean values of Relative (left) and Absolute (right) differences for RCP2.6 at regional scale

Mean of relative differenze [%] RCP2.6				
Region	**Period**	**ΔMHS**	**Δ95HS**	**ΔSSL**
N-W	2020-2050	-8	-5	-9
	2060-2099	-8	-4	-11
N-C	2020-2050	-11	-10	-11
	2060-2099	-14	-12	-13
N-E	2020-2050	-7	-6	-12
	2060-2099	-10	-8	-13
S	2020-2050	-12	-9	-10
	2060-2099	-14	-10	-11

Mean of absolute difference [Days] RCP2.6	
ΔSSS	**ΔSSE**
+9	-14
+8	-13
+7	-17
+7	-19
+11	-18
+11	-20
+9	-15
+11	-15

Table 11: Mean values of Relative (left) and Absolute (right) differences for RCP8.5 at regional scale

Mean of relative difference [%] RCP8.5				
Region	**Period**	**ΔMHS**	**Δ95HS**	**ΔSSL**
N-W	2020-2050	-11	-8	-12
	2060-2099	-40	-30	-34
N-C	2020-2050	-15	-11	-13
	2060-2099	-45	-36	-38
N-E	2020-2050	-11	-8	-13
	2060-2099	-34	-27	-34
S	2020-2050	-16	-12	-12
	2060-2099	-49	-36	-34

Mean of absolute difference [Day] RCP8.5	
ΔSSS	**ΔSSE**
+13	-17
+15	-49
+13	-20
+5	-57
+15	-21
+22	-55
+13	-18
+20	-54

and -17 days for the former.

Analogously to what seen for reductions in MHS, the Northern-Center and Southern regions are the most affected ones, especially for RCP8.5, with an anticipation of -20/-18 days for 2020-2050 and -57/-54 in 2069-2099 for SSE, leading to mean reductions in the SSL of -92($\sim -35\%$)/-85($\sim -38\%$) days (Table 10 and Table 11). It is important to note that these variations in Starting and Ending of the Snow Season, in the best case scenario (RCP2.6), still result in a mean reduction of the snow season length of almost a month: 25 days in 2020-2050 and 30 in 2069-2099

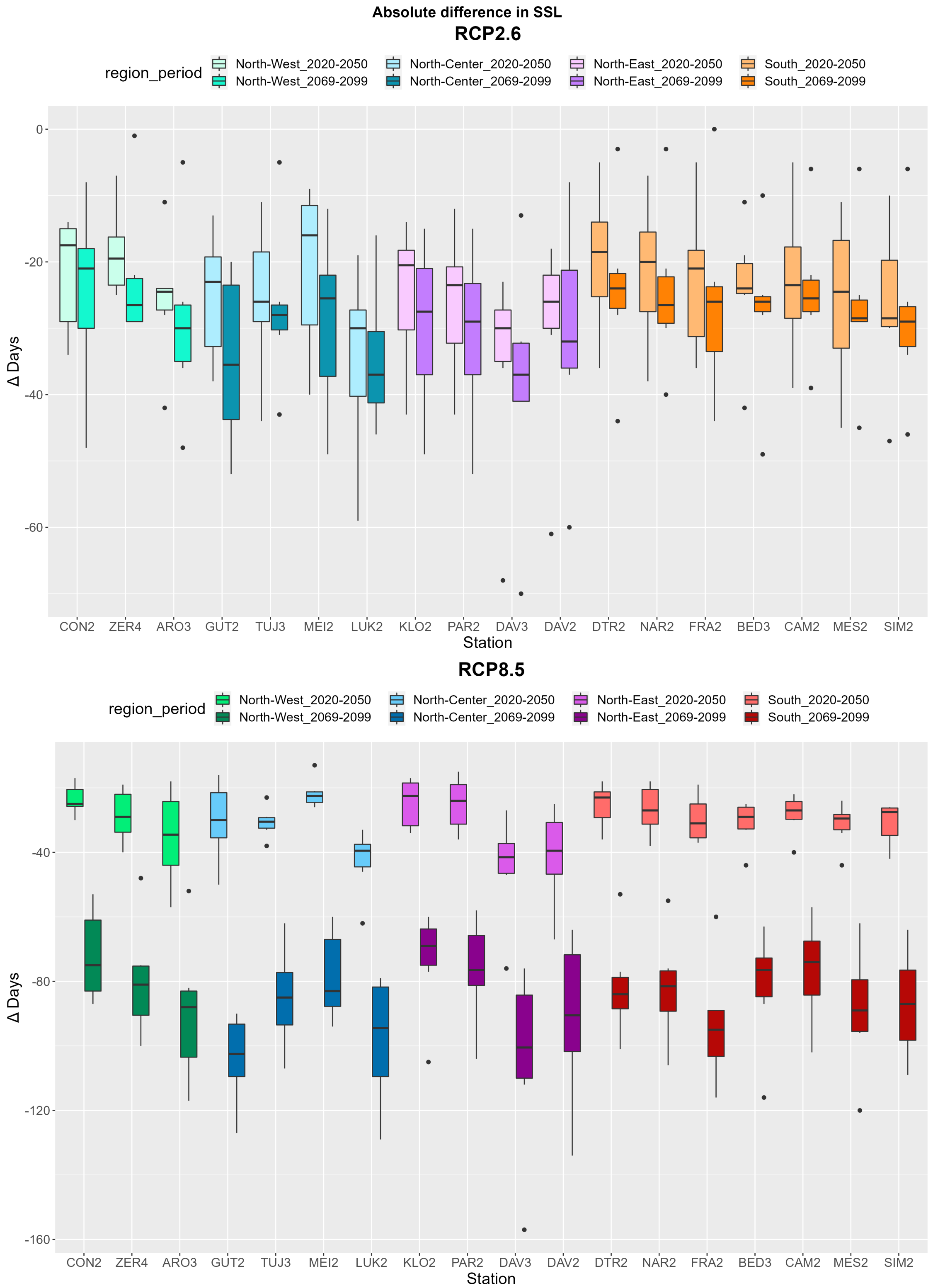

Figure 48: Absolute difference in SSL between the Future periods (2020-2050, 2069-2099) and the Historical one. Top: RCP2.6. Bottom: RCP8.5. Regions are subdivided by color: green for North-West, purple for North-center, blue for North-East, orange/red for South

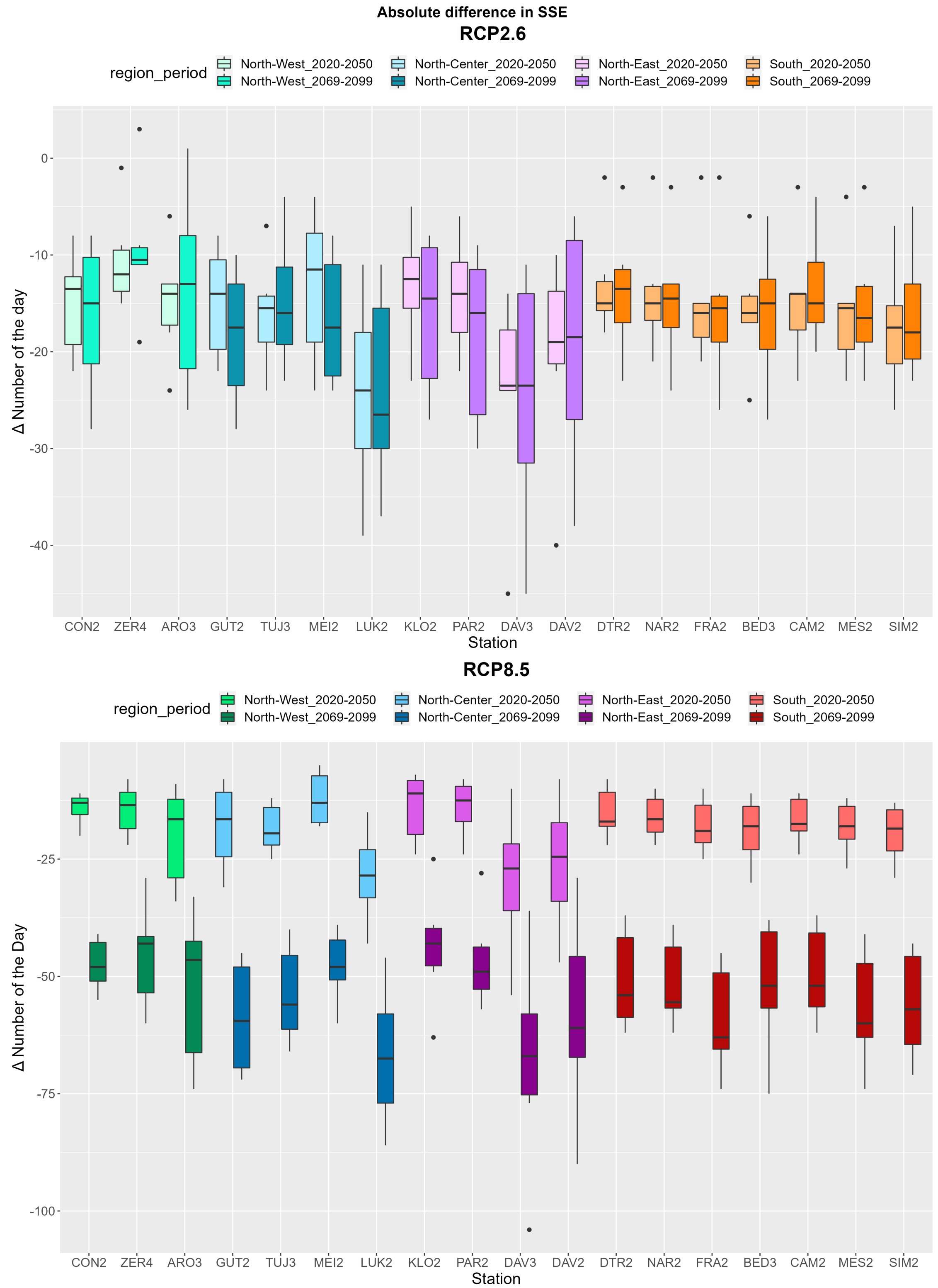

Figure 49: Absolute difference in SSE between the Future periods (2020-2050, 2069-2099) and the Historical one. Top: RCP2.6. Bottom: RCP8.5. Regions are subdivided by color: green for North-West, purple for North-center, blue for North-East, orange/red for South

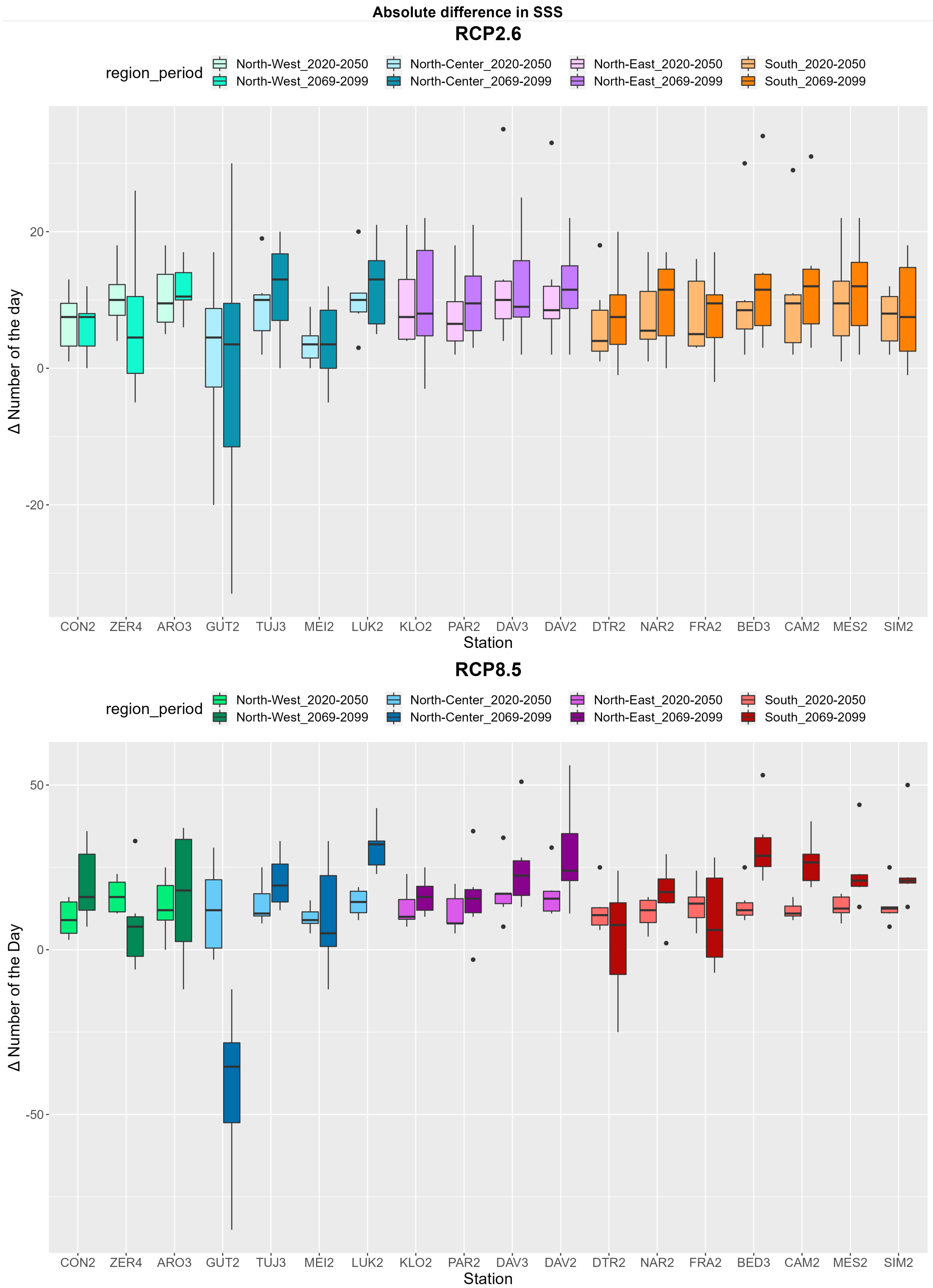

Figure 50: Absolute difference in SSS between the Future periods (2020-2050, 2069-2099) and the Historical one. Top: RCP2.6. Bottom: RCP8.5. Regions are subdivided by color: green for North-West, purple for North-center, blue for North-East, orange/red for South

The only outlier from the rather homogeneous effect of climate change on the analysed stations is the station GUT2 (Figure 50). Its anticipation or smaller delay is due to a more frequent ephemeral behaviour with respect to the other stations.

The future value of meteorological variables and, consequently, of the evolution of the snowpack are strictly related to the Climate Change signal present in the used climate model chains. Each pixel of the model chains carries a different signal, thus, it is important to check how strong this signal is once the QM is run. In fact, if the pixel signal is still very strong at the station scale even after QM and all stations belonging to the same pixel show similar results, it means that in a study at the station scale the results are not representative and that model chains with higher resolution (12km) are necessary to carry out a meaningful analysis. Figure 51 shows the difference in MHS between the Future periods (2020-2050, 2069-2099) and the Historical one for stations belonging to a shared pixel. It is visible how the signal is not very strong within the pixels as the differences in MHS do not share the same values, however an influence is noticeable in the different mean value between pixels. This means that downscaling to the stations provided an added value to the study as it indeed goes down to the local scale.

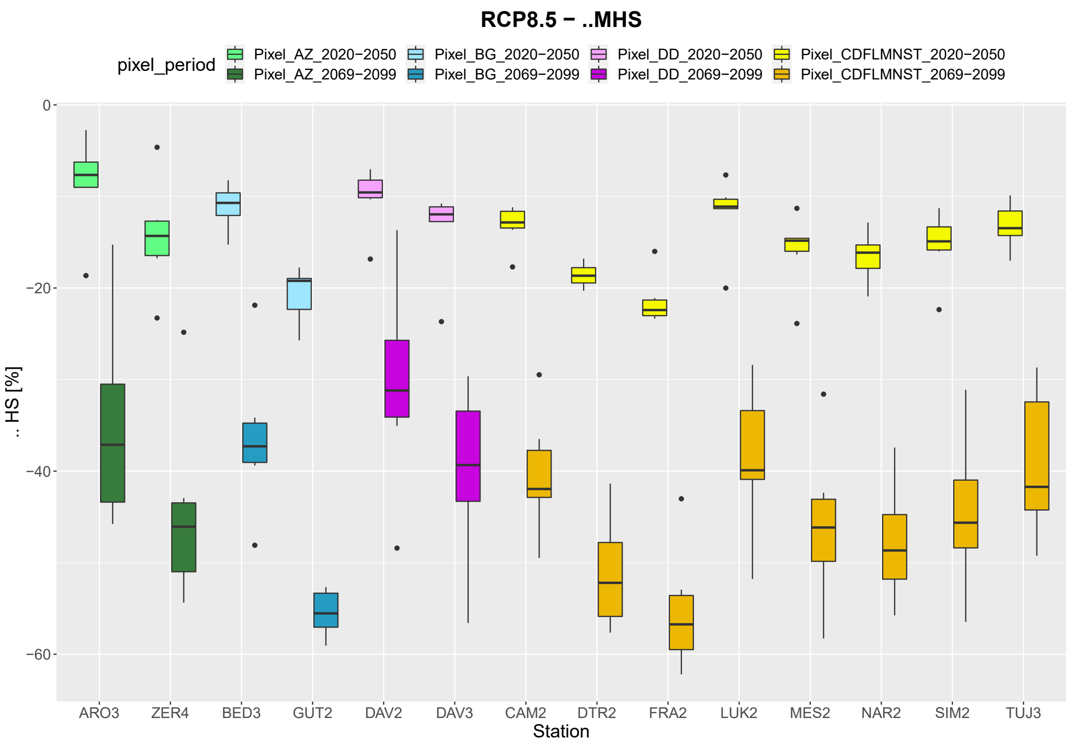

Figure 51: Relative difference in MHS between the Future periods (2020-2050, 2069-2099) and the Historical one. Top: RCP2.6. Bottom: RCP8.5. Pixel are subdivided by color: green for Pixel AZ (ARO3, ZER4), blue for Pixel BG (BED3, GUT2), pink for Pixel DD (DAV2, DAV3), yellow for Pixel CDFLMNST (CAM2, DTR2, FRA2, LUK2, MES2, NAR2, SIM2, TUJ3)

4.3 Macro-regional Analysis

Often climate change impacts are studied for large areas, however, this may result in an homogenisation of the results. In fact, in complex terrains as the one that characterises the Alps, flattening the differences can result in mean signals that do not completely represent the inner ones. However, a larger overview is important to detect common trend. Thus, in this study, two larger *Macro-regions* were defined and compared: Northern and Southern sides of the Alps ridge.

4.3.1 Method

To study the climate change signal on the two sides of the Alps a process of averaging model by model among stations, as previously applied at the regional level (Section 4.2.1) was used to reach the macro-region scale.

4.3.2 Results

The most stricking effect from the analysis of climate models on such a wide area is that the differences seen at the regional scale disappear: beside MHS (Figure 52), North and South show very similar responses for all the Snow Metrics (Figures in Appendix D). In fact, SSL mean values in the South differ from the North of only 2% and both mean SSS and mean SSE vary from 1 to 5 days (Table 12 and Table 13). In Figure 52, the effects on MHS on the Northern (in green) and Southern (in orange-red) sides of the Swiss Alps is shown for the periods 2020-2050 and 2069-2099 for the scenarios RCP2.6 (top) and RCP8.5 (bottom).

It is very important to note, that despite the small difference between Northern and Southern effects, the differences with the Historical period are relevant: for SSL the difference is of the magnitude of $\sim -10\%$ in 2020-2050 for RCP2.6 and RCP8.5, in 2069-2099 is still around $\sim -10\%$ for RCP2.6, but it goes up to $\sim -35\%$ for RCP8.5; For RCP2.6, the changes in SSL are the results of a delay of 9 days in SSS, and an anticipation of 16 days on SSE for both periods. For RCP8.5 the variations in SSL are due to a delay of 13(1-19) days in SSS in 2020-2050 (2069-2099), and an anticipation of 18(54) days in SSE in 2020-2050 (2069-2099). The trend shown by the shortening of the Snow Seasons, and its cause found especially in the anticipation of the melting, are in accordance with previous studies which report a shortening of 2 week in 2035 and of 11 weeks in 2085 [44] considering the scenario A2 [1], analogous to RCP8.5 .

MHS is the Snow Metric whose mean experiences the largest reduction going down of 10% in the North and 13% in the South for RCP2.6, and of 12%(North)-16% (South) in 2020-2050 and 40%(North)-45%(South) in 2069-2099 for RCP8.5 (Table 12 and Table 13).

Table 12: Mean values of Relative (left) and Absolute (right) differences in RCP2.6 at macro-region scale

Mean of relative difference [%] RCP2.6				
Region	**Period**	**ΔMHS**	**Δ95HS**	**ΔSSL**
N	2020-2050	-9	-7	-11
	2060-2099	-10	-7	-12
S	2020-2050	-12	-9	-9
	2060-2099	-14	-10	-11

Mean of absolute difference [Days] RCP2.6	
ΔSSS	**ΔSSE**
+9	-16
+9	-17
+9	-15
+10	-15

Table 13: Mean values of Relative (left) and Absolute (right) differences in RCP8.5 at macro-region scale

Mean of relative difference [%] RCP8.5				
Region	**Period**	**ΔMHS**	**Δ95HS**	**ΔSSL**
N	2020-2050	-12	-9	-13
	2060-2099	-40	-31	-35
S	2020-2050	-16	-12	-12
	2060-2099	-46	-36	-34

Mean of absolute difference [Days] RCP8.5	
ΔSSS	**ΔSSE**
+13	-19
+14	-53
+13	-17
+19	-54

[1]The scenario A2 belongs to the Special Report on Emissions Scenarios (SRES), published by IPCC in 2001.The SRES define four narrative storylines, labelled A1, A2, B1 and B2, describing the relationships between the forces driving greenhouse gas and aerosol emissions and their evolution during the 21st century for large world regions and globally . Each storyline represents different demographic, social, economic, technological, and environmental developments that diverge in increasingly irreversible ways [26]

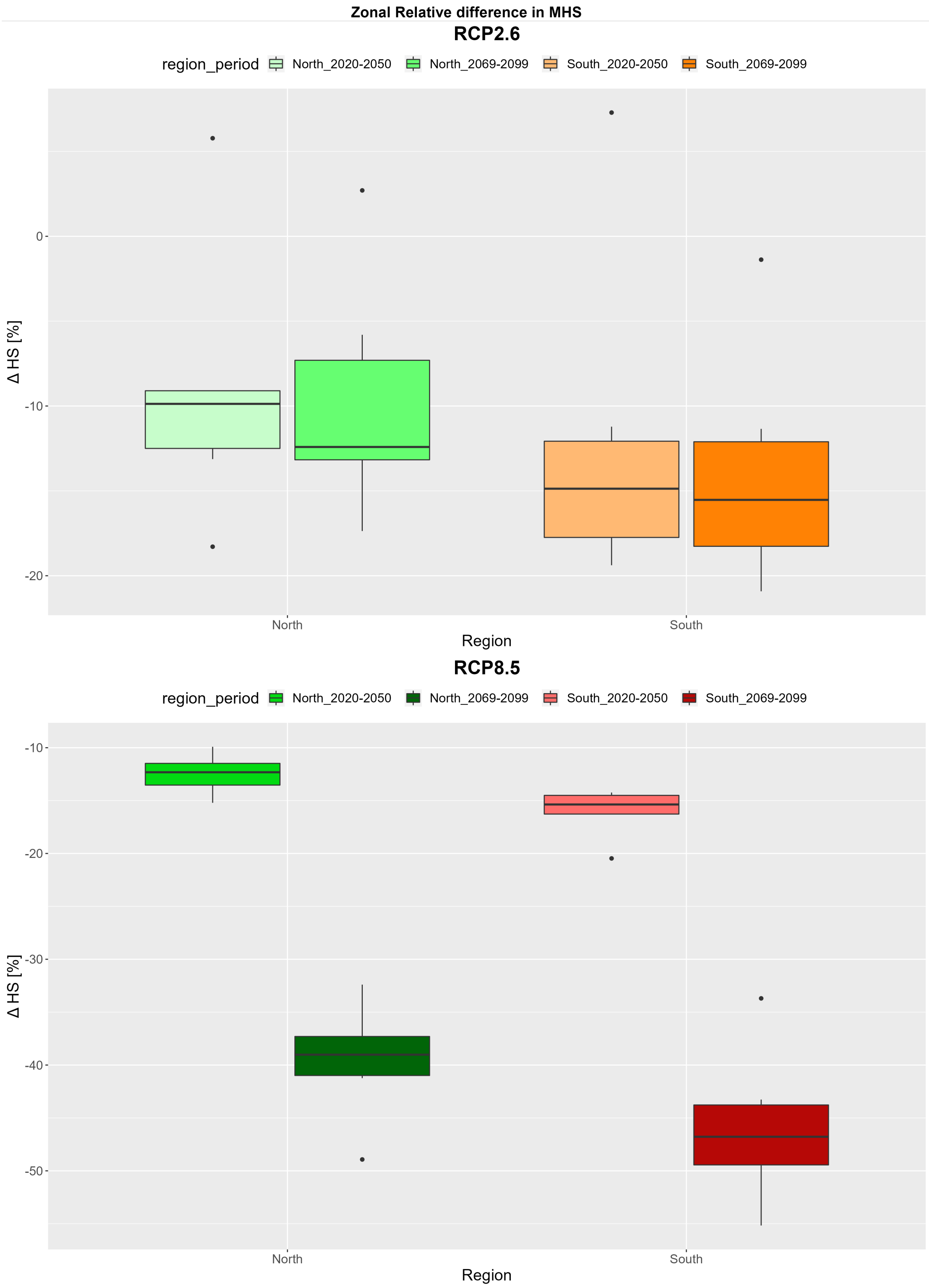

Figure 52: Relative difference in MHS between the Future periods (2020-2050, 2069-2099) and the Historical one, shown at macro-region scale. Top: RCP2.6. Bottom: RCP8.5. Macro-regions are subdivided by color: green for North, orange/red for South

Snow cover, and its characteristics, (SSL, SSS, SSE, MHS and 95HS) are strictly related to the changes in precipitation and air temperature, thus, to explain the observed changes in the Snow Metrics and the North-South behaviour MMTA, PSUM and MDTAA0 were analysed. In Figure 53 and 54 the Absolute difference in MMTA and Relative difference in MPSUM in the two macro-regions is reported.

For both RCPs and periods the northern high alpine terrains are projected to experience a higher increase in temperature with respect to the south. This difference between the two sides is expected especially in the summer months, while in winter and spring they show similar trends. For RCP2.6, MMTA is projected to increase, for both periods, up to $+3°C$ in July and August on the northern side, at up to $+2°C$ on the southern one. RCP8.5 shows an even further warming in summer of both sides at the End of Century: up to $+7.5°C$ in the north and $+6°C$ in the south.

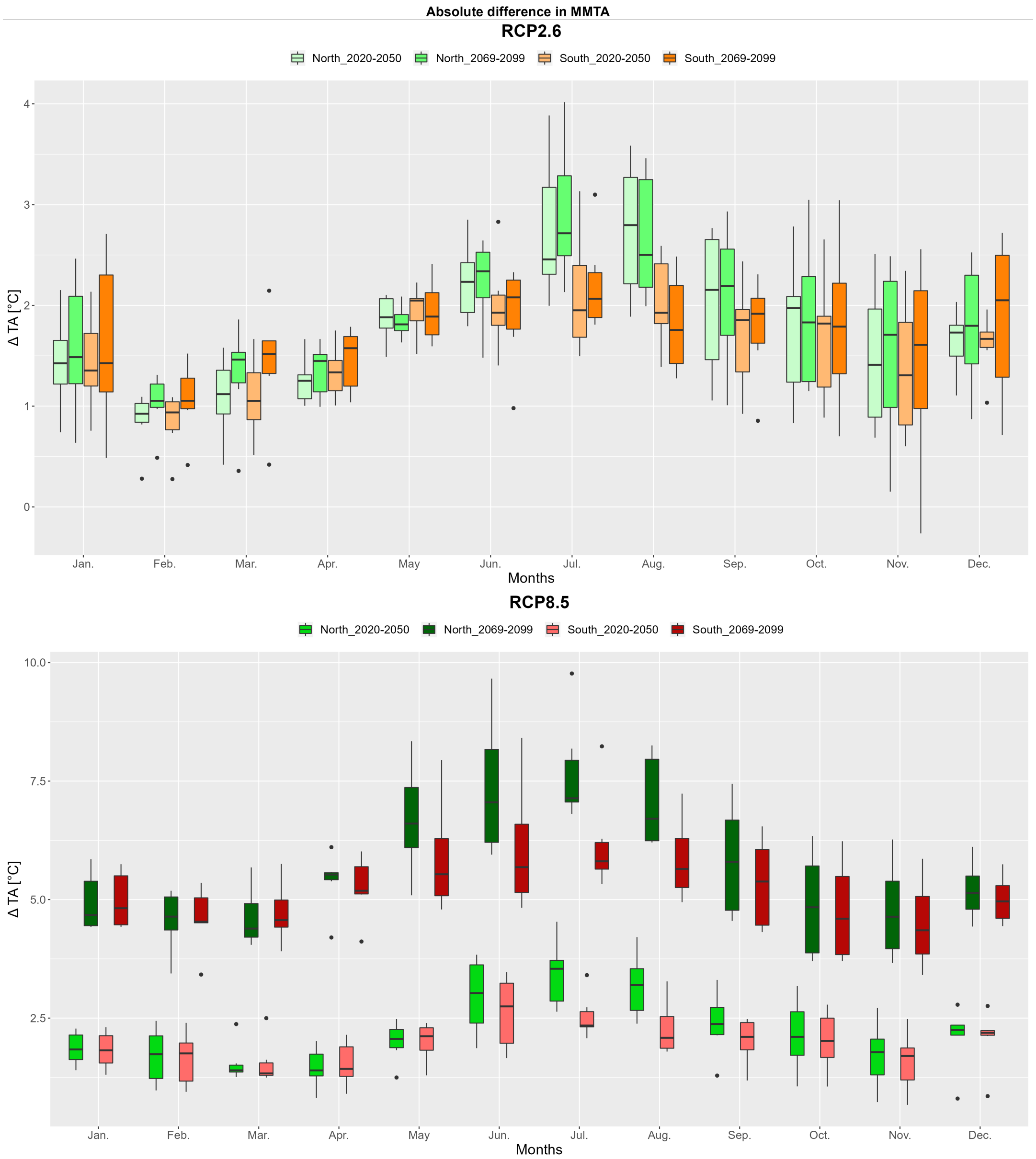

Figure 53: Absolute difference in Mean Monthly Air Temperature in the northern and southern sides of the Alps at Mid and End of Century with respect to the Historical period.

While the results are in accordance with Kotlarski et al. (2022) [8] for what concerns the months of maximum increase, they are not for what concerns the side that is expected to experience the larger rise. This might be due to the differences in the definition of North and South of the two studies: the south macro-region, for Kotlarski et al, includes both northern and southern sides of the present study (Figure 63 in Appendix E). Nevertheless, the results of the temperature gradients projected for both periods and scenarios in the current study are in accordance with the maps of temperature gradients in the study of Kotlarski et al. (2022) [8] (Figure 64 in Appendix E).

In accordance to previous studies [59], for what concerns MPSUM (Figure 54), RCP2.6 (top graph) shows a more homogeneous variation along the year even though winter months are expected to experience an increase in precipitation while summer month are expected to be drier. RCP8.5 (bottom graph), on the other hand, projects a stronger polarization of the precipitation in winter, resulting in drier summer. In both scenario and periods, the southern side is awaited to undergo a larger increase in precipitation in comparison to the northern one. An mean increase from 0 to 25% in winter (DJF) for RCP2.6 and from 0 to 50% in RCP8.5 is in accordance with the precipitation gradients maps reported in Kotlarski et al. (2022) [8] (Figure 65 in Appendix E).

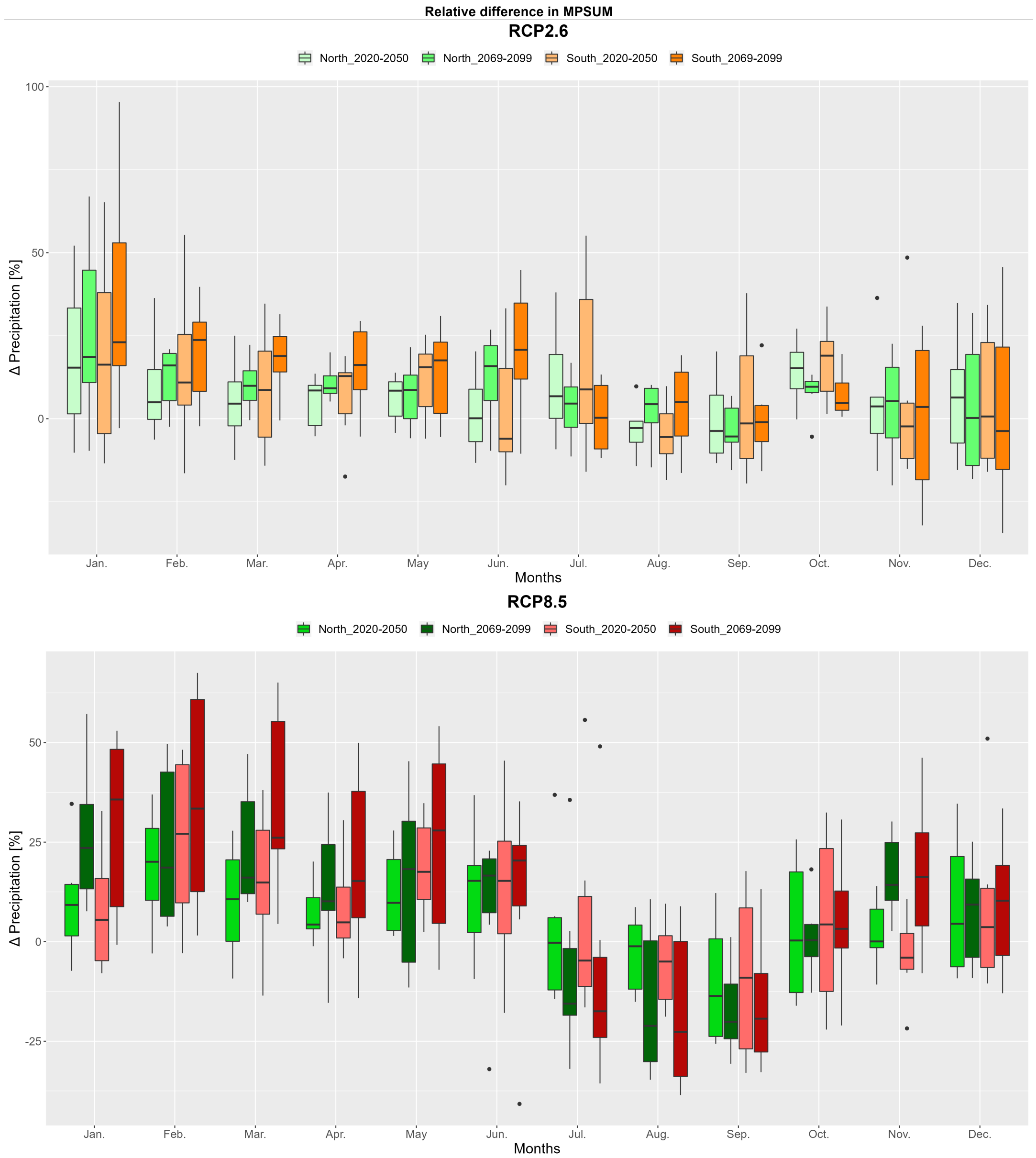

Figure 54: Relative difference in Monthly Precipitation in the northern and southern sides of the Alps at Mid and End of Century with respect to the Historical period.

The increase of winter precipitation may lead to the idea that it could offset the effects of the contemporaneous rise in air temperature. Previous studies, which however did not target high elevation terrains, indicate a stronger dominance of air temperature gradients effects [60]. This result would explain the result of Figure 52 for which MHS is awaited to be smaller in the south. Despite the precipitation analysis showed a stronger increase in the south, the turning point is given by the temperature increase: even though the norther side is expected to experience larger air temperature gradients in summer, along winter and spring months the gradients show the same magnitude on the both sides, altering the accumulation and melting periods. In fact, considering that the historical temperatures (Figure 55) are higher in the south, an analogous ΔTA in winter and spring, makes the south more incline to experience a continuous building-melting of the snowpack resulting in a smaller MHS.

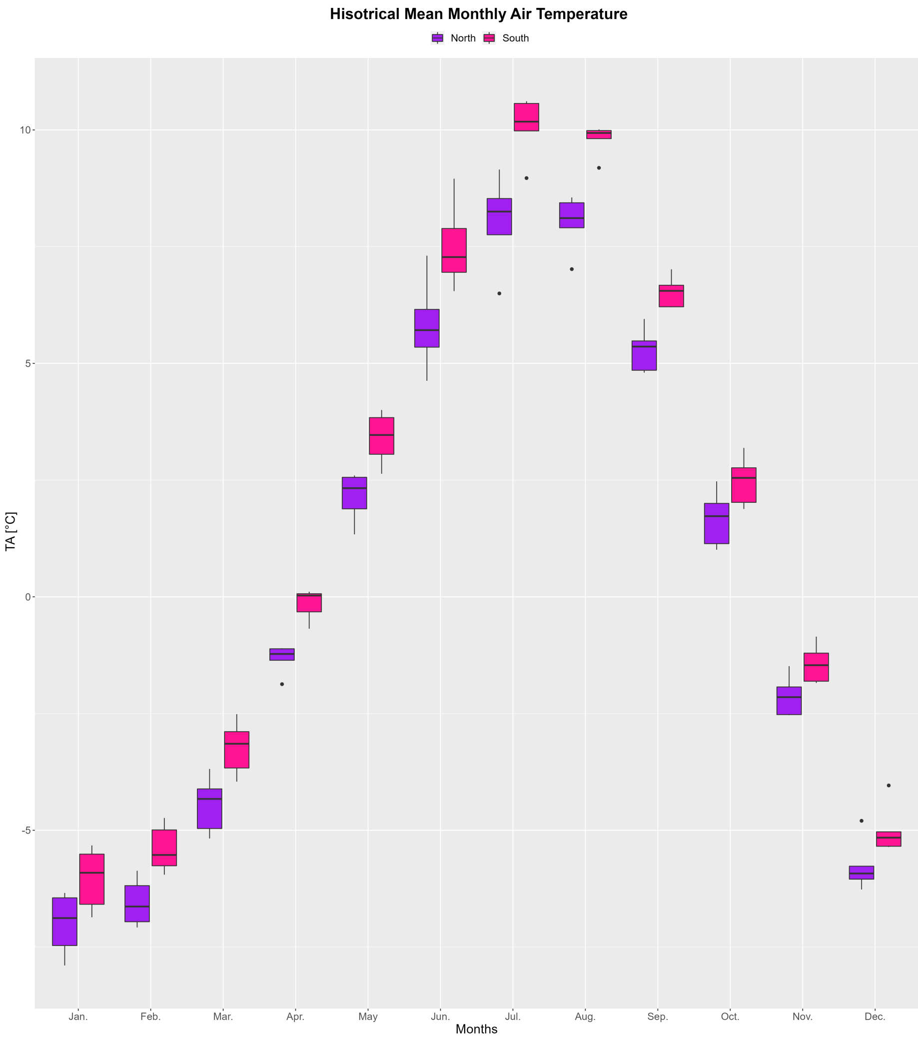

Figure 55: Historical MMTA values. North in purple, South in pink

Figure 56 shows MDTAA0 values that validate the previously made conjecture that the rise in TA is going to the major player in the changes in MHS over the Alps and that the Southern side TA is going to be often warmer than on the Northern side even though it is going to experience a less intense variation. It is, in fact, visible how the number of days for which mean TA is above 0°C, from January to May, is larger on the southern side for both scenarios and periods.

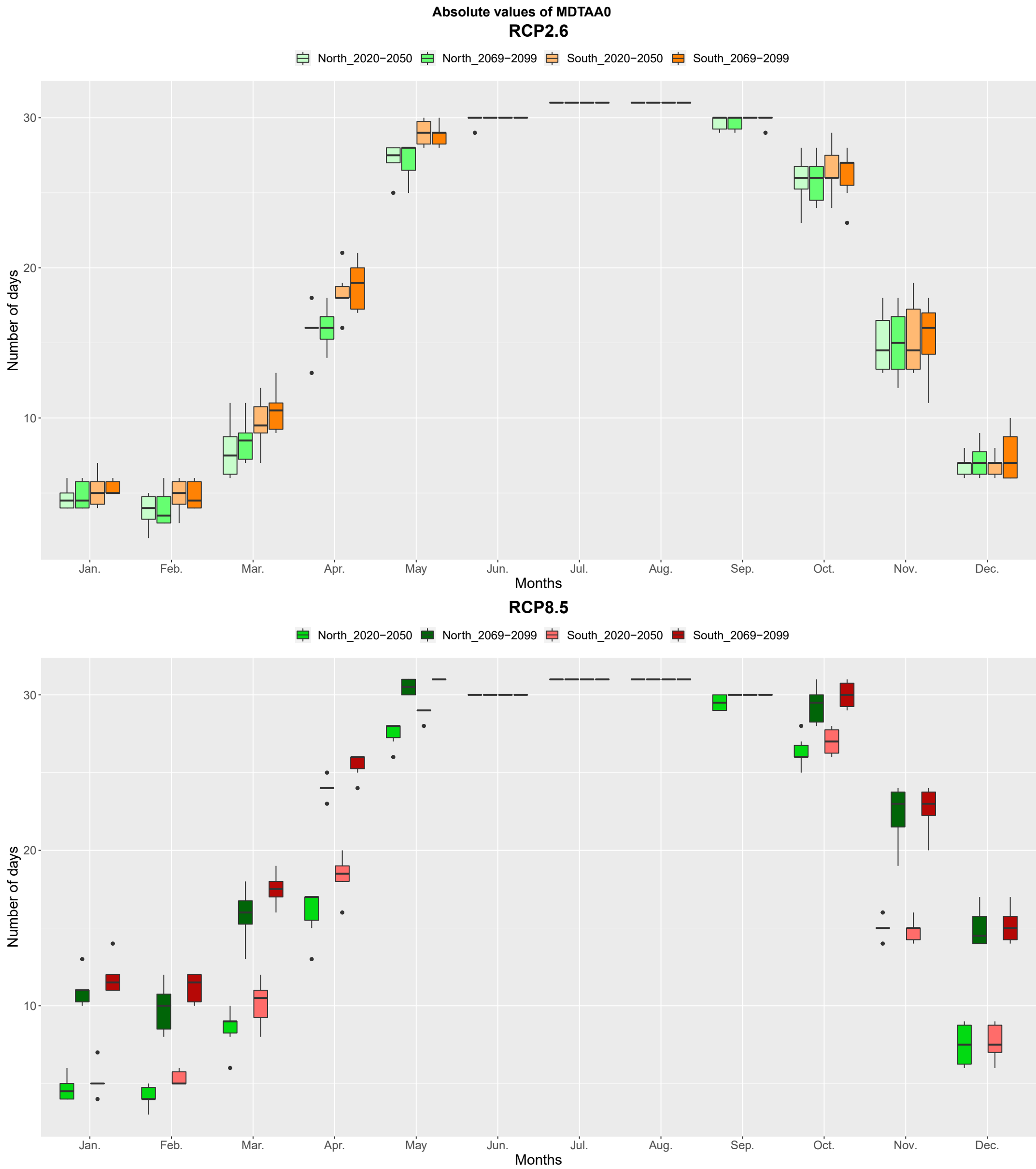

Figure 56: Absolute values of Mean monthly number of days with air temperature above 0°C MDTAA0. Top: RCP2.6. Bottom: RCP8.5

4.4 Consequences on hydrology: melted snow runoff

The Alps are well known to be the European *Water towers* as they store large quantities of water in form of snow and ice which gets partially released along the year. The discharge regime for rivers that origin in the Alpine region and transport water to the lowlands is influenced mainly by glaciers and snow. The changes in high alpine Snow Cover, thus, might have large implications on the downstream water supply as well as on the health of the whole catchment. Snow, when melts, creates a meltwater runoff that partially replenish the groundwater flow, partially flows as throughflow in the soil and partially becomes direct overland flow. Evaporation and plants transpiration aside, these three flows will contribute, with different timings, together with the precipitation, to the discharge of the river of the catchment. Thus, even though the link between snow runoff and river discharge is not straight forward, it is very strong. In this Section the Mid and End of Century meltwater runoffs are studied in comparison with the historical one.

4.4.1 Method

To study the changes in runoff a new variable had to be considered: *MS SN Runoff*. SNOWPACK provides it as an output. This variable is the flux of water leaving the snowpack as meltwater in terms of $[Kg\, m^{-2} h^{-1}]$.

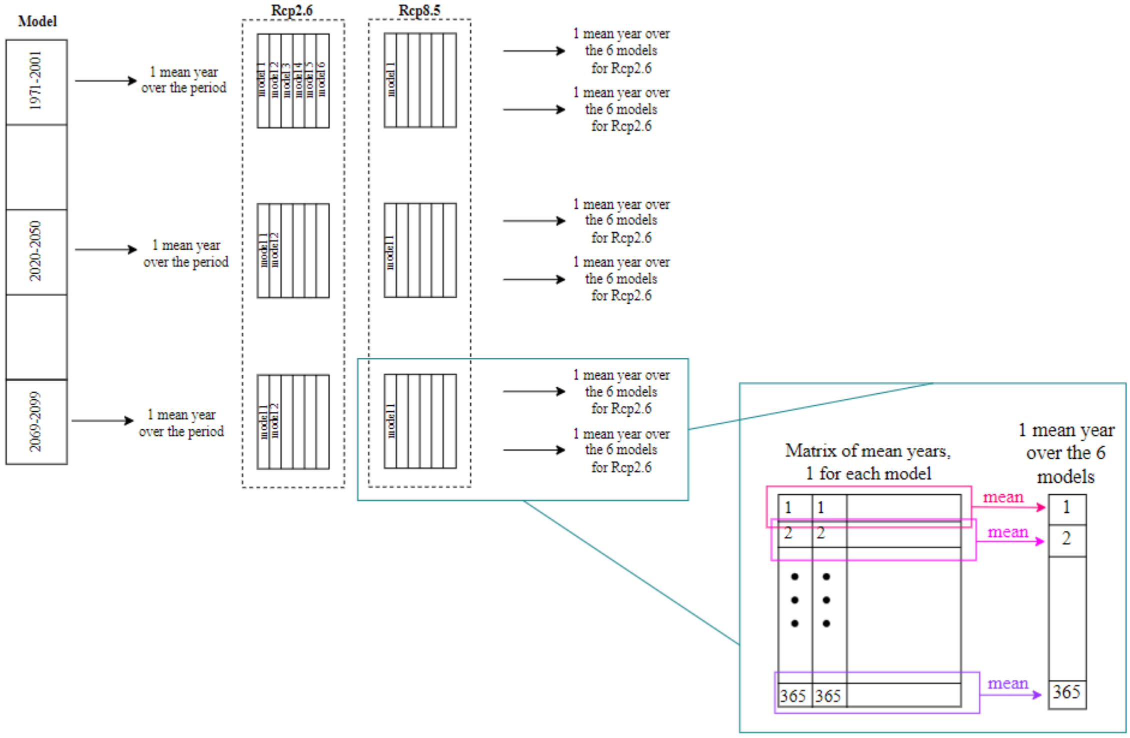

Figure 57: Scheme of the process to generate mean-year runoff data for each period and scenario at every station.

4.4.2 Results

Analogously to the behaviour found for Snow Metrics with respect to periods as scenarios, also the runoff shows similar differences with respect to the historical period for both periods of RCP2.6 and the Mid Century in RCP8.5, while the End of Century for RCP8.5 widely diverges. In the above mentioned period+scenarios that change analogously, 3 behaviours were detected in the variation of the runoff:

- Historical peak > Future peaks (RCP2.6 + 2020-2050 RCP8.5)
- Historical peak $\sim$ Future peaks (RCP2.6 + 2020-2050 RCP8.5)
- Historical peak < Future peaks (RCP2.6 + 2020-2050 RCP8.5)

Where the terms peak identifies the largest runoff among a window of 5 days in which the sum of the runoffs is maximum. 1/4 of the stations (CON2, KLO2,MEI2, PAR2) (Figure 58) show the first behaviour, 1/2 (CAM2, DTR2, FRA2, LUK2, MES2, NAR2, SIM2, TUJ3, ZER4) the second, 1/4 (ARO3, BED3,DAV2,DAV3) the third. For what concerns 2069-2099 in RCP8.5 the pattern is: strong reduction in peak value and strong anticipation of such peak.

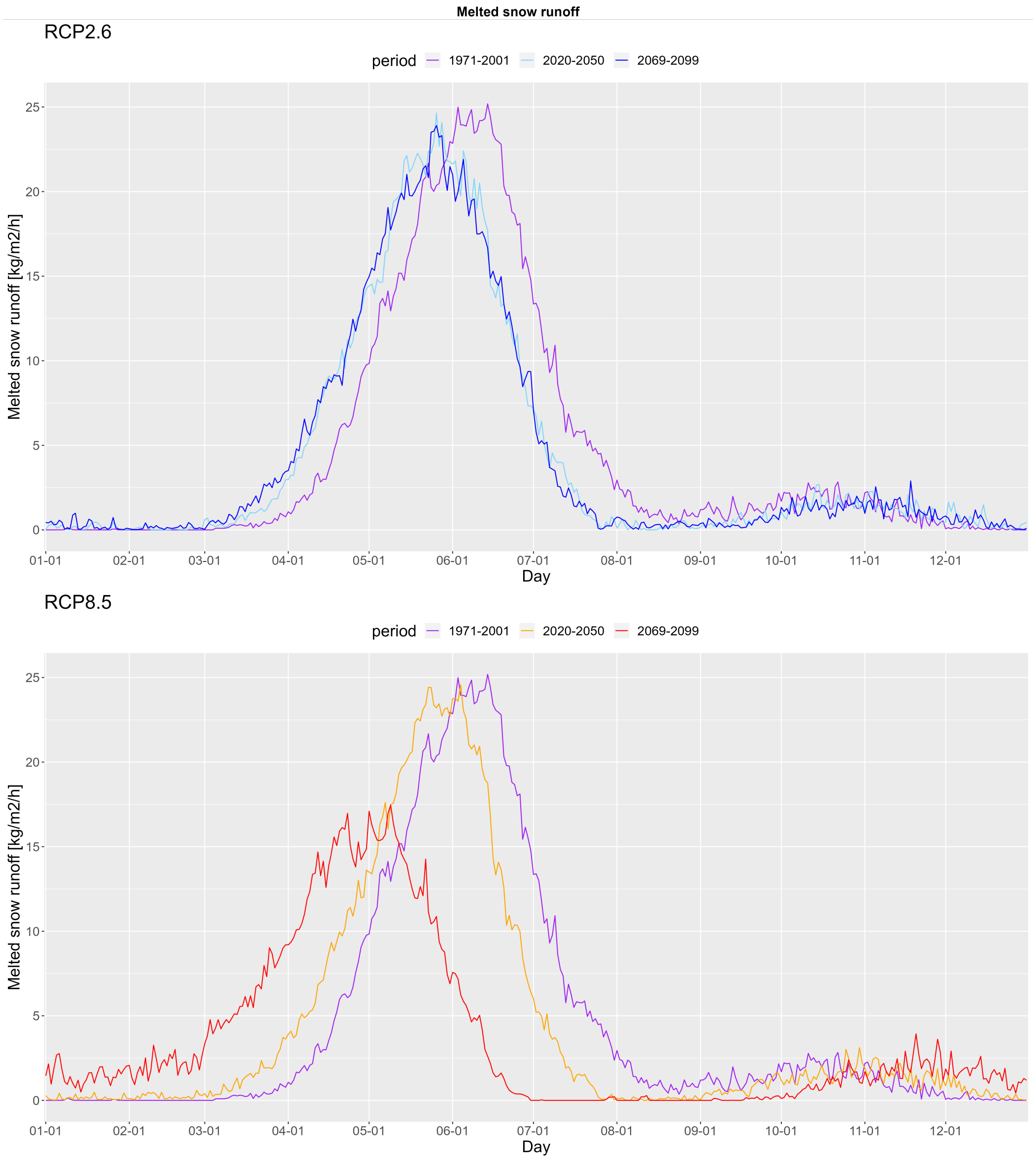

Figure 58: Mean-year runoff at Station CON2. Top: RCP2.6, Historical in purple, Mid Century in light-blue, End of Century in blue. Bottom: RCP8.5, Historical in purple, Mid Century in orange, End of Century in red

The common feature to all the periods and scenario is the anticipation of the peak of runoff (Figure 58). 3/4 of the stations, for RCP2.6 and 2020-2050 RCP8.5, show an anticipation of ~ 11 days, the remaining 1/4 of ~ 18 days. For what concerns 2069-2099 RCP8.5, all the stations show an anticipation of at least 35 days, with a mean of 40 days. Furthermore, it is important to note how, beside the peak, also the nature of the runoff changes:

- Historical period: the runoff starts, at the earliest at the beginning of March, with mean starting day on the 12^{th} of March, lasts around ~ 300 days, and goes to zero at the latest the last days of November, with mean ending day on the 17^{th} of November.
- RCP2.6 and 2020-2050 RCP8.5: it follows historical behaviour but with a tendency of going down to zero, or to very small flows, late July/August.
- 2069-2099 RCP8.5: the runoff goes to zero in summer rather than during winter (mean ending date on the 7^{th} of June) and in winter has a not negligible contribution to the water balance of the surrounding environment.

These results are in accordance with previous studies on the effect of climate change on rivers [11] [61]. The cause of the anticipation in the runoff peak can be traced back to the earlier increase in air temperature. As visible in the central graph in Figure 59, MMTA goes above 0°C a month earlier, reaching 2 months for RCP8.5 at the End of the Century. As visible in the top graph, MDTAA0 start to largely increase in the months of March and April for RCP2.6, kickstarting the melting in advance. For RCP8.5 at the End of the Century, MDTTA0 is much larger in any month, causing the previously seen continuous melting in the winter and spring months.

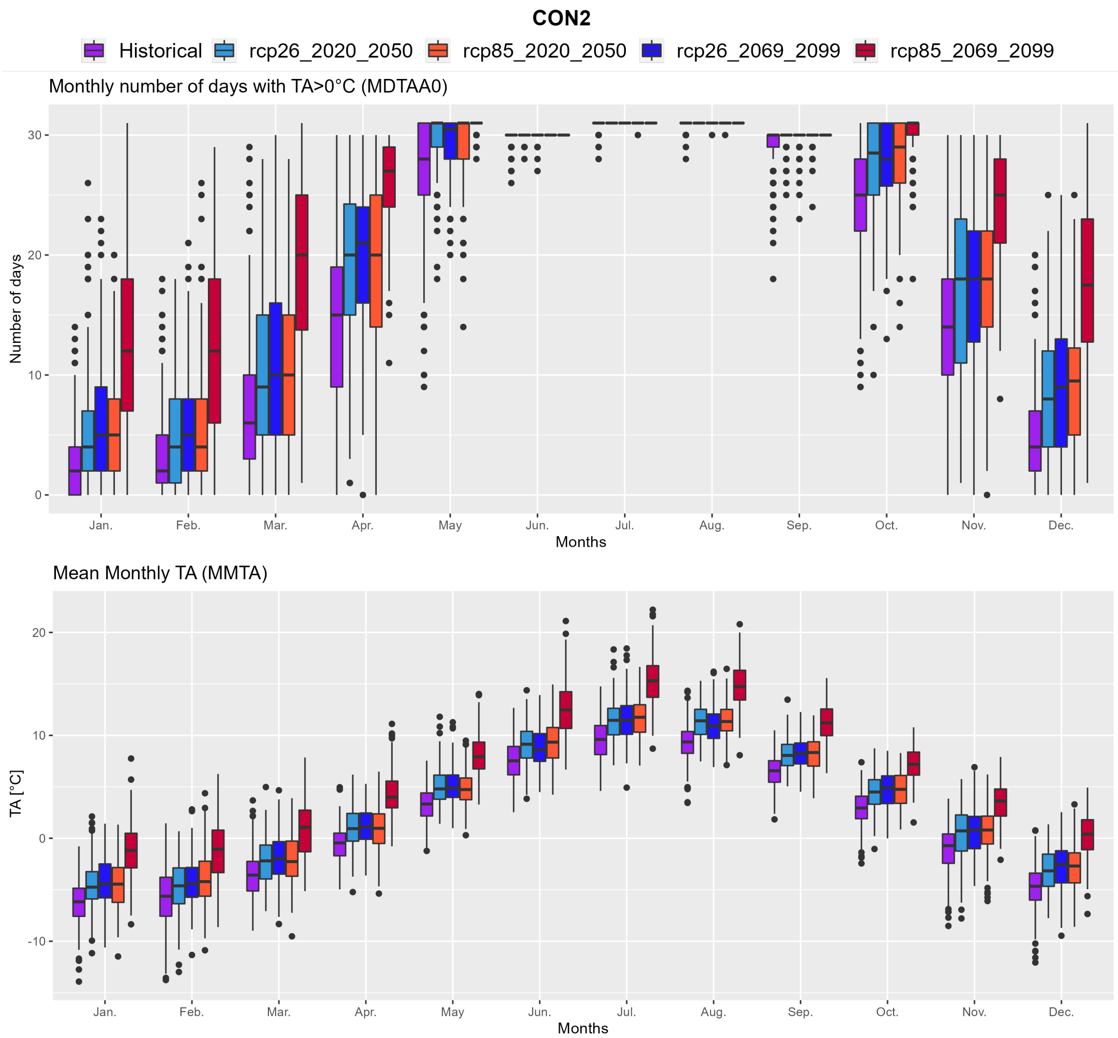

Figure 59: Climate Metrics at CON2 station. Bottom: MDTAA0. Top: MMTA. Historical values are shown in purple, RCP2.6 is shown in light-blue for 2020-2050, in blue for 2069-2099, RCP8.5 is shown in orange for 2020-2050, red for 2069-2099.

While in the Historical period, the supply of water from the snowpack to the surrounding environment continuously occurs from spring to beginning of winter, already in RCP2.6 and 2020-2050 RCP8.5 this supply becomes intermittent or absent in the middle of summer, to worsen for RCP8.5 when the snow contribution to the water balance of the catchment stretches from autumn to beginning of summer. This means that, also in the best case scenario (RCP2.6), in summer, when the water demand is the highest, alpine terrains around 2000 m.a.s.l. might not provide any meltwater-from-snow supply for at least a month, and in the worst case scenario (RCP8.5), by the End of Century, no contribution will arrive the whole summer and a bit of autumn.

5 Limitations

The findings of the present study have to be seen in light of some limitations.

7 main limitations were identified:

1. Limited number of stations especially on the southern side of the Alps
2. Limited number of used RCM
3. Neglect of solar exposure and shading in two steps of the study: (a) during the process of matching MCH-IMIS stations, as well as (b) during the impact analysis.
4. Use of reconstructed ILWR from SNOWPACK
5. Use of low resolution climate models
6. Daily resolution of climate models
7. Use of univariate QM
8. Use of artificial TA threshold for the precipitation partition

The listed limitations have different impacts on the study:

(1) A larger number of stations, located also on the Italian territory, would strengthen the trends within regions that are now too feeble. An attempt to acquire such data was done. However, due to both scarcity of data that would fit the requirements among the acquired ones and lack of time for a further and deeper research, it was not successful.

(2) A larger number of RCM could provide a further insight on the possible variability of the results. In this study, only two RCM were used as they were the only one available at the moment with the necessary variables, but future generations of climate models could over come this issue.

(3) Solar exposure plays an important role in the evolution of the snowpack as solar radiations cover a large share of the snowpack energy balance. (a) In the MCH-IMIS matching process a different approach could be used. Rather than having a single station for both PSUM and ISWR reconstruction, two stations could be used: the nearest for PUSM, as here done, and for ISWR the one with the most similar solar exposure among a pool of close stations. However, finding close stations with such characteristic is hard, as they have to be close enough not too have biases in cloudiness. (b) In the comparison of Climate Change effects within and between regions, taking into account the solar exposure and shading of the stations might highlight a difference response of the snowpack to future changes, especially for what concerns beginning and ending of the snow season.

(4) The absence of ILWR measurement at IMIS stations implied the need to rely on the inner SNOWPACK reconstruction. The resulting overestimation during melting period is likely to have affected to some extent the result concerning the Snow Season Ending date. However, thanks to the differences between future and historical value, the bias was lowered.

(5) No common signal due to the pixel was detected among the stations belonging to the same pixel, which means that it is not strictly necessary to look into more detail to have a local response. However, studies focused on comparing the results between low (50km) and high(<12km) resolution models showed that even though the results between the two models are in line, the high-resolution

climate models approach is strongly suggested in case of high altitudes and complex topography [62], as they would increase the accuracy of the results as they better represent local phenomena. In the current study models with higher resolution could not be used as too few RCP scenarios were available for such models, however more scenarios are likely to be released in the future.

(6) The daily resolution of the climate models undermines the reconstruction of the daily cycle of meteorological variables. According to the used disaggregation method this can have different implications e.g. for what concerns radiations, in case of clouds, this results in an average cloudiness along the whole day. Climate Models values are also available at higher temporal resolutions, however, for EURO-CORDEX hourly values are not validated yet.

(7) The use of the univariate QM did not allow the correction of the issue raised by the climate change model on the partition phase of precipitation as links between variables are not taken into account. The use of a multivariate QM process is likely to avoid such inconsistency eliminating, furthermore, the need of defining unrealistic air temperature thresholds.

(8) Even though TA thresholds were defined so that the mean cumulative solid precipitation curve of the models would be the closest to the one obtain considering the solid precipitation reconstructed from HS measurements, they were computed for the calibration period and strictly applied to the whole period 1971-2099. However, It is not sure that such assumption holds in the future. Setting a fixed temperature threshold does not indeed allow to account for future rises in temperature and, consequently, in a higher possibility for TA to be above the threshold. This might foster the already happening changes in snow cover. This problem could be solved applying a multivariate QM as it would not require the definition of the artificial TA thresholds.

6 Conclusions

The present research study aimed at studying the effects of Climate Change on the snow cover in Swiss Alpine terrains in the 21^{st} Century, with a specific eye on the differences between the northern and southern sides of the ridge. To do so, observation data from 18 meteorological stations located above 2000 m.a.s.l. were used in couple with EURO-CORDEX data, at 50km resolution (EUR-44). Two emission scenarios, RCP2.6 and RCP8.5, were considered to study the range of possible impacts at Mid Century (2020-2050) and End of Century (2069-2099) with respect to the Historical period of reference (1971-2001). Since the stations are spread across the whole Swiss alpine arc, clustering in Valais (North-West), at the border between Bern and Uri (North-Center), in Grison (North-East), and in Ticino (South), the results are believed to be representative of several local effects which can be found also in other stations.

Despite differences in magnitude, all stations showed a clear reduction in snow season length, with, as main cause, an earlier ending, rather than a delayed starting. In fact, while a rather homogeneous delay in Snow Season Starting date of 7-11 days, for RCP2.6 and 13-22 days for RCP8.5, was detected among all stations, the Snow Season is expected to end 15-18 days in advance for RCP2.6, and around 55 days for RCP8.5 in agreement with previous studies. It is noteworthy to mention that an analysis of the signal of stations belonging to the same climate change model pixel showed how the influence of the pixel is small in comparison to the local signal. This finding highlights how the use of punctual measurement data provided an added value to the simple analysis of the climate signal at pixel scale.

In accordance with earlier works [60], despite the increase of precipitation in winter, the reason of these changes is to be traced back mainly to the rise in temperatures. In fact, for RCP2.6, in half of the stations air temperature was shown to be above $0°C$ a month in advance (from May to April) already in the period 2020-2050, with the consequent stronger anticipation of the melting period, especially in the North-Center, North-East and Southern stations.

The described delays and anticipations are reflected in the changes in Snow Season Length, which projected it to shorten of 20-30 days for RCP2.6 and 80-92 for RCP8.5 day by 2069-2099. Furthermore, the results demonstrate a simultaneous reduction in both Mean Snow Height and maximum Snow Height. The stations in the South and North-Center are the ones experiencing the largest impact on Mean Snow Height, with a reduction of 12-16% ($\sim$ 16-20 cm) in 2020-2050, and 14-45% ($\sim$ 20-60 cm) in 2069-2099. The least affected stations, in the North-West, showed how no less than a reduction of 8% can be expected.

The larger overview of climate signal on the Northern and Southern side of the Alps show a flattening of the differences in Snow Metrics across the mountain ridge despite a strong variation with respect to historical values. Solely Mean Snow Height is expected to be more largely impacted on the Southern side with respect to the Northern one: results show, in fact, a reduction of 10% in the North in contrast with the 13% in the South for RCP2.6, and of 12%(North)-16% (South) in 2020-2050 and 40%(North)-45%(South) in 2069-2099 for RCP8.5. This different signal on the two sides can be traced back to the rising temperatures: despite a larger increase in precipitation and temperature on the Northern side, the Southern side is expected to still be the warmer slope during winter and spring months. Thus, the smaller Mean Snow Height reflects the expected continuous building-melting of the snowpack as result of the warmer temperatures on this side.

The meltwater runoff from snow is likely to be heavily affected due to the changes in snowcover. The historical bell-shaped regime with a long tail till winter is going to give way, in the best scenario (RCP2.6), to a shorter tail, ending in summer, and a shift of 11-18 days of the maximum release towards the beginning of the year. In the worst case (RCP8.5), the results show a reduction of 7[mm/h] at the peak and an anticipation of 40 days of the maximum release. Furthermore, a continuous meltwater supply is expected along the whole winter due to higher temperatures at the expenses of summer days which will see a drop to 0 [mm/h] by the end of July. Both the anticipation of the peak in runoff and the continuous meltwater flux can be linked to the increase in air temperature. These new regimes may cause reductions in snow-meltwater supply in summer month, not only for drinkable water but for energy production as well. In a country, like Switzerland, where 12.3% of the total energy consumption comes from hydropower, it may have a large impact.

As a suggestion for further steps and improvements, the author proposes to work on the limitations of the methodology of the present study as well as on the criticality that the present generation of climate change model showed. Firstly, due to time restrictions, data from a limited number of stations could be collected while a larger number of stations would strengthen the trends within regions that are now too feeble. Secondly, an analysis taking into account the sun exposure of the stations would avoid possible biases in the comparisons of the results. Furthermore, the use of a multivariate QM would eliminate the need of defining unrealistic air temperature thresholds which might foster the changes in snowcover. Additionally, future generations of climate model chains are expected to overcome the shortage of high resolution models (<12km) with a plurality of scenarios, as well as an increased number of available RCM with a large abundance of variables and validated hourly data. Higher resolution models would increase the reliability of the results as local phenomena liked to orography would be better described, a larger number of RCM would instead provide a larger view on the possible variability of the future results. As in this study hourly resolution was necessary, it would eliminate the need for disaggregation processes, eliminating the biases in the daily cycles of variables.

Acknowledgements

I would like to express my deep gratitude to Dr. Adrien Michel, my research supervisor, who guided me with his advises, patience and encouragements through the whole research and writing process. Our discussions and his constructive suggestions helped me to develop my personal skills as young researcher which I will treasure for my future career. I would like to also thank him as Adrien, not as supervisor, for the good spirit he has shown in all these months making me laugh even when I found it hard to.

Furthermore, I am particularly grateful for the help, support and opportunity given me by Professor Michael Lehning who invested time on my study and welcomed me first in CRYOS group at EPFL and then in the Snow Processes research group at SLF, allowing me to step into the world of scientific research.

I wish also to acknowledge the help provided by Professor Jost von Hardenberg, who reviewed my work providing valuable support.

I would also like to thank very much the people that made my staying in Switzerland a great adventure: firstly my flatmates in Lausanne, with whom I learned what it means to live in a house full of people, sharing good and bad days and receiving support in every moment, then to the whole CRYOS group that made me feel welcomed right away and, between a coffee and a beer at Sat, helped me to grow as a young engineer, thirdly, to my WG-mates in Davos who turned the Cave into a Home. Very special thanks go to Claudia, Mahdi, Caro and Riccardo without whom all of this would have not been the same.

I would like to also thank who supported me from back home. A strong thanks goes to Valentina, with whom the distance was only physical. I am particularly grateful to Giulio, who understood how important this experience would have been for me and supported me along the way, and to my parents who never stopped pushing me to believe in myself and in what I was doing not only in the last few months but along my whole academic journey. Last but not least, I want to strongly thank the two people that have been with me at every step of these two years, of which this thesis is only the conclusion: Alessia and Luca. Even though spread across Europe our friendship has often been a safe haven.

Thank you, thank you all for making this rollercoaster an amazing journey.

Appendices

Appendix A

- Model 1 = KNMI-RACMO22E + MOHC-HadGEM2-ES
- Model 2 = SMHI-RCA4 + ICHEC-EC-EARTH
- Model 3 = SMHI-RCA4 + MIROC-MIROC5
- Model 4 = SMHI-RCA4 + MOHC-HadGEM2-ES
- Model 5 = SMHI-RCA4 + MPI-M-MPI-ESM-LR
- Model 6 = SMHI-RCA4 + NCC-NorESM1-M

Station	TA Threshold											
	Model 1 Rcp2.6	Model 1 Rcp8.5	Model 2 Rcp2.6	Model 2 Rcp8.5	Model 3 Rcp2.6	Model 3 Rcp8.5	Model 4 Rcp2.6	Model 4 Rcp8.5	Model 5 Rcp2.6	Model 5 Rcp8.5	Model 6 Rcp2.6	Model 6 Rcp8.5
ARO3	1.8	2.2	3.4	3.8	4	4	3	2.8	3.4	3.4	3	3.4
CON2	2.2	2.8	3.8	3.2	3.8	3.4	2.6	2.8	3.4	3	3.4	3.2
DAV2	2.4	2.8	3.8	4	4	4	3.4	3.2	4	3.8	3.8	4
DAV3	2.4	2.8	4	4	4	4	3.4	3.4	4	4	3.8	4
GUT2	4	4	4	4	4	4	4	4	4	4	4	4
KLO2	2.4	3.2	4	4	4	4	3.8	4	4	4	4	4
LUK2	1.2	1.6	2.4	2.4	2.8	3.2	2.2	2.2	2.4	2.2	2.2	2.2
MEI2	2.2	3.2	3.4	3	3.2	3.2	2.4	2.8	3.4	3	3.4	3.4
PAR2	2.4	3	3.4	3.4	3.6	3.4	2.8	2.6	3.2	3	3.6	3.2
TUJ3	3	3.6	4	4	4	4	4	4	4	4	4	4
ZER4	2.8	3.2	4	4	4	4	4	4	4	4	4	4
BED3	2.2	3	4	3.8	4	4	3.6	3.8	4	4	4	4
CAM2	2.4	2.8	3.6	3.6	4	4	3.4	3.6	3.6	4	4	3.6
DTR2	3	3.6	4	3.8	4	4	3.6	4	4	4	4	4
FRA2	3.4	3.8	4	4	4	4	4	4	4	4	4	4
MES2	1.6	2	3	3.2	3.4	4	2.4	2.6	3.2	2.6	3	3.6
NAR2	2.8	3.2	4	4	4	4	4	4	4	4	4	4
SIM2	1.4	2	3.2	3	3.4	3.6	2.6	2.6	3.	3	2.8	3.4

Appendix B

.INI FILE:

```
[Input]
COORDSYS = CH1903
TIME_ZONE = 1
METEO = SMET
METEOPATH = input/
STATION1 = Time_adapted_Disaggregated_QM_EUR-44_KNMI-
    RACMO22E_MOHC-HadGEM2-ES_r1i1p1_rcp26_1971-2099_ARO3
SNOW = SMET
SNOWPATH = input/
SNOWFILE1 = SOIL

[Output]
COORDSYS = CH1903
TIME_ZONE = 1
METEOPATH = output/
WRITE_PROCESSED_METEO = FALSE
EXPERIMENT = FINAL_Time_adapted_Disaggregated_QM_EUR-44_KNMI-
    RACMO22E_MOHC-HadGEM2-ES_r1i1p1_rcp26_1971-2099_ARO3
SNOW_WRITE = FALSE
PROF_WRITE = TRUE
PROF_FORMAT = PRO
AGGREGATE_PRF = FALSE
PROF_START = 0.0
PROF_DAYS_BETWEEN = 0.04166667
TS_WRITE = TRUE
TS_FORMAT = SMET
TS_START = 0.0
TS_DAYS_BETWEEN = 0.04166667
OUT_HAZ = FALSE
FIRST_BACKUP = 100000

CUMSUM_MASS = FALSE
PRECIP_RATES = TRUE
OUT_CANOPY = FALSE
OUT_HAZ = FALSE
OUT_SOILEB = FALSE
OUT_HEAT = TRUE
OUT_T = TRUE
OUT_LW = TRUE
OUT_SW = TRUE
OUT_MASS = TRUE
```

```
OUT_METEO = TRUE
OUT_STAB = TRUE

[Snowpack]
CALCULATION_STEP_LENGTH = 15.0
ROUGHNESS_LENGTH = 0.002
HEIGHT_OF_METEO_VALUES = 7.5
HEIGHT_OF_WIND_VALUE = 7.5
ENFORCE_MEASURED_SNOW_HEIGHTS = FALSE
SW_MODE = INCOMING
ATMOSPHERIC_STABILITY = MO_HOLTSLAG
CANOPY = 0
MEAS_TSS = FALSE
CHANGE_BC = FALSE
THRESH_CHANGE_BC = -1
SNP_SOIL = TRUE
SOIL_FLUX = TRUE
GEO_HEAT = 0.06

[SnowpackAdvanced]
T_CRAZY_MIN = 100
THRESH_RAIN = 1.8

[Filters]
ENABLE_METEO_FILTERS = TRUE
TA::FILTER1 = MIN_MAX
TA::ARG1::MIN = 240
TA::ARG1::MAX = 320
RH::FILTER1 = MIN_MAX
RH::ARG1::MIN = 0.01
RH::ARG1::MAX = 1.2
RH::FILTER2 = MIN_MAX
RH::ARG2::SOFT = TRUE
RH::ARG2::MIN = 0.05
RH::ARG2::MAX = 1.0
RSWR::FILTER1 = MIN_MAX
RSWR::ARG1::MIN = -10
RSWR::ARG1::MAX = 1500
RSWR::FILTER2 = MIN_MAX
RSWR::ARG2::SOFT = TRUE
RSWR::ARG2::MIN = 0
RSWR::ARG2::MAX = 1500
TSS::FILTER1 = MIN_MAX
TSS::ARG1::MIN = 200
```

```
TSS::ARG1::MAX = 320
TSG::FILTER1 = MIN_MAX
TSG::ARG1::MIN = 200
TSG::ARG1::MAX = 320
VW::FILTER1 = MIN_MAX
VW::ARG1::MIN = -2
VW::ARG1::MAX = 70
VW::FILTER2 = MIN_MAX
VW::ARG2::SOFT = TRUE
VW::ARG2::MIN = 0.2
VW::ARG2::MAX = 50.0
ENABLE_TIME_FILTERS = TRUE

[Interpolations1D]
RSWR::linear    = extrapolate
ISWR::linear    = extrapolate
ILWR::linear    = extrapolate
ENABLE_RESAMPLING = TRUE
WINDOW_SIZE = 43200
PSUM::RESAMPLE = ACCUMULATE
PSUM::ACCUMULATE::PERIOD = 900
HS::RESAMPLE = LINEAR
TSS::RESAMPLE = LINEAR
TA::RESAMPLE = LINEAR
TSG::RESAMPLE = LINEAR
RH::RESAMPLE = LINEAR
VW::RESAMPLE = NEAREST
VW::NEAREST::EXTRAPOLATE = TRUE
RSWR::RESAMPLE = LINEAR
ISWR::RESAMPLE = LINEAR
ILWR::RESAMPLE = LINEAR
DW::RESAMPLE = NEAREST
DW::NEAREST::EXTRAPOLATE = TRUE

[Generators]
RH::GENERATORS = CST
RH::CST::VALUE = 0.700000
PSUM::GENERATORS = CST
PSUM::CST::VALUE = 0.000000
TA::GENERATORS = SIN
TA::SIN::TYPE = Yearly
TA::SIN::MIN = 268.260000
TA::SIN::MAX = 285.560000
TA::SIN::PHASE = 0.083000
```

VW : : GENERATORS = CST
VW : : CST : : VALUE = 1.000000
DW : : GENERATORS = CST
DW : : CST : : VALUE = 0
TSG : : GENERATORS = CST
TSG : : CST : : VALUE = 273.150000
ISWR : : GENERATORS = CST
ISWR : : CST : : VALUE = 0
HS : : GENERATORS = CST
HS : : CST : : VALUE = 0

Appendix C

Metrics Statistics						
Station	Dataset	Metric	Mean	Median	95%	25%
ARO3	Reconstructed Timeseries	SSL	195	205	213	175
		SSS	325°	320°	352°	314°
		ESS	156 °	158°	171°	152°
		MHS	0.99	1.01	1.25	0.84
		95HS	1.70	1.63	2.16	1.5
	Joined CC Models	SSL	223	225	269	208
		BSS	305°	304°	335°	294°
		ESS	164°	163°	191°	152°
		MHS	1.03	1	1.61	0.82
		95HS	2.13	2.09	3.06	1.8
BED3	Reconstructed Timeseries	SSL	238	240	271	284
		SSS	296°	299°	316°	284°
		SSE	170 °	168°	185°	166°
		MHS	1,72	1.53	2.51	1.39
		95HS	3.25	2.76	4.82	2.66
	Joined CC Models	SSL	251	249	289	235
		SSS	295°	296°	319°	285°
		SSE	182°	182°	208°	172°
		MHS	1.72	1.65	2.58	1.39
		95HS	3.50	3.44	4.70	3.02
CAM2	Reconstructed Timeseries	SSL	218	218	244	204
		SSS	312	310	331	303
		SSE	165	165	179	163
		MHS	1.62	1.47	2.22	1.31
		95HS	2.84	2.61	3.90	2.43
	Joined CC Model	SSL	248	248	283	230
		SSS	297	296	321	286
		SSE	180	179	207	168
		MHS	1.65	1.60	2.49	1.30
		95HS	3.19	3.15	4.29	2.65
CON2	Reconstructed Timeseries	SSL	219	220	241	214
		SSS	313	310	330	307
		SSE	167	167	184	159
		MHS	1.82	1.74	2.52	1.47
		95HS	3.13	3.23	4.02	2.74
	Joined CC Models	SSL	235	235	274	221

Metrics Statistics						
Station	Dataset	Metric	Mean	Median	95%	25%
DAV2	Reconstructed Timeseries	SSL	222	222	245	210
		SSS	310	309	332	300
		SSE	166	166	179	162
		MHS	1.17	1.10	1.65	0.94
		95HS	2.08	2.11	2.72	1.76
	Joined CC Models	SSL	246	244	289	229
		SSS	296	297	322	284
		SSE	177	175	206	166
		MHS	1.24	1.20	1.85	0.98
		95HS	2.40	2.36	3.21	2.09
DAV3	Reconstructed Timeseries	SSL	228	228	250	221
		SSS	306	305	322	300
		SSE	169	169	181	163
		MHS	1.33	1.20	1.75	1.15
		95HS	2.28	2.18	2.89	2.00
	Joined CC Models	SSL	241	240	286	225
		SSS	300	300	326	289
		SSE	176	175	207	165
		MHS	1.26	1.22	1.84	1.00
		95HS	2.48	2.46	3.35	2.13
DTR2	Reconstructed Timeseries	SSL	180	188	206	165
		SSS	298	314	357	309
		SSE	143	146	155	137
		MHS	0.99	0.95	1.42	0.85
		95HS	1.78	1.65	2.39	1.44
	Joined CC Models	SSL	206	205	248	188
		SSS	310	308	339	297
		SSE	149	151	174	137
		MHS	0.94	0.91	1.59	0.68
		95HS	1.94	1.90	2.80	1.56
GUT2	Reconstructed Timeseries	SSL	183	185	206	170
		SSS	327	328	350	313
		SSE	144	144	163	131
		MHS	0.98	1.00	1.29	0.80
		95HS	1.87	1.79	2.69	1.53
	Joined CC Models	SSL	193	189	244	174
		SSS	312	317	349	303
		SSE	146	148	174	135

Metrics Statistics						
Station	Dataset	Metric	Mean	Median	95%	25%
KLO2	Reconstructed Timeseries	SSL	190	198	215	180
		SSS	325	326	350	309
		SSE	150	150	165	143
		MHS	1.14	1.10	1.42	0.97
		95HS	1.97	1.90	2.43	1.74
	Joined CC Models	SSL	214	216	259	189
		SSS	307	306	337	295
		SSE	155	157	180	144
		MHS	1.11	1.10	1.66	0.84
		95HS	2.22	2.24	3.17	1.77
LUK2	Reconstructed Timeseries	SSL	248	245	272	239
		SSS	308	308	323	302
		SSE	190	190	207	181
		MHS	2.17	2.20	2.82	1.77
		95HS	3.82	3.73	4.83	3.38
	5* Joined CC Models	SSL	275	270	322	253
		SSS	294	293	318	284
		SSE	201	200	239	186
		MHS	2.17	2.14	3.09	1.79
		95HS	4.10	4.06	5.36	3.48
MEI2	Reconstructed Timeseries	SSL	200	206	217	193
		SSS	322	322	342	310
		SSE	157	158	172	153
		MHS	1.44	1.46	1.94	1.22
		95HS	2.57	2.66	3.44	2.25
	Joined CC Models	SSL	222	221	265	203
		SSS	308	308	336	298
		SSE	164	165	190	153
		MHS	1.35	1.30	2.09	0.98
		95HS	2.76	2.69	3.85	2.33
MES2	Reconstructed Timeseries	SSL	219	218	243	205
		SSS	312	306	338	302
		SSE	165	167	181	158
		MHS	1.30	1.27	1.80	1.02
		95HS	2.39	2.42	3.02	1.98
	Joined CC Models	SSL	240	240	285	224
		SSS	297	297	322	286
		SSE	172	172	200	161

Metrics Statistics						
Station	Dataset	Metric	Mean	Median	95%	25%
NAR2	Reconstructed Timeseries	SSL	191	198	222	176
		SSS	321	315	355	308
		SSE	147	150	158	141
		MHS	1.12	1.12	1.49	1.00
		95HS	2.00	2.09	2.61	1.70
	Joined CC Models	SSL	223	223	263	204
		SSS	305	304	331	296
		SSE	163	163	187	153
		MHS	1.20	1.16	1.86	0.92
		95HS	2.29	2.24	3.23	1.90
PAR2	Reconstructed Timeseries	SSL	208	210	231	203
		SSS	316	311	339	308
		SSE	159	160	176	154
		MHS	1.20	1.20	1.73	1.03
		95HS	2.10	2.13	2.94	1.78
	Joined CC Models	SSL	229	232	272	209
		SSS	302	302	328	289
		SSE	166	167	196	155
		MHS	1.27	1.26	2.03	0.94
		95HS	2.52	2.50	3.42	2.11
SIM2	Reconstructed Timeseries	SSL	215	215	244	209
		SSS	288	306	326	302
		SSE	167	172	180	159
		MHS	1.32	1.31	1.87	1.06
		95HS	2.36	2.37	3.24	2.10
	Joined CC Models	SSL	252	250	294	235
		SSS	297	296	324	286
		SSE	184	183	212	172
		MHS	1.49	1.44	2.26	1.15
		95HS	2.92	2.88	3.96	2.43
TUJ3	Reconstructed Timeseries	SSL	206	212	234	196
		SSS	317	310	354	305
		SSE	157	157	170	154
		MHS	1.34	1.28	1.82	1.08
		95HS	2.37	2.19	3.33	1.89
	Joined CC Models	SSL	241	239	285	227
		SSS	300	300	326	289
		SSE	175	175	203	165

Metrics Statistics						
Station	Dataset	Metric	Mean	Median	95%	25%
ZER4	Reconstructed Timeseries	SSL	197	200	224	183
		SSS	318	310	348	306
		SSE	149	152	160	145
		MHS	1.04	1.01	1.37	0.84
		95HS	1.75	1.71	2.40	1.44
	Joined CC Models	SSL	241	239	285	227
		SSS	300	300	326	289
		SSE	175	175	203	165
		MHS	1.39	1.33	2.06	1.09
		95HS	2.69	2.63	3.77	2.31

Appendix D

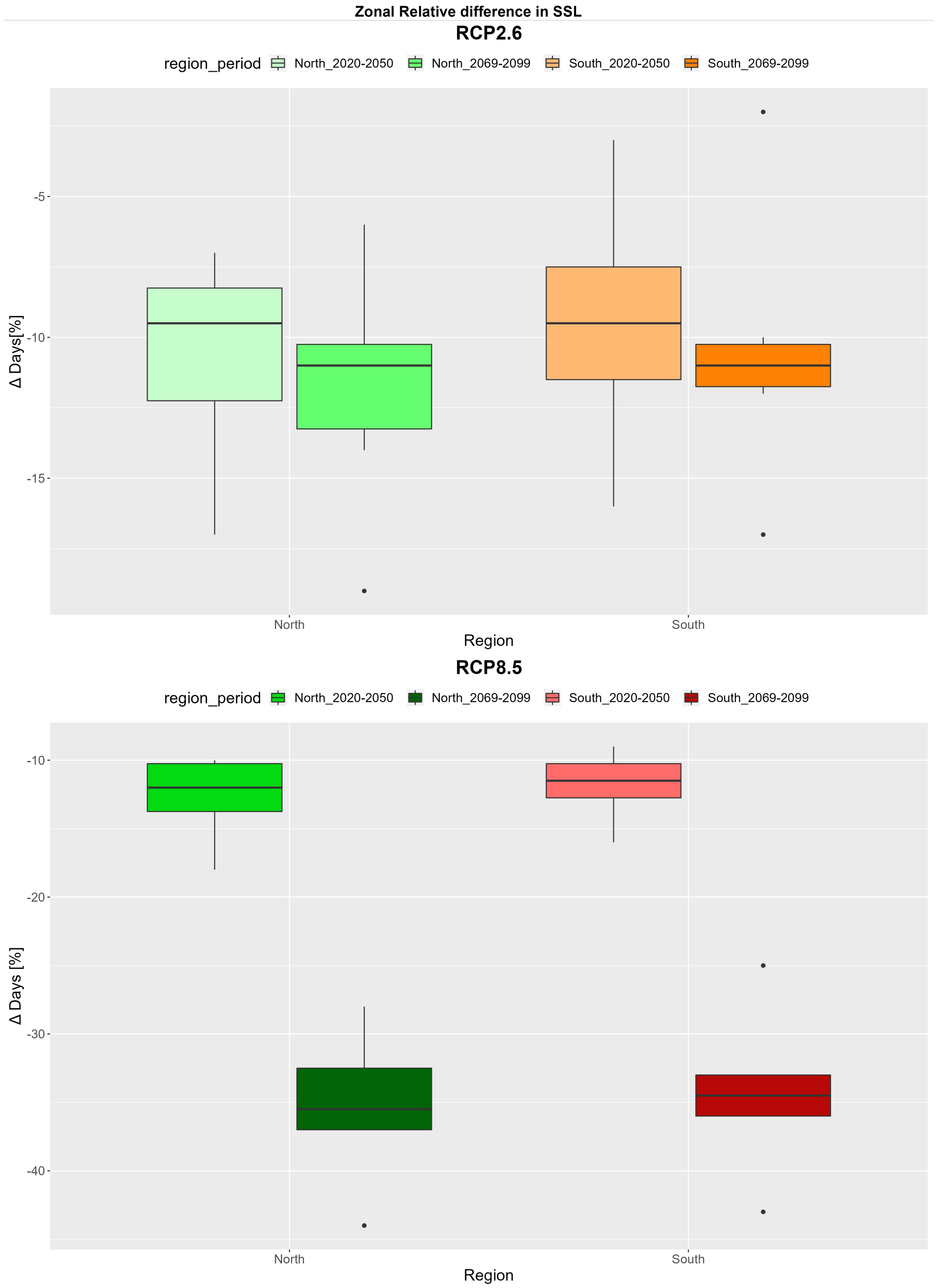

Figure 60: Relative difference in SSL between the Future periods (2020-2050, 2069-2099) and the Historical one, shown at macro-region scale. Top: RCP2.6. Bottom: RCP8.5. Macro-regions are subdivided by color: green for North, orange/red for South

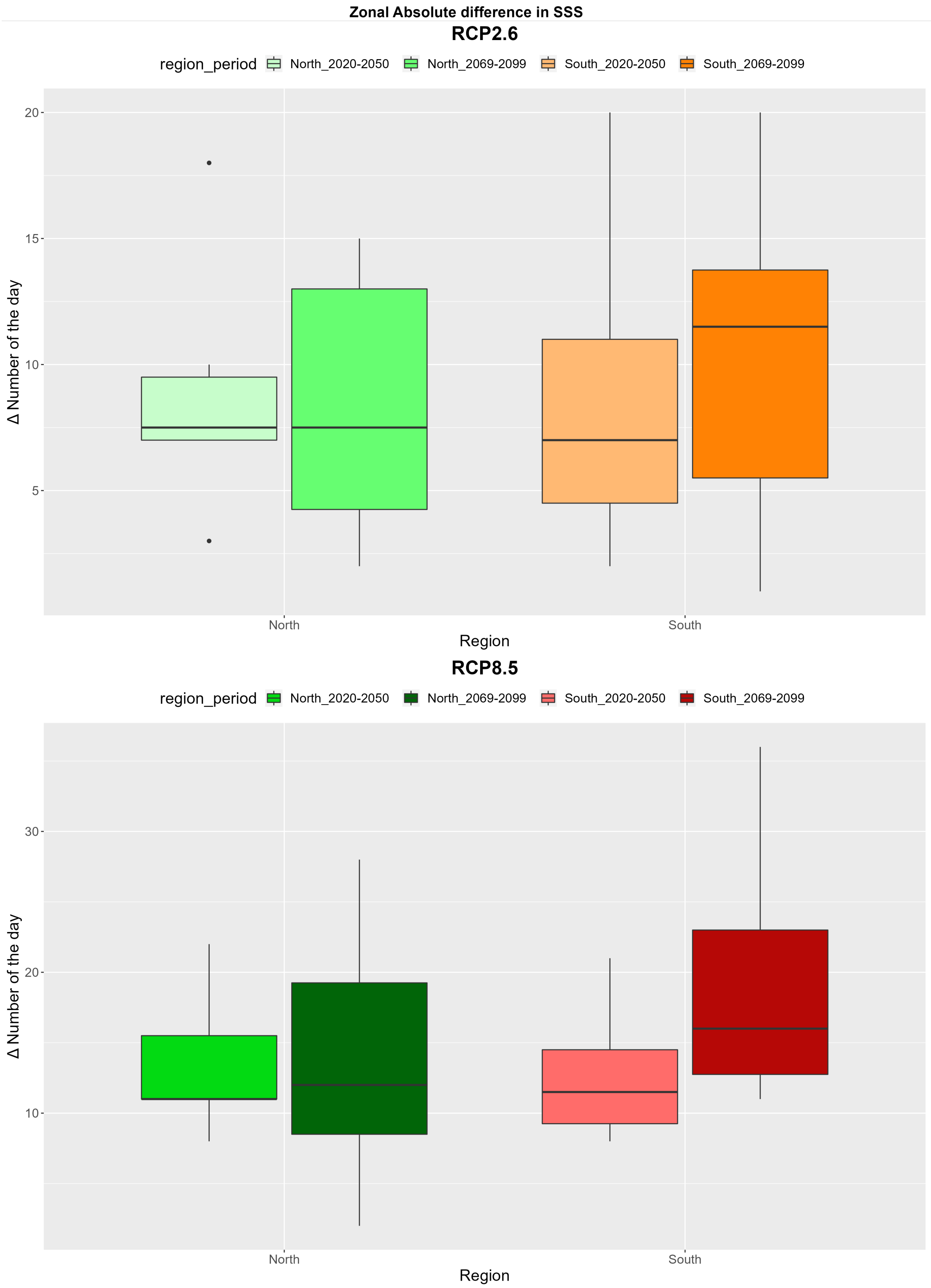

Figure 61: Absolute difference in SSS between the Future periods (2020-2050, 2069-2099) and the Historical one, shown at macro-region scale. Top: RCP2.6. Bottom: RCP8.5. Macro-regions are subdivided by color: green for North, orange/red for South

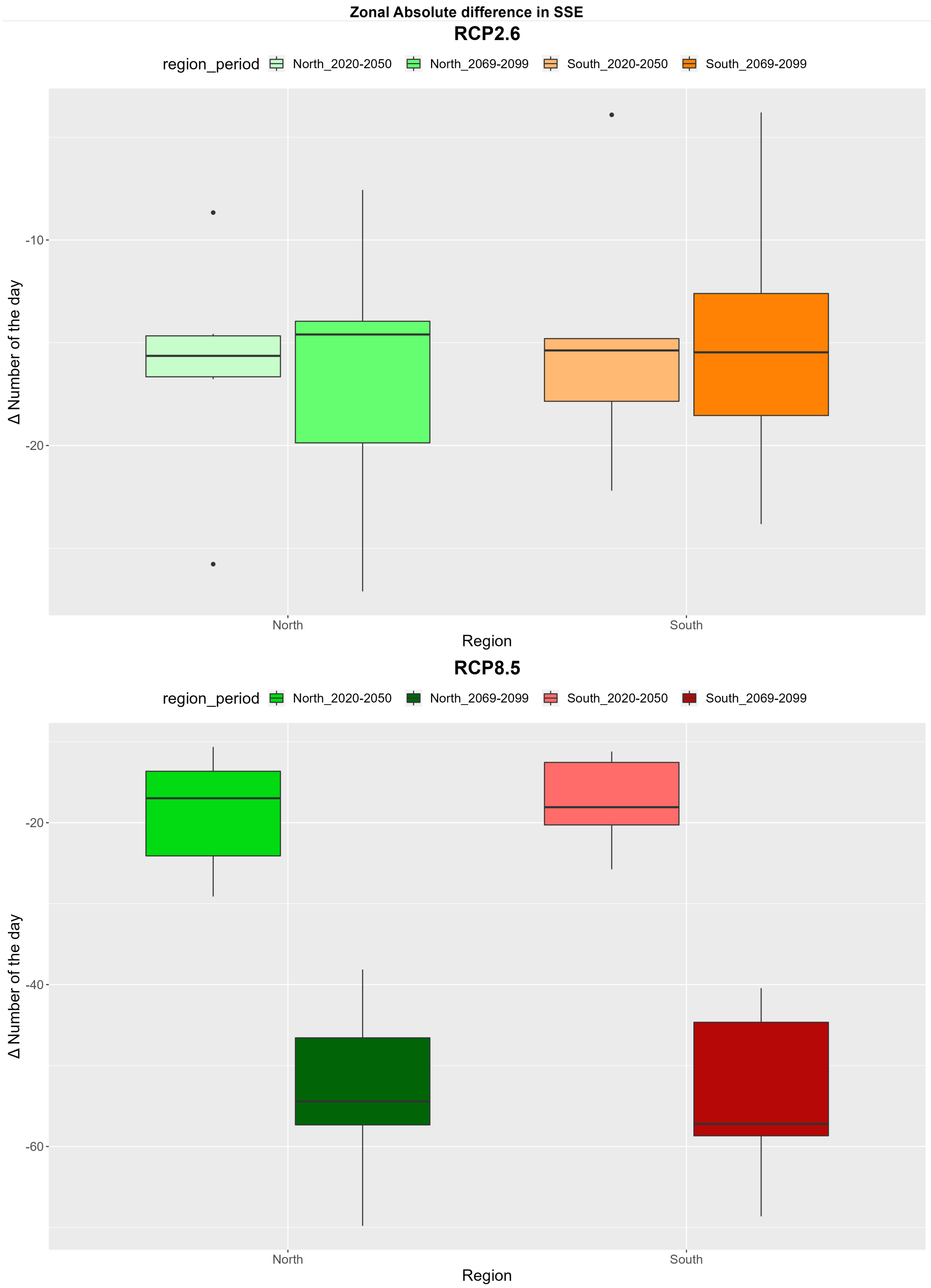

Figure 62: Absolute difference in SSE between the Future periods (2020-2050, 2069-2099) and the Historical one, shown at macro-region scale. Top: RCP2.6. Bottom: RCP8.5. Macro-regions are subdivided by color: blue for North, orange/red for South

Appendix E

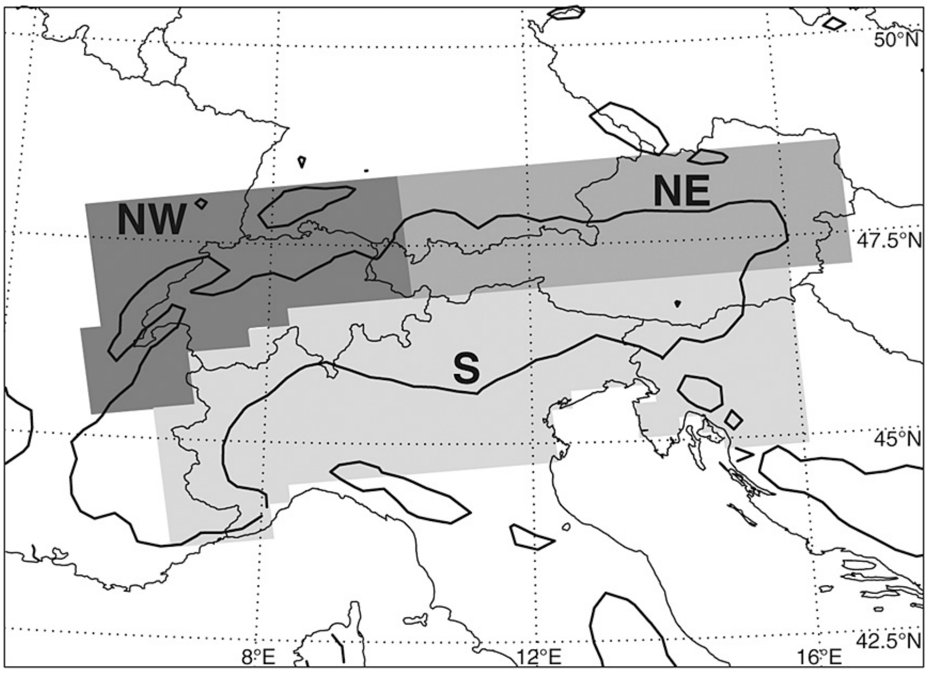

Figure 63: Subdivision in Zones in the study of Kotlarski et al. (2022) [8]

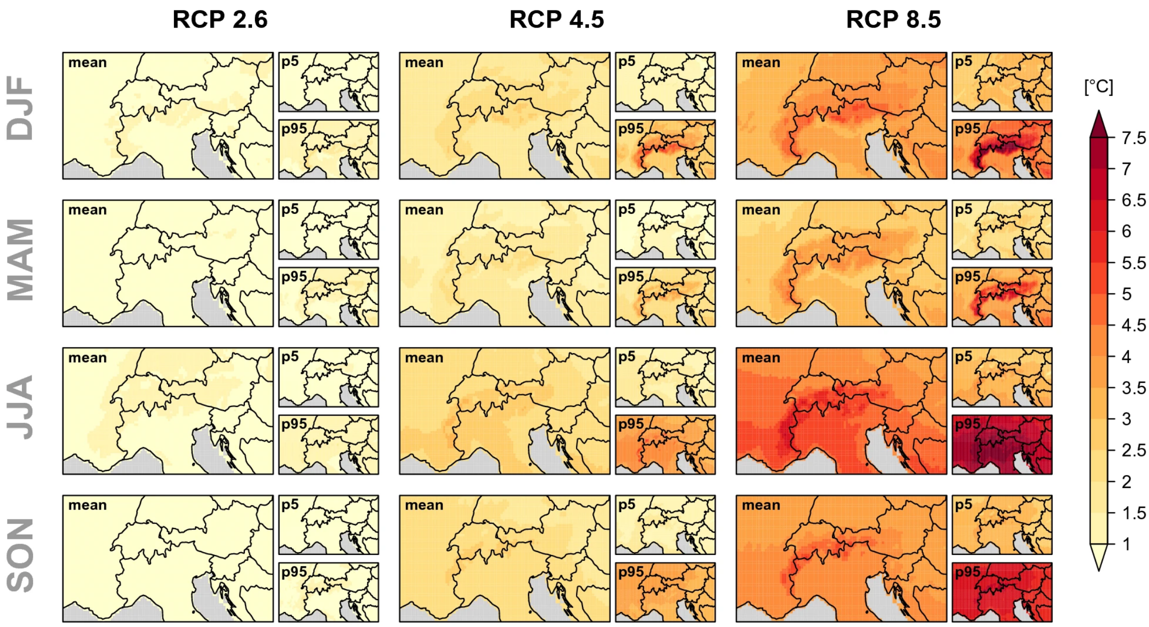

Figure 64: Horizontal pattern of the projected seasonal mean temperature change between 1981–2010 and 2070–2099 [°C] over the Alpine domain and for the three emission scenarios considered. Columns refer to the individual emission scenarios and lines to the seasons. The large panel of each triple shows the ensemble mean change of the EUR-11 sub-ensemble. The small panels indicate the lower (p5; upper panel) and upper estimate (p95; lower panel) of the EUR-11 sub-ensemble. Note that mean values and upper and lower estimates have been computed for each grid cell separately and that there is no individual experiment showing these specific patterns [8].

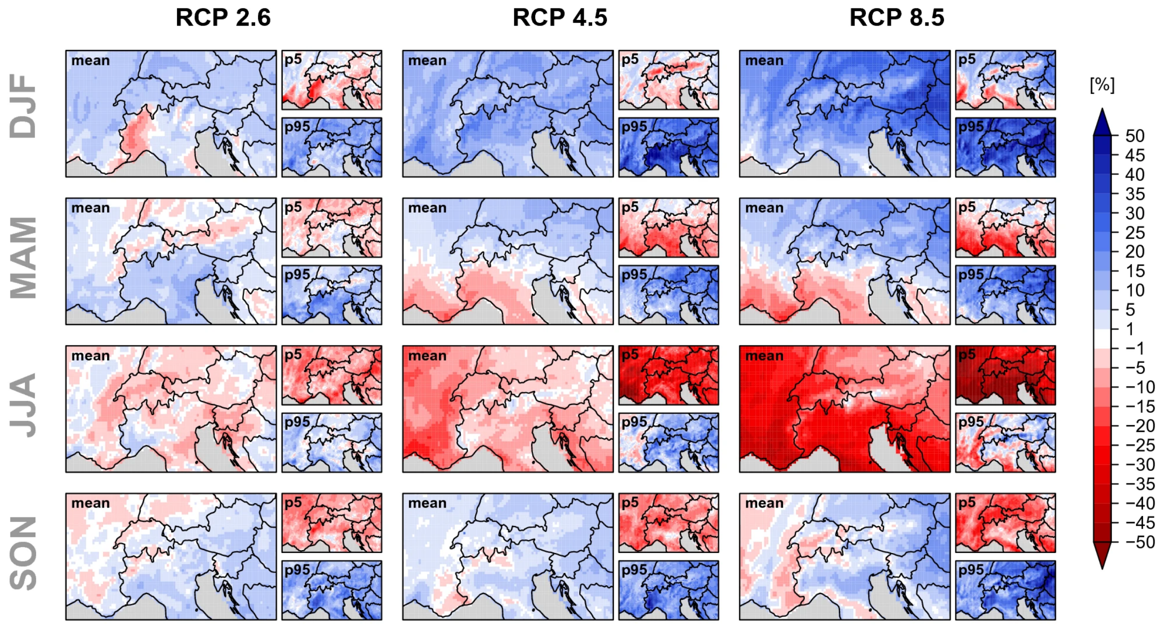

Figure 65: Horizontal pattern of the projected seasonal mean precipitation change [%] between 1981–2010 and 2070–2099 over the Alpine domain and for the three emission scenarios considered. Columns refer to the individual emission scenarios and lines to the seasons. The large panel of each triple shows the ensemble mean change of the EUR-11 sub-ensemble. The small panels indicate the lower (p5; upper panel) and upper estimate (p95; lower panel) of the EUR-11 sub-ensemble. Note that mean values and upper and lower estimates have been computed for each grid cell separately and that there is no individual experiment showing these specific patterns [8].

References

[1] Notarnicola C. "Overall negative trends for snow cover extent and duration in global mountain regions over 1982–2020". In: *Sci Rep* 12.13731 (2022). DOI: 10.1038/s41598-022-16743-w (cit. on p. 2).

[2] Matiu M. et al. "Observed snow depth trends in the European Alps: 1971 to 2019". In: *The Cryosphere* 15.1343-1382 (2021). DOI: 10.5194/tc-15-1343-2021 (cit. on p. 2).

[3] Beniston M. et al. "The European mountain cryosphere: a review of its current state, trends, and future challenges". In: *The Cryosphere* 12 (2018), pp. 759–790. DOI: 10.5194/tc-12-759-2018 (cit. on p. 2).

[4] IPCC. "IPCC Special Report on the Ocean and Cryosphere in a Changing Climate". In: *IPCC* (2019) (cit. on p. 2).

[5] Beniston M., Keller F, Koffi B., and Goyette S. "Estimates of snow accumulation and volume in the Swiss Alps under the changing climatic conditions". In: *Theor. Appl. Climatol.* 76 (2003), pp. 125–140. DOI: 10.1007/s00704-003-0016-5 (cit. on p. 2).

[6] Marty C. "Regime shift of snow days in Switzerland". In: *Geophysical Research Letters* (2008). DOI: 10.1029/2008gl033998 (cit. on p. 2).

[7] Gobiet A. and Kotlarski S. "Future Climate Change in the European Alps". In: *Climate Science* (2020). DOI: 10.1093/acrefore/9780190228620.013.767 (cit. on p. 2).

[8] Kotlarski S., Gobiet A., Morin S., Olefs M., Rajczak J., and R. Samacoït. "21st Century alpine climate change". In: *Clim Dyn* (2022). DOI: 10.1007/s00382-022-06303-3 (cit. on pp. 2, 53, 68, 69, 95, 96).

[9] Schmucki E, Marty C., Fierz C., and Lehning M. "Simulations of 21st century snow response to climate change in Switzerland from a set of RCMs". In: *Int J. Climatol.* 35 (2015), pp. 3262–3273. DOI: 10.1002/joc.4205,2015 (cit. on p. 2).

[10] Marty C., Bavay M., Farinotti A., and Huss M. "Snow: Hydro-CH2018 synthesis report chapters: "future changes in hydrology""". In: *Hydro-CH2018 Project* (2020). DOI: 10.16904/slf.2 (cit. on p. 2).

[11] Michel A., Schaefli B., Wever N., Zekollari H., Lehning M., and Huwald H. "Future water temperature of rivers in Switzerland under climate change investigated with physics-based models". In: *Hydrol. Earth Syst. Sci.* 26 (2022), pp. 1063–1087. DOI: 10.5194/hess-26-1063-2022 (cit. on pp. 2, 15, 74).

[12] The Federal Council. *Energy-Facts and Figures*. URL: https://www.eda.admin.ch/aboutswitzerland/en/home/wirtschaft/energie/energie---fakten-und-zahlen.html#:~:text=Electricity%5C%20is%5C%20mainly%5C%20generated%5C%20by,by%5C%20around%5C%2014.5%5C%25%5C%20since%5C%201990. (cit. on p. 2).

[13] Abegg B., Agrawala S., Crick F., and de Montfalcon A. "Climate change impacts and adaptation in winter tourism". In: *Theor. Appl. Climatol.* (2007), pp. 25–60. DOI: 10.1787/9789264031692-en (cit. on p. 2).

[14] Schmucki E., Marty C., Fierz C., Weingartner R., and Lehning M. “Impact of climate change in Switzerland on socioeconomic snow indices”. In: *Climate change in the European Alps* 127 (2017), pp. 875–8889. DOI: 10.1007/s00704-015-1676-7 (cit. on p. 2).

[15] Bavay M., Lehning M., Joan T., and Löwe H. “Simulations of future snow cover and discharge in Alpine headwater catchments”. In: *Hydrological Process* 23 (2009), pp. 95–108. DOI: 10.1002/hpy.7195 (cit. on p. 2).

[16] McColl R. W. *Encyclopedia of World Geography*. URL: https://yale.databasin.org/pages/coping-uncertainty/ (cit. on p. 3).

[17] National Centre for Climate Services. *CH2018 – Climate Scenarios for Switzerland, Technical Report, National Centre for Climate Services*. 2018. ISBN: 978-3-9525031-4-0 (cit. on pp. 3, 4, 6, 12–14, 21, 30, 37, 41).

[18] MeteoSwiss. *South side of the Alps*. URL: https://www.nccs.admin.ch/nccs/en/home/regions/grossregionen/south-side-of-the-Alps.html (cit. on p. 4).

[19] MeteoSwiss. “Klimaregionen der Schweiz. In: Die Beobachtungsnetze der Schweizerischen Meteorologischen Anstalt”. In: *Arbeitsberichte der MeteoSchweiz* 93 (1980). DOI: https://yale.databasin.org/pages/coping-uncertainty/ (cit. on p. 6).

[20] MeteoSwiss. *The Climate of Switzerland*. URL: https://www.meteoswiss.admin.ch/home/climate/the-climate-of-switzerland.html (cit. on pp. 6, 17).

[21] Zubler E. M., Scherrer S. C.and Croci-Maspoli M., Liniger M. A., and Appenzeller C. “Key climate indices in Switzerland; expected changes in a future climate””. In: *Climatic change,* 123.2 (2014), pp. 255–271. DOI: 10.1007/s10584-013-1041-8 (cit. on p. 7).

[22] Hartmann D.L. *Global Physical Climatology*. Elsevier, 2015. ISBN: 978-0-12-328531-7 (cit. on pp. 7, 8).

[23] Eltahir E. and Krol A. *Climate Models*. URL: https://climate.mit.edu/explainers/climate-models#:~:text=Climate%5C%20models%5C%20are%5C%20computer%5C%20programs,the%5C%20climate%5C%E2%5C%80%5C%94under%5C%20different%5C%20conditions (cit. on p. 8).

[24] NOAA. *Climate Models*. URL: https://www.climate.gov/maps-data/climate-data-primer/predicting-climate/climate-models#:~:text=Climate%5C%20models%5C%2C%5C%20also%5C%20known%5C%20as,the%5C%20ocean%5C%2C%5C%20atmosphere%5C%2C%5C%20land (cit. on pp. 8, 9).

[25] Jacob D. “Regional Climate Models: Linking Global Climate Change to Local Impacts”. In: *Encyclopedia of Complexity and Systems Science* (2009), pp. 7591–7602. DOI: 10.1007/978-0-387-30440-3_449. (cit. on p. 9).

[26] IPCC. *About the IPCC*. URL: https://www.ipcc.ch/about/ (cit. on pp. 9, 66).

[27] Wayne G. P. *The Beginner’s Guide to Representative Concentration Pathways*. Skeptical Science, 2013 (cit. on p. 9).

[28] Moss R., Edmonds J., and Hibbard K. et al. “The next generation of scenarios for climate change research and assessment”. In: *Nature* 463 (2010), pp. 747–756. DOI: 10.1038/nature08823 (cit. on p. 10).

[29] JVan Vuuren DP., Stehfest E., Den Elzen MGJ., Deetman S., Hof A., Isaac M., Klein Goldewijk K., Kram T. Mendoza Beltran A., and Oostenrijk R. "RCP2.6: Exploring the possibility to keep global mean temperature change below 2°C". In: (2011). DOI: 10.1007/s10584-011-0152-3 (cit. on pp. 10, 11).

[30] IPCC. *Sixth Assessment Report - Technical Summary*. URL: https://www.ipcc.ch/report/ar6/wg1/downloads/report/IPCC_AR6_WGI_TS.pdf (cit. on p. 11).

[31] PRIMAVERA. *Uncertainty in climate projections*. URL: https://uip.primavera-h2020.eu/sites/default/files/Uncertainty_Climate_Models.pdf (cit. on p. 11).

[32] WHawkins E. *Sources of uncertainty in CMIP5 projections*. Climate Lab Book, 2013 (cit. on p. 12).

[33] Yale framework. *Recognizing and Coping with Uncertainty in Climate Impact Analysis and Adaptation Strategies*. URL: https://yale.databasin.org/pages/coping-uncertainty/ (cit. on p. 12).

[34] Rajczak J., Kotlarski S., Salzmann N., and Schär C. "Robust climate scenarios for sites with sparse observations: a two-step bias correction approach". In: *International Journal of Climatology* 36 (2016), pp. 1226–1243. DOI: 10.1002/joc.4417 (cit. on pp. 13, 37).

[35] Feigenwinter I., Kotlarski S., Casanueva A., Fischer AM., Schwierz C., and Liniger MA. "Exploring quantile mapping as a tool to produce user-tailored climate scenarios for Switzerland". In: *Technical Report MeteoSwiss* 270 (2018), p. 44. DOI: file:///C:/Users/chiesa/Downloads/MeteoSchweiz_Fachbericht_270_final\%20(3).pdf (cit. on p. 14).

[36] Bartelt P. and Lehning M. "A physical SNOWPACK model for the Swiss avalanche warning, Part I: numerical model". In: *Cold Regions Science andTechnology* 35 (2002), pp. 123–145. DOI: 10.1016/S0165-232X(02)00074-5 (cit. on pp. 15, 17, 22).

[37] Bony S et al. "Climate Models and Their Evaluation". In: *IPCC* (2018) (cit. on p. 15).

[38] Brun E., Martin E., Simon V., Gendre C., and Coleou C. "An energy and mass model of snow cover suitable for operational avalanche forecasting". In: *J. Glaciol.* 35 (1989), pp. 333–342. DOI: 10.3189/S0022143000009254 (cit. on p. 15).

[39] Essery R. "Snow Modelling". In: *ECMWF Seminar on Polar Meteorology* (2006), pp. 4–8 (cit. on p. 15).

[40] Vionnet V., Brun E., Morin S., Boone A., Faroux S., Le Moigne P., Martin E., and Willemet J.-M. "The detailed snowpack scheme Crocus and its implementation in SURFEX v7.2". In: *Geosci. Model Dev.* 5 (2012), pp. 773–791. DOI: 10.5194/gmd-5-773-2012 (cit. on p. 15).

[41] Boone A. "Description du Schema de Neige ISBA-ES". In: *Centre National de Recherches Météorologiques* (2002) (cit. on p. 15).

[42] Jordan R. "A One-Dimensional Temperature Model for a Snow Cover: Technical Documentation for SNTHERM". In: *Cold Regions Research and Engineering Lab* 89 (1991) (cit. on p. 15).

[43] Schmucki E., Marty C, Fierz C., and Lehning M. “Evaluation of the mdoelled snow depth and snow water equivalent at three contrasting sites in Switzerland using SNOWPACK simulations driven by different meteorological data input”. In: *Cold Regions Science and Technology* 99 (2014), pp. 27–37. DOI: 10.1016/j.coldregions.2013.12.004 (cit. on pp. 16, 29).

[44] Marty C., Schlögl S., Bavay M., and Lehning M. “How much can we save? Impact of different emission scenarios on future snow cover in the Alps”. In: *The Cryosphere* 11 (2017), pp. 517–529. DOI: 10.5194/tc-11-517-2017 (cit. on pp. 16, 66).

[45] IMIS: WSL Institute for Snow and SLF Avalanche Research. *IMIS measuring network*. URL: https://www.slf.ch/en/%20avalanche-bulletin-and-snow-situation/measured-values/%20description-of-automated-stations.html (cit. on p. 17).

[46] Earth System Grid Federation (ESGF). *What is ESGF?* https://esgf.llnl.gov/ (cit. on p. 21).

[47] Copernicus Europe’s eyes on Earth. *Climate Data Store*. https://cds.climate.copernicus.eu/!/home (cit. on p. 21).

[48] SLF. *SNOWPACK table of contents*. URL: file:///C:/Program%5C%20Files/Snowpack/doc/html/index.html (cit. on p. 22).

[49] Lehning M., Bartelt P., Brown B., Russi T., Stockli U., and Zimmerli M. “A network of automatic weather and snow station and supplementary model calculation providing snowpack information for avalanche warning”. In: *International snow science workshop proceedings* (1998), pp. 225–233. DOI: https://www.dora.lib4ri.ch/wsl/islandora/object/wsl\%3A16814/datastream/PDF/Lehning-1998-A_network_of_automatic_weather-\%28published_version\%29.pdf (cit. on p. 23).

[50] Guido Van Rossum and Fred L Drake Jr. *Python reference manual*. https://www.r-project.org/, 1995 (cit. on p. 24).

[51] Unsworth and Monteith. “Long-wave radiation at the ground”. In: *Q. J. R. Meteorolo. Soc.* 101 (1975), pp. 13–24 (cit. on p. 29).

[52] Sicart J. E., Pomeroy J. W., Essery R. L. H., and Bewley D. “Incoming longwave radiation to melting snow:observations, sensitivity and estimation innorthern environments”. In: *Wiley InterScience* 20 (2006), pp. 3697–3708. DOI: 10.1002/hyp.6383 (cit. on p. 29).

[53] Bender E., Lehning M., and Fiddes J. “Changes in Climatology, Snow Cover, and Ground Temperatures at High Alpine Locations”. In: *Front. Earth Sci.* (2020). DOI: 10.3389/feart.2020.00100 (cit. on p. 29).

[54] Marty C., Philipona R., Fröhlich, and C. et al. “Altitude dependence of surface radiation fluxes and cloud forcing in the alps: results from the alpine surface radiation budget network”. In: *Theor.Appl.Climatol* 72 (2002), pp. 137–155. DOI: 10.1007/s007040200019 (cit. on p. 30).

[55] *Linux software*. https://www.linux.it/ (cit. on p. 35).

[56] Themeßl M.J., Gobiet A., and Leuprecht A. “Empirical-statistical downscaling and error correction of daily precipitation from regional climate models”. In: *International Journal of Climatology* 31 (2010), p. 44. DOI: 10.1002/joc.2168 (cit. on p. 37).

[57] Ihaka R. and Gentleman R. *The R Project for Statistical Computing*. Centrum voor Wiskunde en Informatica Amsterdam, 1991 (cit. on p. 39).

[58] Förster K., Hanzer F., Winter B., Marke T., and Strasser U. "An open-source MEteoroLOgical observation time series DISaggregation Tool (MELODIST v0.1.1)". In: *Geosci. Model Dev.* 9 (2016), pp. 2315–2333. DOI: 10.5194/gmd-9-2315-2016 (cit. on p. 39).

[59] Gobiet A., Kotlarski S., Beniston M., Heinrich G., Rajczak J., and Stoffel M. "21st century climate change in the European Alps". In: *Science of the Total Environment* 493 (2014), pp. 1138–1151. DOI: 10.1016/j.scitotenv.2013.07.050 (cit. on p. 68).

[60] Vries H., Lenderink G., and van Meijgaard E. "Future snowfall in western and central Europe projected with a high-resolution regional climate model ensemble". In: *Geophysics Research Letters* 41 (2014), pp. 4294–4299. DOI: 10.1002/2014GL059724 (cit. on pp. 69, 77).

[61] Muelchi R., Rössler O., Schwanbeck J., Weingartner R., and Martius O. "River runoff in Switzerland in a changing climate – runoff regime changes and their time of emergence". In: *Hydrol. Earth Syst. Sci.* 25 (2021), pp. 3071–3086. DOI: 10.5194/hess-25-3071-2021 (cit. on p. 74).

[62] Lüthi S., Ban N., Kotlarski S., Streger C.R., Jonas T., and Schär C. "Projection of Alpine Snow-Cover in a High-Resolution Climate Simulation". In: *Atmopshere* 463 (2019), p. 18. DOI: 10.3390/atmos10080463 (cit. on p. 76).